U.PORTO

FEUP FACULDADE DE ENGENHARIA
UNIVERSIDADE DO PORTO

EFFECT OF CABLE DAMAGE ON THE STRUCTURAL BEHAVIOUR OF A CABLE-STAYED BRIDGE

HENRIQUE FRANZENER HYPPOLITO

Dissertation submitted for partial satisfaction of the requirements of the degree of

MASTER IN CIVIL ENGINEERING STRUCTURES

Advisor: Doctor Professor Elsa de Sá Caetano

JUNE 2020

MASTER IN CIVIL ENGINEERING STRUCTURES 2019/2020

DEPARTMENT OF CIVIL ENGINEERING

Tel. +351-22-508 1901

Fax +351-22-508 1446

✉ mestec@fe.up.pt

Edited by

FACULTY OF ENGINEERING OF UNIVERSITY OF PORTO

Rua Dr. Roberto Frias

4200-465 PORTO

Portugal

Tel. +351-22-508 1400

Fax +351-22-508 1440

✉ feup@fe.up.pt

http://www.fe.up.pt

Para meus pais.

“Tente mover o mundo – o primeiro passo será mover a si mesmo.”

Platão

ACKNOWLEDGMENT

First of all, I want to express my sincere gratitude to my advisor Prof. Dr. Elsa de Sá Caetano for the support and guidance during the development of this work.

I would also like to extend my gratitude to all the professors in the Department of Structures of Civil Engineering for the time dedicated to the students of the Master in Structures of Civil Engineering. Without their dedication and patience during the classes we would not be able to have the proper knowledge and preparation to work as structural engineers.

The last, but not the least, I want to thank my family and specially to my girlfriend, Isabelle, for the support and dedication during this period.

ABSTRACT

Since old civilizations, the application of cables to support loads has been a popular technique. At the beginning of the nineteenth century wrought iron bars, and later steel wires, with a reliable tensile strength were developed and become an interesting option to be used as inclined stays. However, during the first applications to cable-stayed bridges in the middle of the 19th century, problems were faced due to misunderstanding of the structural behaviour and construction process. With the breakthrough in computer-aided analysis in the mid-1960s, the use of the cable-stayed system started to be implemented and quickly extended around the world.

In most cases, the cables of a cable-stayed bridge are composed of steel wire strands. As many of the structures are placed in a very aggressive environment, near to the coast, the steel elements are more susceptible to corrosion. To guarantee the lifetime of the structure, special requirements for cable protection have been developed along the years. Nowadays, old structures have been the object of monitoring and maintenance works to assure serviceability conditions.

In this work, the Edgar Cardoso Bridge (1982), located in Figueira da Foz, Portugal, will be the object of study. This bridge is arranged in a pure fan system with 24 stays and main span of 225m. As the bridge already presents some members affected by corrosion, the objective of this work is to characterize the mechanism of degradation and how it can be monitored. During the process, a Finite Element Model (FEM) was developed and validated with measurement data collected in the bridge. Based on the FEM model, four scenarios of damage were simulated where the cable area was reduced by 10%, 20% and 40%, at individual level or on all stay cables, to simulate cable loss.

The first conclusion taken from this work is that measurements can provide a reliable source of information to validate the finite element models. After the analysis, it was also found that the structure has a tolerable safety factor for design conditions and the cables can support area reduction between 20 and 40%. With the simulation of the four scenarios of damage, it was possible to confirm that the cables are de most fragile element of the bridge. Thus, to monitor a possible damage development, the displacement of the deck is the most advisable parameter to be measured, because this was the value with higher variation in all cases studied.

KEYWORD: Cable-stayed Bridges, Cables, Damage, Structural modelling, Monitoring.

RESUMO

Desde as antigas civilizações, a aplicação de cabos para suportar cargas tem sido uma técnica popular. No início do século XIX, barras de ferro forjadas, e mais tarde fios de aço, com uma força de tração fiável foram desenvolvidos e tornaram-se uma opção interessante para ser usados como tirantes inclinados. No entanto, nas primeiras aplicações em pontes atirantadas, problemas no entendimento do comportamento estrutural e no processo de construção levaram a algumas falhas. Somente após a descoberta da análise assistida por computador, em meados da década de 1960, o uso de pontes atirantadas foi efetivamente implementado e se estendeu para o mundo.

Na maioria dos casos, os cabos de uma ponte atirantada são compostos por fios de aço. Como a maioria das estruturas são construídas em um ambiente muito agressivo, perto da costa, os elementos de aço ficam mais suscetíveis à corrosão. Para garantir o tempo de vida útil, requisitos especiais de proteção do cabo foram desenvolvidos ao longo dos anos. Atualmente, estruturas antigas têm sido objeto de trabalhos de monitorização e manutenção para garantir condições de serviço.

Neste trabalho, a Ponte Edgar Cardoso (1982), localizada na Figueira da Foz, em Portugal, será objeto de estudo. Esta ponte é constituída por um sistema em forma de leque com 24 tirantes e extensão do vão central de 225m. Como a ponte já apresenta alguns membros afetados pela corrosão, o objetivo deste trabalho é caracterizar os mecanismos degradação e as formas mais eficientes de os monitorizar. Com este propósito foi desenvolvido um Modelo de Elementos Finitos (FEM) e validado com dados de medições efetuadas na ponte. Com base no modelo foram simulados quatro cenários de dano à estrutura onde a área do cabo foi reduzida em 10%, 20% e 40%, de forma individual ou em conjunto, para simular o dano nos cabos.

A primeira conclusão tirada deste trabalho é que as medições podem fornecer uma fonte fiável de informação para validar os modelos de elementos finitos. Após a análise verificou-se também que a estrutura tem um fator de segurança aceitável para as condições de dimensionamento e que os cabos podem suportar uma redução da área entre 20 e 40%. Com a simulação dos quatro cenários de dano foi possível concluir também que os cabos são o elemento mais frágil da ponte. Assim, o parâmetro mais aconselhável para ser medido num processo de monitoramento dos danos, é o deslocamento do tabuleiro, sendo este o parâmetro com maior variação em todos os casos estudados.

PALAVRAS-CHAVE: Pontes Atirantadas, Cabos, Dano, Modelação estrutural, Monitoração.

GENERAL INDEX

ACKNOWLEDGMENT i

ABSTRACT iii

RESUMO v

1 INTRODUCTION 1

1.1 FRAMEWORK 1
1.2 OBJECTIVES 1

2 STATE-OF-THE-ART 2

2.1 CABLE-STAYED BRIDGES – HISTORICAL REVIEW 2
2.2 CABLES 7
2.2.1 CABLE TYPES 7
2.2.2 CORROSION PROTECTION 9
2.2.3 ANCHORAGE SYSTEMS 11
2.3 CABLE LOSS 13
2.4 STRUCTURAL MONITORING 14

3 STRUCTURE DESCRIPTION 21

3.1 STAYS 21
3.2 DECK 22
3.3 PYLON 23
3.4 DAMAGE IDENTIFICATION 24

4 STRUCTURAL MODELLING 25

4.1 MODELLING PROCESS 25
4.2 LOAD CASES 29
4.2.1 DEAD LOAD 30
4.2.2 TRAFFIC LOAD 30
4.2.3 WIND ACTION 34
4.2.4 SEISMIC LOAD 41
4.2.5 LOAD COMBINATIONS 45
4.3 VALIDATION OF THE FINITE ELEMENT MODEL 49
4.3.1 SELF-WEIGHT 49

4.3.2 CABLE GEOMETRY 50
4.3.3 MODE SHAPES AND NATURAL FREQUENCIES 51
4.4 SENSITIVITY ANALYSIS 51

5 SIMULATION OF DAMAGE SCENARIOS 55

5.1 PARAMETERS FOR DAMAGE ANALYSIS 55
5.2 DAMAGE SCENARIOS 57

6 RESULTS AND DISCUSSIONS 59

6.1 DAMAGE SCENARIO 1 – LOSS ON THE LONG CABLE 59
6.1.1 AXIAL LOAD 59
6.1.2 DISPLACEMENT 61
6.1.3 MODAL RESPONSE 62
6.1.4 ADJACENT MEMBERS 62
6.2 DAMAGE SCENARIO 2 – LOSS ON THE MEDIUM CABLE 63
6.2.1 AXIAL LOAD 63
6.2.2 DISPLACEMENT 64
6.2.3 MODAL RESPONSE 65
6.2.4 ADJACENT MEMBERS 66
6.3 DAMAGE SCENARIO 3 – LOSS ON THE SHORT CABLE 66
6.3.1 AXIAL LOAD 67
6.3.2 DISPLACEMENT 68
6.3.3 MODAL RESPONSE 68
6.3.4 ADJACENT MEMBERS 69
6.4 DAMAGE SCENARIO 4 – UNIFORM LOSS ON ALL THE CABLES 70
6.4.1 AXIAL LOAD 70
6.4.2 DISPLACEMENT 71
6.4.3 MODAL RESPONSE 72
6.4.4 ADJACENT MEMBERS 72
6.5 DISCUSSION 73

7 CONCLUSIONS 77

REFERENCES 79

FIGURES INDEX

Figure 1 - Albert Bridge (London, 1873) 2
Figure 2 - Dryburgh Bridge (England, 1817) 3
Figure 3 - Bridge over the River Saale (Germany, 1824) 3
Figure 4 - Brooklyn Bridge (New York, 1883) 3
Figure 5 - Strömsund Bridge (Sweden,1955) 4
Figure 6 - Severins Bridge (Cologne,1959) 4
Figure 7 - Maracaibo Bridge (Venezuela,1962) 5
Figure 8 - Friedrich-Ebert Bridge (Germany,1967) 5
Figure 9 - Pasco-Kennewick Bridge (United States, 1978) 6
Figure 10 - Barrios de Luna Bridge (Spain, 1984) 6
Figure 11 - Tatara Bridge (Japan, 1999) 7
Figure 12 - Sutong Yangtze River Bridge (China, 2008) 7
Figure 13 - Seven-wire strand 8
Figure 14 - Multi-wire helical strand 8
Figure 15 – Locked-coil system 9
Figure 16 - Parallel -strand cable 9
Figure 17 - Cable corroded 9
Figure 18 - HDPE pipe usage 10
Figure 19 – Dehumidification system applied on the Bay Bridge, United States. 10
Figure 20 – Typical components of stay cable anchorage (Freyssint, 2010) 11
Figure 21 - Socket for parallel wire strand 11
Figure 22 - Internal dumpers: a - Elastomeric (IED), Hydraulic (IED) and Radial (IRD) dampers (Freyssinet, 2014); b – Elastomeric damper; c – Friction damper (VSL, 2002) 12
Figure 23 - Anchorage system with eyed bars of the Asashi Kaikyo Bridge 12
Figure 24 - Accidental forces for design of cable bridges 13
Figure 25 - Øresund Bridge SHM sensors (phase II), Denmark-Sweden 14
Figure 26 – a) Strain gauges b) accelerometer. 15
Figure 27 - Total Station 16
Figure 28 - (a) Impulse hammer; (b) eccentric mass vibrator; (c) electrodynamic shaker over three load cells; d) impulse excitation device for bridges. 17
Figure 29 - Forced vibration tests: (a) Tatara cable-stayed bridge; (b) Yeongjong suspension bridge; (c) high force shaker 18
Figure 30 - (a) Force balance accelerometers; (b) multichannel data acquisition and processing system for ambient vibration tests; (c) strong motion triaxial seismograph. 19
Figure 31 - Stress-ribbon footbridge at the FEUP Campus 19
Figure 32 - Edgar Cargoso bridge,1982. 21
Figure 33 - General view from the saddles arrangement and the design. 22
Figure 34 - Deck cross section 22
Figure 35 - Deck view 23
Figure 36 - Pylon view and geometry 23
Figure 37 - Pylon base structure 24
Figure 38 - Edgar Cargoso Bridge 3D model 25
Figure 39 - Link element variations 27
Figure 40 - Releases at the deck bar elements 27
Figure 41 - Link between the steel deck and the concrete slab 28
Figure 42 - Cable connection to the pylon to through link element. 28

Figure 43 – Pin bearing in the pylon zone 29
Figure 44 - Suspenders at the edge of the deck 29
Figure 45 - Carriageway width 31
Figure 46 - Load Model 1 (LM1) 31
Figure 47 – Traffic load model 1 distribution 32
Figure 48 - Cable tension influence lines 33
Figure 49 - Moment influence line 33
Figure 50 - Edgar Cargoso bridge location 34
Figure 51 - Application of the wind force along the z direction, Fz(ze). 37
Figure 52 - Seismic zones for continental Portugal according to the action type. 41
Figure 53- SAP2000 response spectrum by the Eurocode 8. 45
Figure 54 - Mode shapes for the Edgar Cardoso Bridge 51
Figure 55 - Bridge axial load diagram 52
Figure 56 - YY bending moment diagram for the bridge deck (Dead load case). 52
Figure 57 - Structure displacement (Dead load case). 53
Figure 58 - LM4 distribution for the damage analysis 56
Figure 59 - Members analyzed in the damage scenarios 56
Figure 60 - Cables where the damage was applied 57
Figure 61 - Cable affected by the damage scenario 1 (loss on the long cable) 59
Figure 62 - Cable affected by the damage scenario 2 (loss on the medium cable) 63
Figure 63 - Cable affected by the damage scenario 3 (loss of short cable). 67

GRAPHICS INDEX

Graphic 1 - Transversal Influence Line 32
Graphic 2 - Force coefficient cfx,0 for bridge decks (NP EN 1991-1-4, 2019) 37
Graphic 3 - Force coefficient to rectangular sections with sharp edges 38
Graphic 4 - Boundary effect coefficient ψλ 39
Graphic 5 - Response spectrum shape 42
Graphic 6 - Seismic behavior factor 44
Graphic 7 - Probabilistic approach for load and resistance definition 46
Graphic 8 - Recommended values of ψ factor .....**Erro! Marcador não definido.**
Graphic 9 - Example of a damage scenario done for a medium cable 58
Graphic 10 - Axial load variation for damage scenarios 1 (loss of long cable on the West side) 60
Graphic 11 - Variation of stress for the damage scenario 1 (loss of long cable) 60
Graphic 12 - Variation of displacement for the damage scenario 1 (loss of long cable) 61
Graphic 13 - Axial load variation for damage scenario 2 (loss of medium cable) 64
Graphic 14 - Variation of stress for the damage scenario 2(loss of medium cable) 64
Graphic 15 - Variation of displacement for the damage scenario 2 (loss of medium cable). 65
Graphic 16 - Axial load variation for damage scenarios 3 (loss of short cable). 67
Graphic 17 - Variation of stress for the damage scenario 3 (loss of short cable) 67
Graphic 18 - Variation of displacement for the damage scenario 3 (loss of short cable) 68
Graphic 19 - Axial Force variation for the damage scenario 4 (uniform loss) 70
Graphic 20 - Stress variation in the cables for the damage scenario 4 71
Graphic 21 - Displacement variation for the damage scenario 4 (uniform loss). 71

TABLES INDEX

Table 1 - Section properties 25
Table 2 - Other permanent loads 30
Table 3 - Terrain category and terrain parameters 35
Table 4 - Average wind velocities 36
Table 5 - Peak velocity pressure 36
Table 6 - Force coefficients applied to the bridge deck 37
Table 7 - Boundary effect determination values 38
Table 8 - Pressure coefficient for cylinders with circular cross-section 39
Table 9 - Structural coefficient (cscd) calculation 40
Table 10 - Wind force values and coefficients 40
Table 11 - Wind force value applied to the z direction on the deck 40
Table 12 - Maximum base ground acceleration 42
Table 13 - Response spectrum parameters for soil type B 43
Table 14 - Maximum values of the behaviour factor q (EN 1998-2:2005+A2:2011) 44
Table 15 - Shear reactions for seismic action 45
Table 16 - Indicative design working life 46
Table 17 - Recommended values for γ factor 49
Table 18 - Deck self-weight verification 49
Table 19 - Stay's axial forces 50
Table 20 - Comparation of the natural frequencies 51
Table 21 - Axial forces on the main span cables 52
Table 22 - Pylon section resistance analysis 53
Table 23 - Axial forces on a medium cable of the main span after area reduction of the large cable 55
Table 24 – Cables identification 60
Table 25 – Displacement points identification 61
Table 26 - Displacements on the tower top for the damage scenario 1 (loss of long cable). 62
Table 27 - Modal variation for the damage scenario 1(loss of long cable) 62
Table 28 - Variation of stress in the double "I" section for the damage scenario 1 (loss of long cable). 63
Table 29 - Variation of stress in the pylon section for the damage scenario 1(loss of long cable). 63
Table 30 - Displacements at the tower top for the damage scenario 2 (loss of medium cable). 65
Table 31 - Modal variation for the damage scenario 2 (loss of medium cable) 65
Table 32 - Variation of stress in the double "I" section for the damage scenario 2 (loss of medium cable). 66
Table 33 - Variation of stress in the pylon section for the damage scenario 2(loss of medium cable). 66
Table 34 - Displacements on the tower top for the damage scenario 3 (loss of short cable). 68
Table 35 - Modal variation for the damage scenario 3 (loss of short cable) 68
Table 36 - Variation of stress in the double "I" section for the damage scenario 3 (loss of short cable) 69
Table 37 - Variation of stress in the pylon section for the damage scenario 3 (loss of short cable) 70
Table 38 - Displacements at the tower top for the damage scenario 4 (uniform loss). 71
Table 39 - Modal response variation for the damage scenario 4 (uniform loss). 72
Table 40 - Variation of stress in the double "I" section for the damage scenario 4 (uniform loss) 72
Table 41 - Variation of stress in the pylon section for the damage scenario 4 (uniform loss). 73
Table 42 - Variation of stress in the cables most affected in each damage scenario. 73
Table 43 - Variation of the axial force for each damage scenario. 74

Table 44 - Displacement variation for each damage scenario..... 74
Table 45 - Displacements on the tower top for the all the damage scenarios. 74
Table 46 - Variation in the vibration modes for different damage scenarios..... 75
Table 47 – Stress variation for the double “I” beam 75
Table 48 - Stress variation for the pylon section..... 76

1
INTRODUCTION

1.1 FRAMEWORK

Cable-stayed bridges have become a popular solution to overcame large spans, since they combine an economical and aesthetical advantages for certain constructed spans. In the past half-century, the developments in construction technics, new high-strength materials, and computer technology for structural analyses were fundamental for the diffusion of this structural technique.

Nowadays, the biggest concern about old cable-stayed bridges is the integrity of the cable stays. As these elements are mainly made of high-strength steel, they are very susceptible to suffer corrosion during the bridge lifetime. As the substitution of a stay could be economically inviable, to ensure a proper protection and maintenance is fundamental for the correct functionality of the bridge. According to that, engineers are focused on the structural health monitoring (SHM). This technique is based on the installation of measurement devices to collect data from the structure that can help professionals anticipate some problematic event.

In Portugal, the Edgar Cardoso Bridge is the first cable stayed bridges in the country in its type, opening to traffic in 1982. This structure was designed by the engineer and professor Edgar Cardoso, responsible for other beautiful landmarks around the world and recognized as one of the world's greatest structural engineers. Unfortunately, nowadays the bridge suffers from some corrosion issues on the cables and has been the object of rehabilitation works and monitoring processes.

1.2 OBJECTIVES

In the contest exposed in the last section, the objectives of this work are:

- To develop a finite element model of the structure based on reliable measurements made on the structure.
- To simulate damage scenarios that represent the loss of cross section due to corrosion.
- To identify the elements that are more sensitive to failure.
- To identify which parameters are more influenced by cable loss, so that they can be used as a guideline for further monitoring process.

2
STATE-OF-THE-ART

2.1 CABLE-STAYED BRIDGES – HISTORICAL REVIEW

Since old civilizations, the application of cables to support loads has been a popular technique. At the seventeenth century a bridge proposed by Verantius (Italy,1617) was one of the first projects to include inclined stays to support the deck. In the following years Löscher (Germany,1784) also proposed a system of inclined stays very similar to those used nowadays [4].

In 1823, a bridge conceived by Marc Seguin characterized the first use of draw iron wires. This solution had problems related with the durability, since there was no efficient method to prevent corrosion at that time. In alternative, some engineers used pin connected eye-bars in chains as the main load-carrying elements. This system was applied in remarkable structures across the European continent. One of the classic examples is the Albert Bridge (Figure 1) in London, finished in 1873 this bridge is composed by a mixed system of cable stays and suspension [1].

Figure 1 - Albert Bridge (London, 1873)

At the beginning of the nineteenth century wrought iron bars, and later steel wires, with a reliable tensile strength were developed and become an interesting option to be used as inclined stays. But in the early cable-stayed bridges it was very difficult to find an even distribution of the load between all cables. Moreover, imperfections during fabrication and erection could easily lead to a structure where some stays were slack, and others overstressed. The stays were generally attached to the girder and pylon by pinned connections that did not allow a controlled tensioning [1]. By that time, several cable-stayed bridges were proposed and constructed. However, because of the problems faced due to

misunderstanding of structural behaviour and construction process, some failures occurred. The Dryburgh Bridge (England, 1817) (Figure 2) and the bridge over the River Saale (Germany, 1824) (Figure 3) are examples of these structural failures. Therefore, for some decades, the uncertainty about cable-stayed bridges lead engineers to consider suspension bridges instead [5].

Figure 2 - Dryburgh Bridge (England, 1817)

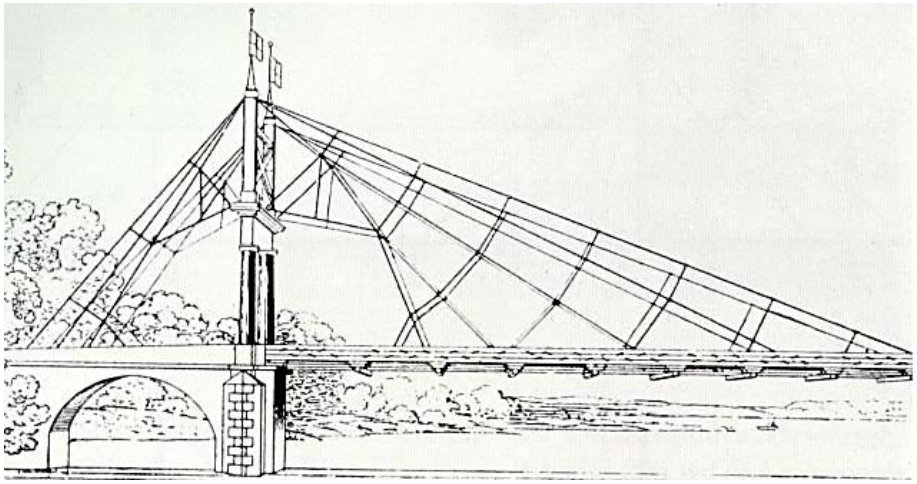

Figure 3 - Bridge over the River Saale (Germany, 1824)

In the middle of the 19th century cable-stayed systems started to be implemented in several suspension bridges as a complementary form to increase global stiffness and the stability against wind actions. At that time, a huge development in construction of suspension bridges was accomplished. The Brooklyn Bridge (Figure 4) opened in 1883, designed by John A. Roebling with main span of 486 m, was the first to use steel cables instead of iron and is the most notable exemplar of these hybrid systems. In the United States, J. Roebling was also responsible for other structures with the same characteristics as the Ohio River Bridge (1867) and Niagara Falls railway Bridge (1855) [5].

Figure 4 - Brooklyn Bridge (New York, 1883)

During the World War II the number of bridges destroyed in West Germany reached, approximately, 15000 [6]. This fact created a necessity to develop innovative solutions to rebuild these structures in a short time. The cable-stayed system emerged as an efficient manner to combine quick erection, aesthetic qualities, and comparatively low costs. Soon, this technique became recognized as an alternative to the classical bridge types, as suspension and arch systems, for medium spans (150-300m) [5].

However, it was in Sweden that the first modern cable-stayed bridge considered in the literature was built, in 1955. The Strömsund Bridge (Figure 5) was designed by the German engineer Dischinger, composed by two side spans of 75m and a main span of 183m. The stays were arranged as a pure fan system with cables radiating from the pylon top. The erection of the Strömsund Bridge also marked the beginning of a new era by implementing new structural analysis techniques. This new approach allowed engineers to calculate cable forces throughout the construction period and thereby assuring the efficiency of all cables in the final stage. From that point, a big expansion on cable-stayed bridges has begun [1].

Figure 5 - Strömsund Bridge (Sweden,1955)

Another remarkable structure was the Severins Bridge (Figure 6) completed in 1959 in Cologne, Germany. This bridge is the first application of an A-shaped pylon combined with transversely inclined cables planes. Also, this was the first asymmetrical two-span bridge with pylon at only one of the riverbanks. This bridge is still in use and became one of the most successful bridges of this type [1]. Following the innovative process, the North Elbe Bridge, with a main span of 172m, constituted the first application of single-plane cables was built in 1962 [5].

Figure 6 - Severins Bridge (Cologne,1959)

The success of German constructions and the breakthrough in computer-aided analysis in the mid-1960s extended the cable-stayed system to the rest of the world. The globalization reached the Asiatic continent where the Onomichi Bridge (1968) was the first long cable-stayed bridge in Japan with main span of 215 m. Besides, it is good to point that this structure was made with 82% of corrosion-resistant weathering steel [6].

The multi-span Maracaibo Bridge (Figure 7), in Venezuela, designed by Morandi and finished in 1962 is an exemplar of the so-called “first generation” of cable-stayed bridges. These structures were composed by a small number of stay cables, usually 2 to 6 pairs of stays in the main span, separated by a large distance (more then 30m). This conception results in high tensions in the cables and high stress in the anchorage zone. Because of that, complicated anchorages were needed, and several ropes were used to form each stay [5].

Figure 7 - Maracaibo Bridge (Venezuela,1962)

The evolution of new technologies for structural analysis lead to the introduction of multiple-cable systems where each stay is a single prefabricated strand. This system involves a high degree of indeterminacy, impossible to solve by hand, but well reached with the new technology [1]. The first use of this new system was made in the Friedrich-Ebert Bridge (Figure 8) opened in 1967 over the Rhine river in Bonn, Germany. The bridge has a central steel deck that span over 280m supported by 20 stays, on each side, connected to two pylons. The multiple-cable technique increases the flexural stiffness of the deck and reduces the stress concertation, simplifying the anchorages. In addition, the reduction of spacing between cables allow a simpler phased construction by free cantilever [5].

Figure 8 - Friedrich-Ebert Bridge (Germany,1967)

By the end of 1970s, a new generation of cable-stayed bridges have been launched. The concept applied for the first time in the Pasco-Kennewick Bridge (Figure 9) in 1978 has a deck entirely supported by the cable-stayed system. The structural behaviour was very different from the other bridges constructed so far. The deck now acts as a compressive chord of a truss hang up to the towers by inclined stays [5]. At this period, the usage of concrete deck was begging to become popular. In 1984, the Barrios de Luna Bridge (Figure 10) built in Spain gave a strong indication that concrete was a competitive material to be used not only in the pylons but also in the deck of cable-stayed bridges [1].

Figure 9 - Pasco-Kennewick Bridge (United States, 1978)

Figure 10 - Barrios de Luna Bridge (Spain, 1984)

At the end of the 20th century major achievements in the construction of cable-stayed bridges have been made. For the first time a span with more than five hundred meters has been placed. The Skarnsund Bridge (Norway,1991) and the Yangpu Bridge (China, 1993) were the first to break this boundary. However, the greatest realizations were made by the end of the decade with the Normandy Bridge in France (1995) with a main span of 856m and the Tatara Bridge (Figure 11) that opened to traffic in 1999 with the record of 890m in Japan [1].

Figure 11 - Tatara Bridge (Japan, 1999)

The first 20 years of the 21st century have been marked by a big development of the Asian economy driven mainly by China. Consequently, over thirty cable-stayed bridges with main span greater than 500m were made in this short period of time in China. The most notable bridges to refer are:

- Sutong Yangtze River Bridge (Figure 11), 2008 – main span of 1088m
- Stonecutters Bridge, 2009 – main span of 1018m
- Edong Yangtze River Bridge, 2010 – main span of 926m

Figure 12 - Sutong Yangtze River Bridge (China, 2008)

The limit of this impressive structures is very uncertain. Today many researchers are developing new techniques and materials to reach spans over more than two kilometres. The implementation of materials such as Fibre-Reinforced Polymer (FRP) is a reality in the civil engineering field and is one of the most promising method to achieve those impressive numbers [7].

2.2 CABLES

2.2.1 CABLE TYPES

Basically, cables are arrangements of high strength steel wires. The wires are assembled to form a strand and later used to shape a cable on site or in the shop. The seven-wire (Figure 13) strand is the simplest form to be found in a cable supported bridge. The wires have, in general, 5mm diameter and tensile

strength between 1770 and 1860 MPa. They are normally arranged with a single straight core confined by one level of six wires placed in a helicoidal course [1].

Figure 13 - Seven-wire strand

The multi-wire helical strand, also called spiral strand, is conceived in a similar way to the seven-wire strand. However, this type has multiple wire layers with opposite course directions, as illustrated in Figure 14. As a side effect, when the wires are twisted the total strength drops when compared to the straight element. Approximately, the final strength of a helicoidal strand is 10% lower than the sum of all parallel wires. The nominal modulus of elasticity is also affected by the helicoidal shape of the top layers 15-25% below the value for straight wires. This phenomenon also occurs on the seven-wire strand but with less magnitude [1].

Figure 14 - Multi-wire helical strand

As an alternative to the normal strands there is the locked-coil system. This type of cables is an array of round wires surrounded by an outer layer of special Z-shape wires. The Z-shape wires guarantee a tight surface protecting the interior of corrosion. The final protection against corrosion used to be a surface treatment with painting, nowadays all the wires are galvanized instead. Strands at this system are manufactured in full length and with a diameter range from 40mm to 180mm. Large strands are normally used in cable-stayed bridges with multi-cable systems where every stay is a mono-strand cable [1].

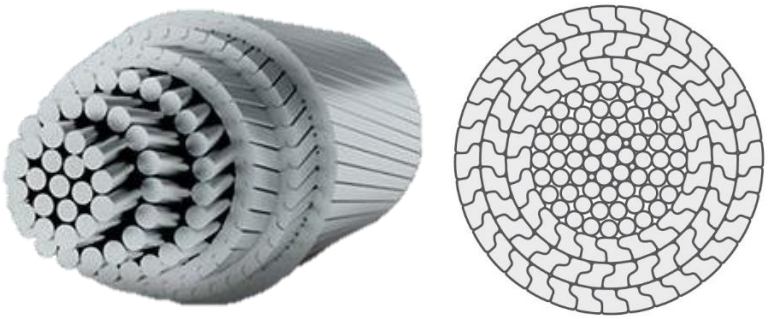

Figure 15 – Locked-coil system

However, difficulties in the design of anchorages and protection against corrosion restricted the usage of this types of systems. Today, the main option adopted in several countries is the parallel-strand cable (Figure 16) [3]. In this system seven-wire strands with a protection layer of high-density polyethylene (HDPE) are arranged together in parallel to form the cable. In many cases the stay is surrounded by a cylindrical pipe in order to reduce the drag coefficient due to the grooved surface [1]. Cables of this type can have between 18 and 90 strands with breaking load up to 24 MN [3].

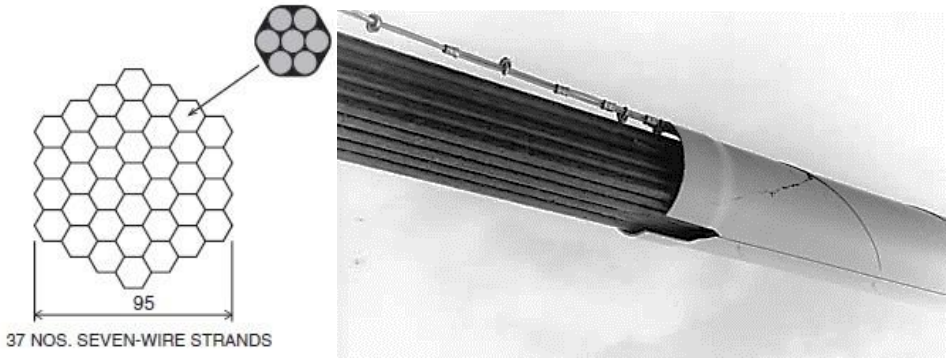

Figure 16 - Parallel -strand cable

2.2.2 Corrosion Protection

Project specifications must guarantee adequate lifetime to the cable stay based on economic conditions. Generally, a 100-year service lifetime period is considered appropriated for suspension and cable-stayed bridges. For this purpose, protection against corrosion is substantial to achieve the required level of durability [8].

In cables composed by many wires the impact of corrosion is more pronounced. Each wire has a small diameter, plus most are inaccessible to direct inspection and maintenance. Thus, voids between wires and the steel material make these cables even more vulnerable to this effect. For example, a cable with a reduction of 1mm in the surface due to corrosion could represent a 64% loss area, a value far from been covered by safety margin [1].

Figure 17 - Cable corroded

Today, as a constructive rule, cable stays should have at least two barriers against corrosion. These two layers are complementary. The internal barrier is applied individually to all wires in the full length of the cable. As a second barrier an external protection should be placed to prevent the internal barrier being consumed. Is very important that the external layer must be water and airtight in both the free length and the anchorage zone.

The internal barrier can be done with metal or non-metal coating. For the metal coating generally pure zinc (galvanization) is used or else zinc-aluminium compound. The quality and the durability of these protections depends on the thickness of the metal coating. Non-metal protection is equivalent to the galvanization, but instead resins or polymers are used.

The external protection used varies with the type of cable stays and with especial requirements of the structure. The most frequently used are some of the following: Stay pipes made of high-density polyethylene (HDPE) (Figure 18), plastic sheath extruded directly on the strand or steel stay pipes made of stainless steel or with protection coatings. Besides, stay pipes also fulfil other functions like mechanical (limiting cable-stay drag), aerodynamics (limiting rain and wind induced instability) and aesthetic (colour) [2].

Figure 18 - HDPE pipe usage

An intermediate cover is also used to avoid humidity inside the core. Generally, wax, grease or resin are placed to fill the blanks. Cement grout was also used in the past, but this method is less effective once cracks due to shrinkage do not create a full tight surface and it is also known that the cement grout can initiate corrosion process. However, another method was found very efficient, to install dehumidifiers to inject dry air inside the cable voids (Figure 19) removing the water needed for the corrosion's chemical reaction. This system was applied by the first time in the Akashi-Kaikyo Bridge constructed in the late 1980s [8].

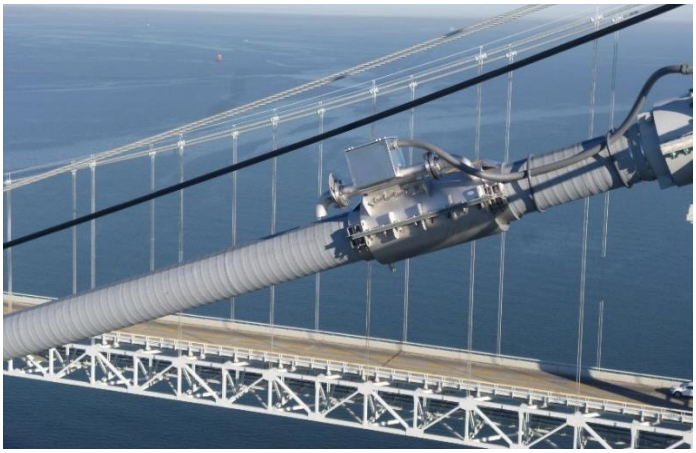

Figure 19 – Dehumidification system applied on the Bay Bridge, United States.

Even though, none of those solutions can offer a full protection against corrosion. Meaning that the only way to prevent this problem is to provide an additional periodic maintenance in the cables.

2.2.3 ANCHORAGE SYSTEMS

Anchorage systems are crucial for the structure, this elements are responsible to transfer the actions that came from the deck and transfer them to the cables(Figure 20). Special requirements are needed to design this system, especially them to have appropriated mechanical resistance and fatigue resistance [8].

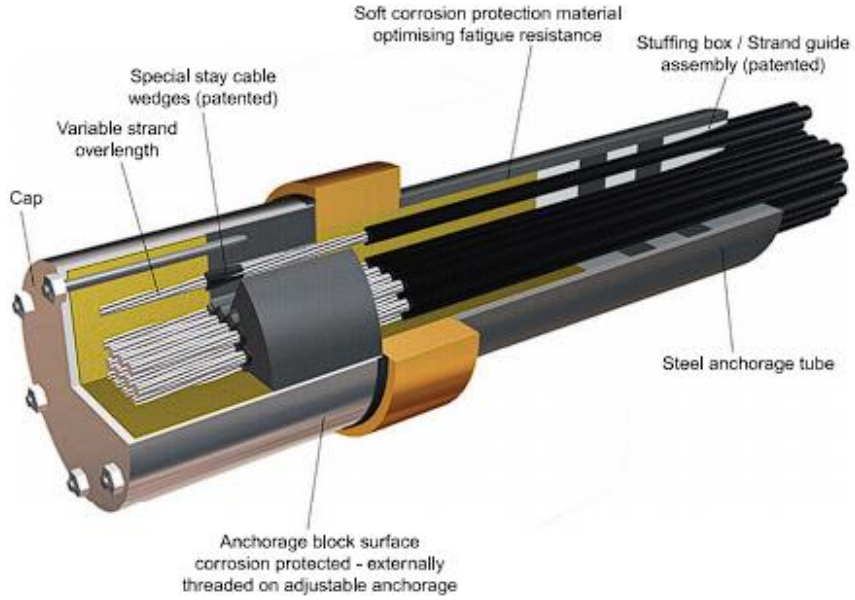

Figure 20 – Typical components of stay cable anchorage (Freyssint, 2010)

A bridge anchor is composed by two main parts: the anchorage head, that is responsible for the load transmission; and the transition zone, where the cable arrangement changes to fit the anchorage system [2]. To anchor parallel-wires strands a special socket was developed in the 1970s, where the wires are displaced through holes in a locking plate at the far end of the socket and provided with button heads to increase the resistance against the slipping of individuals wires. The concavity inside the socket is filled in general with cold cast materials, such as epoxy resin, zinc dust or small, hardened steel balls, in order to reduce fatigue effects.

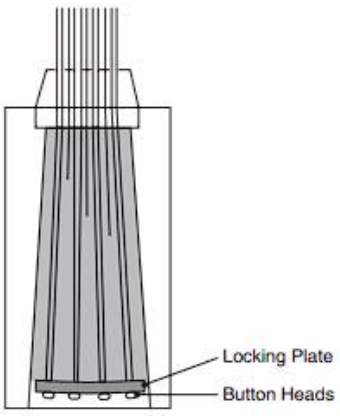

Figure 21 - Socket for parallel wire strand

The principal functions that an anchorage must accomplish are listed below [8]:

- Properly transfer the loads
- Filtering out angular deviation
- Possibility of adjustment
- Corrosion protection
- Removability

Besides, in order to prevent cable vibration internal dampers can be added close by the anchorage element (Figure 22).

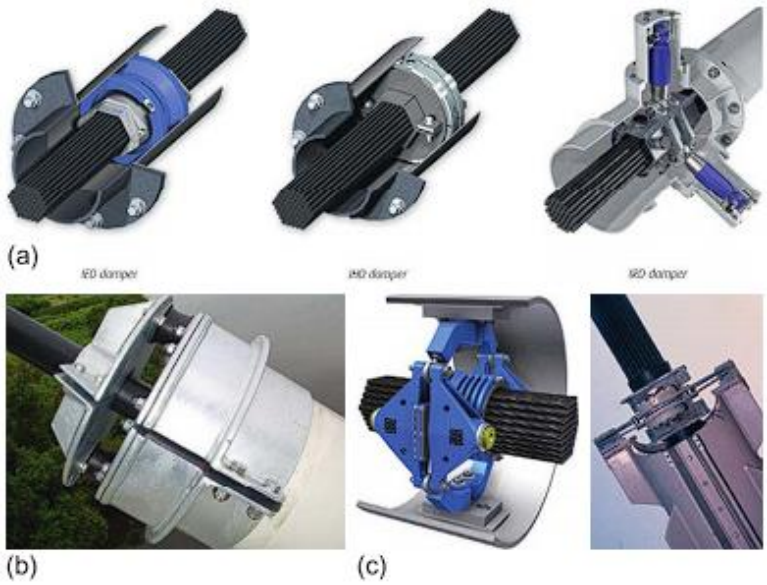

Figure 22 - Internal dumpers: a - Elastomeric (IED), Hydraulic (IED) and Radial (IRD) dampers (Freyssinet, 2014); b – Elastomeric damper; c – Friction damper (VSL, 2002)

A variety of anchor types are available, depending on the solution adopted for the structure. In past solutions, using eye-bars and strand shoes were very common, according to the trends of bridge constructions of the time. Recently, the use is focused on standard solutions based on wire cables that allow the maintenance and implementation of devices such as dehumidifiers.

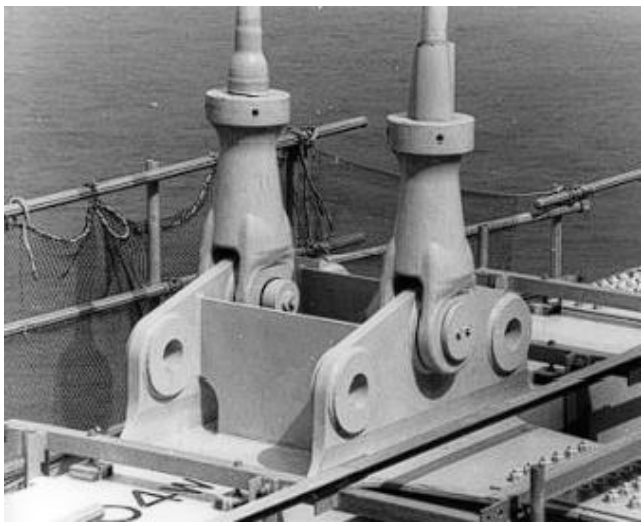

Figure 23 - Anchorage system with eyed bars of the Asashi Kaikyo Bridge

2.3 CABLE LOSS

In cable-stayed bridges, damage, or failure of primary structural components such a pylon, deck, or cables, caused by accidental events can lead to the collapse of the entire bridge [9].

The collapse mechanism of the cable stayed bridge is called "zipper-type collapse", in which the first stay snapped due to an excessive increase of stress from an accidental event or loading [10] [11]. Guidelines, such as PTI D-45.1-12 2012 (Post Tensioning Institute, 2005), Eurocode 1 part 1.7, SETRA, recommend considering cable loss scenarios during design phase, with the implementation of a dynamic amplification factor for static loads that doubles the forces applied to the structure in case of failure.

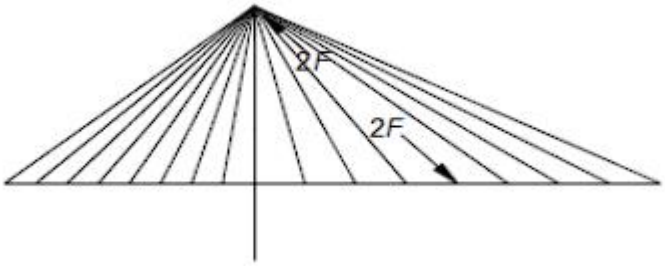

Figure 24 - Accidental forces for design of cable bridges

Furthermore, the bulletin CEB-FIB, 2005, recommends that the design of cable stays for bridges must allow the replacement of these structural members one or more time during the lifetime of the structure.

The damage caused by a cable rupture in a cable stayed bridge could lead to a scenario called “progressive collapse” where the rupture of one element leads to a redistribution of loads that overwhelm other members of the structure, and consequently, rupture. In the past, several structures suffered from damage that directed to the progressive collapse or has affected the usability of the bridge [12].

The loss process in the cable cross-section area will initiate the loss of compression in the bridge girder of a cable-stayed bridge. The loss of bracing on the girder leads to an increase in vertical deflections thus inducing high stresses in the longitudinal girder lying in the plane of the cable loss which then transmits to the longitudinal girder of the other plan of the cables. This pattern of collapse is defined as: Instability –type collapse [14].

In addition, loss of cables leads to overloading of the adjacent cables, and then the load carried by these adjacent cables will be re-distributed to other nearby cables termed unzipping which causes a zipper pattern of progressive collapse. Concrete bridge decks and segmental/ non-continuous bridges decks do not experience this type of collapse pattern. Zipper-type collapse is initiated by the failure of one or more tension elements which then redistribute the forces carried by the failed elements to the remaining structure. The sudden failure induces an impulsive load and the remaining structure responds in a dynamic way, leading to stress concentrations in the next elements along the direction transverse to the principal forces in the elements [15].

When designing a structure to limit state conditions, the event of losing a cable is governed by the Ultimate Limit State design while effects such as deflection, cracking, creep, shrinkage etc. are related to the serviceability of the structure. The loss of a major element may not lead to the collapse of the bridge but can lead to slacking of the cables and thus large deflections in the deck or large vibrations in the deck [11]. This invariably reduces the comfort of the bridge users.

When a cable fails the deck can experience vertical displacement, vibration, and flexural/ buckling at the location of the lost cable. If breakage of the cable occurs at different locations, then the deck may

experience vertical deformations causing varying uplifts along the deck These varying uplifts of the girder can be used to detect which cables in an existing cable-stayed bridge have broken [16]. In decks with twin cable planes, cable loss along one plane introduces eccentricity in the deck supports, leading to large deflections and with the live loads present is a potential cause of instability [17].

2.4 STRUCTURAL MONITORING

Structural health monitoring (SHM) systems are extensively adopted to estimate the behaviour of structures under ambient and forced vibrations in a laboratory environment or in the field and used to monitor structures under other excitations such as earthquakes, traffic, gusts, or live loading [18]. The SHM can play a vital role in the maintenance and health evaluation of cable-supported bridges. In the past three decades, it has been used primarily and effectively for damage detection in bridges, especially where there is some doubt about the performance of a particular design or when the expected loading has been difficult to quantify in the design stages of the bridge. Storms, earthquakes, floods, and accidents are examples of this type of loading. SHM can be used not only for the detection of damage though. It can also be used for the quantification of the severity of damage and the locations of damage [2].

Developments have lead researchers and engineers to use existing SHM techniques and hardware for new purposes. It is not uncommon for SHM equipment to be used temporarily and selectively during the construction of a large bridge to evaluate the construction sequence and to provide data that will help improve the completion of not only the particular bridge, but also other similar bridges in future. The SHM became an important tool to evaluate the need for the retrofit of bridges with the goal of a fail-safe bridge design. In all cases SHM is being used to help close the gap between the theoretical evaluation and the real-life performance of bridges [2].

The measurements on the structure are also important to modal identification of bridges and other civil structures. This information is important for the validation of finite-element models used to predict static and dynamic structural behaviour either at the design stage or at rehabilitation. After appropriate experimental validation, finite-element models can provide essential baseline information that can subsequently be compared with information captured by long-term monitoring systems to detect structural damage [20]. An example of this is the Øresund Bridge (Figure 25), where engineers decided to measure both the static and the dynamic response of the bridge to passing vehicles and trains and the dynamic response of the stay cables to wind. Furthermore, strain gauge measurements were found to be of interest at the locations of maximum expected strain, around the cable outriggers and at several locations on the bottom chord of the bridge. More specifically, the bridge is fitted with 22 triaxial force balance accelerometers, 19 strain gauges, several thermometers to correlate the strain gauge measurements with the variations in temperature, and two bi-axial ultrasonic anemometers to measure the oncoming wind velocities and turbulence intensities [2].

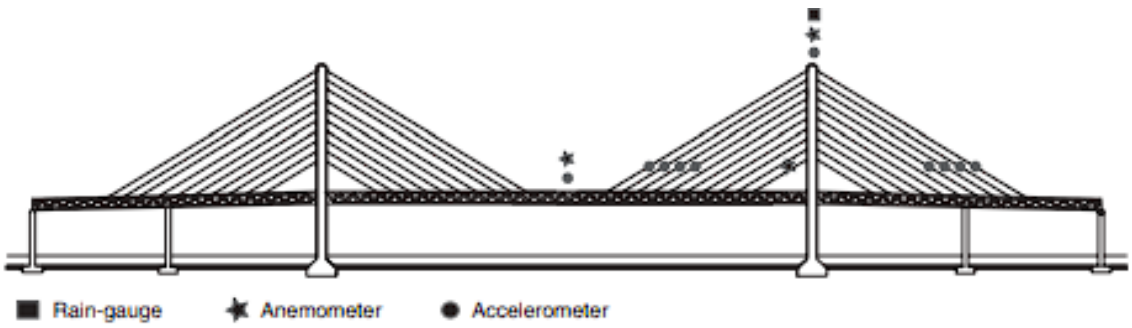

Figure 25 - Øresund Bridge SHM sensors (phase II), Denmark-Sweden

The most common sensors used for bridge monitoring are strain gauges and accelerometers (Figure 26). Each respectively assists in the understanding of the bridge's static and dynamic response to traffic and environmental loading. Based on these measurements, a more accurate evaluation of the structural performance can be made, together with more precise fatigue calculations. The dynamic response of the bridge can also be evaluated globally or locally, often with the goal of determining structural properties that cannot be theoretically evaluated with any great degree of accuracy. These might include structural damping, cable tensions or bridge mode shapes and frequencies [2].

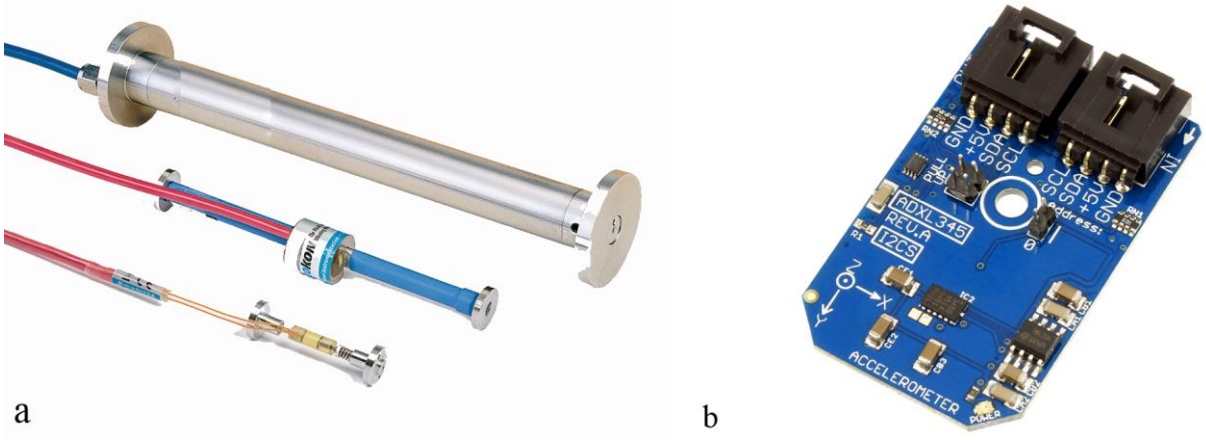

Figure 26 – a) Strain gauges b) accelerometer.

Modern accelerometers, as shown in the Figure 26 are well suited for measurements in the range of 0-50 Hz and are virtually insensitive to high-frequency vibrations. They have contributed significantly to the success of ambient vibration tests. In such tests, the structural ambient response is captured by one or more reference sensors at fixed positions and with a set of roving sensors at different measurement points along the structure and in different setups. The number of points used is conditioned by the spatial resolution needed to characterize appropriately the shape of the most relevant modes of vibration (according to preliminary finite element modelling), while the reference points must be far enough from the corresponding nodal point. This system can be implemented on a normal PC. Some data acquisition and processing systems, specifically designed for ambient vibration tests, are already available [20].

Alternative sensors include inclinometers, relative displacement transducers and, more recently, laser displacement transducers and Global Positioning System (GPS) equipment. Relative displacement transducers are often used to measure local deformations or bearing and expansion joint movements. Laser transducers offer the same capability, but without the need for contact between the measured surfaces. GPS equipment works relatively well in providing mean horizontal displacements, but not so well in providing vertical displacements. The combined Total Station (TPS) (Figure 27) with powerful Laser Doppler Velocimetry (LDV) measurement. With this technology, measurements can be made on a bridge from a distance of up to 2 km with a very high degree of accuracy. A precise TPS can scan a large bridge quickly to allow a powerful laser to measure variations in the position of a bridge for any point on the bridge that the laser is in contact with. Shifts in modal properties, local distortions or global displacements can readily be logged [2].

The most common instrumentation programs are of short duration. Static measurements are performed during the bridge construction and at spaced time intervals after completion, while dynamic measurements are performed at the end of construction. Some sensors are however left at the bridge, which trigger particular events, like earthquakes and severe wind condition, or send alarm signals

whenever excessive vibrations or displacements are attained. More sophisticated SHM perform continuous measurements, storing statistical information and particular records. These systems incorporate communications with a Central Station (Figure 27), which may be located several hundreds of kilometres away, and from where specific commands concerning the signal acquisition and processing can be issued, such as data transfer or change of the signal acquisition parameters [5].

Figure 27 - Total Station

In addition to this measurement's systems test can be done to measurement of the structural response. The Forced Vibration Testing (FVT) techniques employed in Civil Engineering structures constitute straight applications of the so-called Modal Analysis Techniques, which were born in the areas of Mechanical and Aeronautic Engineering some decades ago. These techniques are based on the application of a controlled excitation, and measurement of the response at a set of locations. From the set of excitation and response time histories, estimates of Frequency Response Functions (FRF's) or of Impulse Response Functions (IRF's) can be obtained (for frequency or time domain analysis, respectively) and System Identification algorithms applied, in order to extract the most relevant dynamic parameters of the structure, i.e., the natural frequencies, vibration modes and damping coefficients[18].

The instrumentation systems employed for dynamic testing of structures comprehend the following main components:

- a subsystem for excitation.
- a subsystem for measurement of applied forces and responses.
- a data acquisition modulus, for control of excitation, and for recording and analysing the measured data.

In small and medium-size structures, the excitation can be induced by an impulse hammer (Figure 28a) similar to those currently used in mechanical engineering. This device has the advantage of providing a wide-band input that can stimulate different modes of vibration. The main disadvantages are the relatively low frequency resolution of the spectral estimates (which can preclude the accurate estimation of modal damping factors) and the lack of energy to excite some relevant modes of vibration. Due to this problem, some laboratories have built special impulse devices specifically designed to excite bridges

(Figure 28b). An alternative, also derived from mechanical engineering, is the use of large electrodynamic shakers (Figure 28c), which can apply a large variety of input signals (random, multi-sine, etc.) when duly controlled both in frequency and amplitude using a signal generator and a power amplifier. The shakers have the capacity to excite structures in a lower frequency range and higher frequency resolution. The possibility of applying sinusoidal forces allows for the excitation of the structure at resonance frequencies and, consequently, for a direct identification of mode shapes.

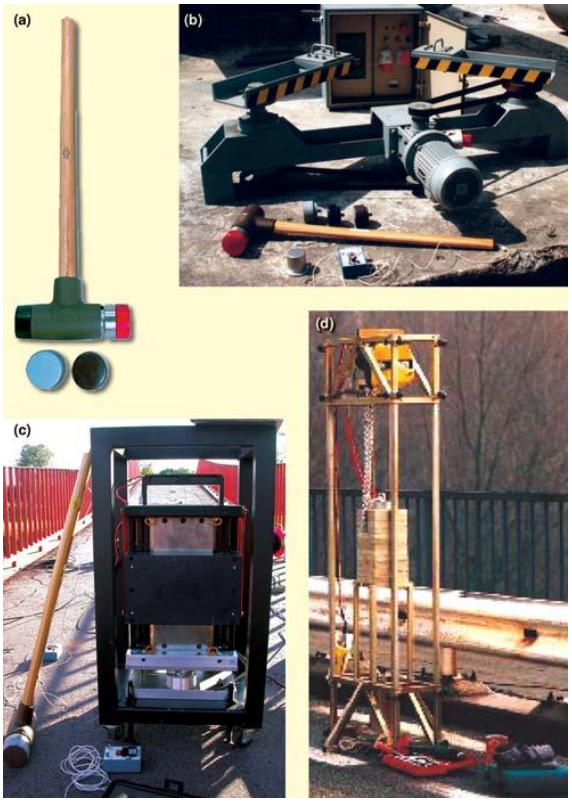

Figure 28 - (a) Impulse hammer; (b) eccentric mass vibrator; (c) electrodynamic shaker over three load cells; d) impulse excitation device for bridges.

This process is identified as input-output modal identification methods whose application relies either on estimates of a set of frequency response functions (FRFs) or on the corresponding impulse response functions (IRFs), which can be obtained through the inverse Fourier transform. These methods attempt to perform some fitting between measured and theoretical functions and employ different optimization procedures and different levels of simplification. Accordingly, they are usually classified according to the following criteria:

- Domain of application (time or frequency)
- Type of formulation (indirect or modal and direct)
- Number of modes analysed (SDOF or MDOF – single degree of freedom or multi degree of freedom)
- Number of inputs and type of estimates (SISO, SIMO, MIMO, MISO – single input single output, single input multi output, multi input multi output, multi input single output).

The main problem associated with forced vibration tests on bridges, buildings, or dams is the difficulty in exciting the most significant modes of vibration in a low range of frequencies with sufficient energy and in a controlled manner. In very large, flexible structures like cable-stayed or suspension bridges, the forced excitation requires extremely heavy and expensive equipment usually not available in most

dynamic labs. The Figure 29 shows the impressive shakers used to excite the Tatara and Yeongjong bridges for dynamic tests [20].

Fortunately, recent technological developments in transducers and A/D converters have made it possible to accurately measure the very low levels of dynamic response induced by ambient excitations like wind or traffic. This has stimulated the development of output-only modal identification methods. Therefore, the performance of output-only modal identification tests became an alternative of great importance in the field of civil engineering. This allows accurate identification of modal properties of large structures at the commissioning stage or during their lifetime without interruption of normal traffic.

Figure 29 - Forced vibration tests: (a) Tatara cable-stayed bridge; (b) Yeongjong suspension bridge; (c) high force shaker

In such tests, the structural ambient response is captured by one or more reference sensors at fixed positions and with a set of roving sensors (Figure 30) at different measurement points along the structure and in different setups. The number of points used is conditioned by the spatial resolution needed to characterize appropriately the shape of the most relevant modes of vibration (according to preliminary finite element modelling), while the reference points must be far enough from the corresponding nodal points.

Figure 30 - (a) Force balance accelerometers; (b) multichannel data acquisition and processing system for ambient vibration tests; (c) strong motion triaxial seismograph

The correlation of modal parameters can be analysed both in terms of identified and calculated natural frequencies and by corresponding mode shapes using correlation coefficients or MAC (modal analysis criteria) values. Beyond that, modal damping estimates can be also compared with the values assumed for numerical modelling. This type of analysis has already been developed for the Vasco da Gama and Luiz I bridge with excellent results and has been applied over the last years at several bridges in Portugal.

The accurate identification of the most significant modal parameters based on output-only tests can support the updating of finite-element models, which may overcome several uncertainties associated with numerical modelling. Such updating can be developed based on a sensitivity analysis using several types of models and changing the values of some structural properties to achieve a good match between identified and calculated modal parameters.

An example of the application of this procedure is the stress-ribbon footbridge at the FEUP Campus where it was studied the dynamic behaviour of the bridge (Figure 21). For this purpose, different finite elements models were developed in order to achieve a good correlation between identified and calculated natural frequencies and mode shapes.

Figure 31 - Stress-ribbon footbridge at the FEUP Campus.

3
STRUCTURE DESCRIPTION

The object of study of this work is the *Edgar Cardoso Bridge* (Figure 32) a Portuguese bridge that opened to traffic in 1982 as the first cable-stayed bridge in the country. This bridge is located in the city of *Figueira da Foz*, about 160km north from Lisbon, and is composed by two side spans with length of 90m and a main span 225m long. This structure was designed by Prof. Edgar Cardoso and constructed by OPCA.

Figure 32 - Edgar Cardoso bridge,1982.

3.1 STAYS

Arranged in a fan system, the cables are made of steel wires with a tensile strength of 1600-1800 MPa. Every cable is anchored end to end at the deck spaced by 30 m and passing through saddles placed on the top of the mast. The stays are formed from 900, 540 and 390 wires, respectively, from the longer to the shorter cable.

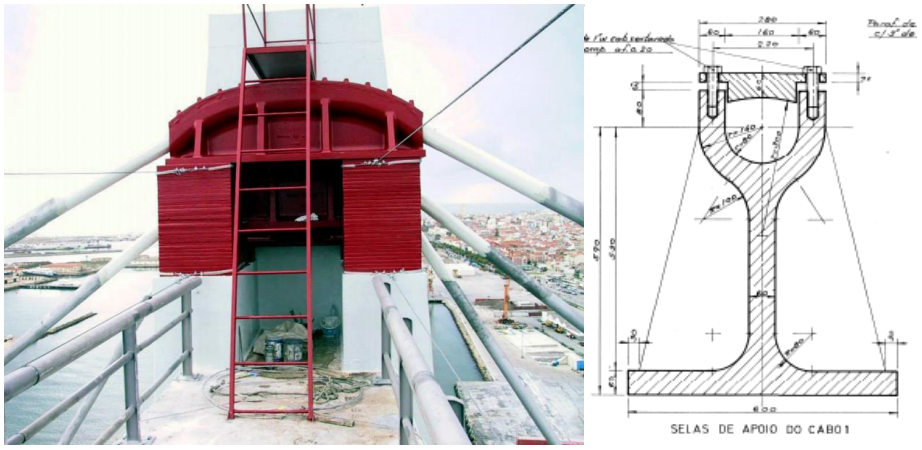

Figure 33 - General view from the saddles arrangement and the design.

3.2 DECK

The deck is composed by steel I-girders supporting a concrete slab of 0.13 to 0.2m thick. With a total width of 20m, the deck is constituted by 2 traffic lanes of 7.5m and a pedestrian lane of 2m on each side (Figure 34).

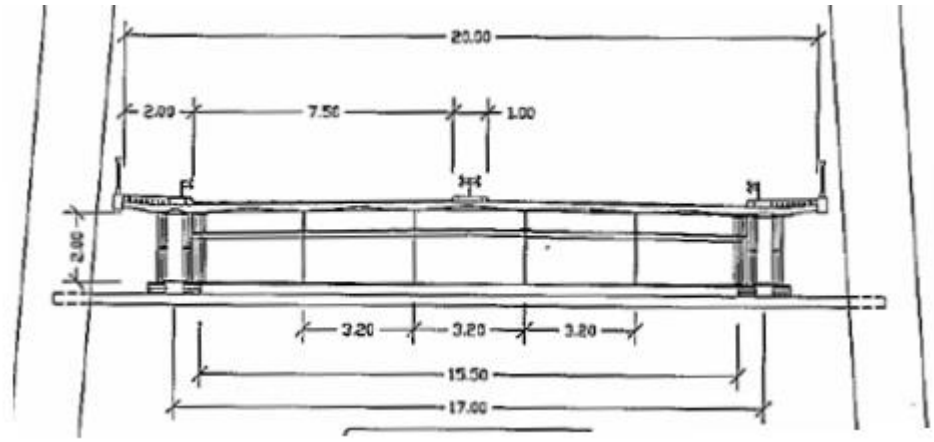

Figure 34 - Deck cross section

The main steel parts that constitute the deck (Figure 35) are:

- Main girders conceived by pairs of I-section on both sides with: 2065mm height, 25mm thick bottom flange, 40mm thick top flange and web thick of 20mm.
- Four HE 600 A longitudinal girders spaced of 3.20m.
- Transversal I-beams with 15.5 span every 10 m following the respective geometry: 2050mm high, 25mm thick flanges and web thick of 16mm.
- The top flange of the main girders is braced by a ½ HE 360 A section diagonal member.

The steel used in the main girders is a S355 grade and for all the other members were used S235.

Figure 35 - Deck view

3.3 PYLON

The bridge has two concrete pylons with 84.4m to support the vertical reactions, as shown in the Figure 36. Each pylon has four concrete legs with hollow squared section. These legs are inclined elements connected at the top by a transversal beam and under the deck by a concrete laminate plate. The concrete used in the pylon, as well as in the deck, has a compression resistance varying in the range from 56 to 72.3 MPa, being characterized by an inspection made in 1998 by Eng. Júlio Appleton and Eng. Armando Rito.

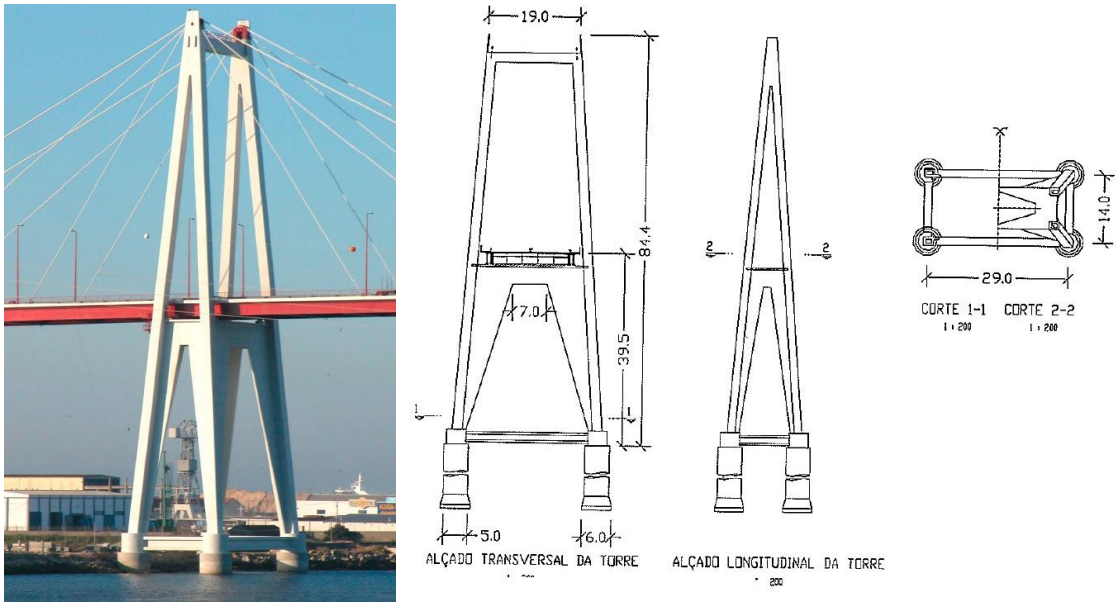

Figure 36 - Pylon view and geometry

At the base level, the towers are supported by four circular hollow piles with an exterior diameter of 5 meters and wall thickness of 0,40m. The pile blocks are interconnected by prestressed I-sections concrete beams (Figure 37).

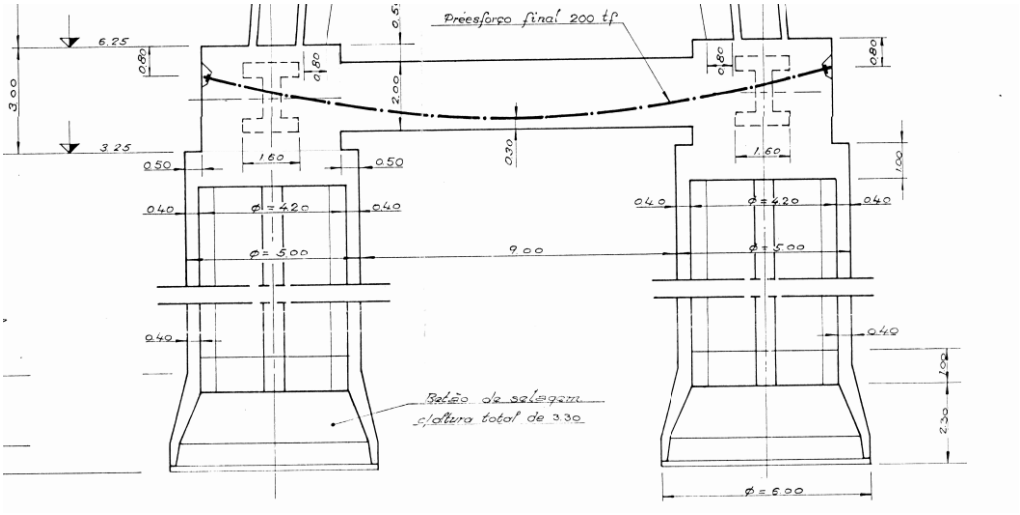

Figure 37 - Pylon base structure

3.4 DAMAGE IDENTIFICATION

During the last two decades the Edgar Cardoso Bridge have been object of rehabilitation works and monitoring process. Figure 38shows some points of corrosion identified in the anchorage zone of one of the cables during one of the monitoring works done in the bridge.

Figure 38 - Corrosion identify on the Edgar Cardoso Bridge [22]

In this context, one of the main objectives of this work is to characterize the damage level that this structure can support. To identify the structural behaviour of the bridge and through which mechanism it will be possible to determinate the development of a more pronounced damage a Finite Element Model (FEM) will be done. The next chapter will discuss the techniques implemented in the modelling process and the corresponding validation.

4
STRUCTURAL MODELLING

4.1 MODELLING PROCESS

To analyse the structural behaviour of the *Edgar Cardoso Bridg*e a complete 3D model was done using the SAP2000 software. Figure 39 represents a perspective of the final model.

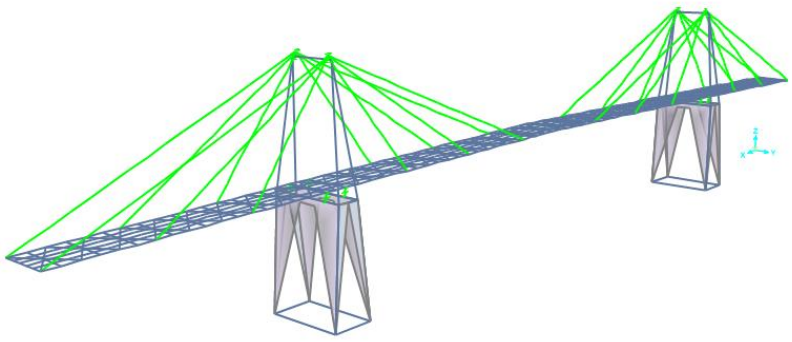

Figure 39 - Edgar Cardoso Bridge 3D model

The modelling process followed the original project made by Eng. Edgar Cardoso [23] and latter information from the rehabilitation report [23] done by the Eng. Julio Appleton, Eng. Armando Rito and their collaborators.

To simulate the steel deck and the pylon, bar elements were used. This type of elements requires section input that were taken from the rehabilitation report mentioned earlier in this section. In addition to all the geometrical properties of the section, it is also mandatory to input the material properties. Table 1 - Section properties shows all the sections and material properties applied to these elements.

Table 1 - Section properties

Section	Properties
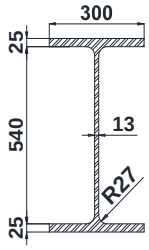 (mm)	Four longitudinal beams HE 600 A Area: 22645.8 mm² Centroid: X: 150 mm Y: 295 mm Radii of gyration: X: 386.50 mm Y: 165.76 mm Principal moments and X-Y directions about centroid: X-X:141208 x10⁴ mm⁴ Y-Y: 11271 x10⁴ mm⁴ Weight per meter: p2=78.5x2.265e-2=1.8 kN/m Steel S235

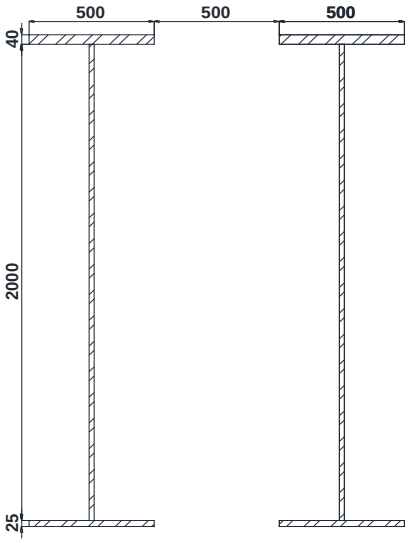

(mm)

Two double "I" beams in the extreme edge of the steel deck.

Area:	145000 mm²
Centroid:	X: 750 mm
	Y: 1131.8 mm
Radii of gyration:	X: 1384.14 mm
	Y: 906.75 mm

Principal moments and X-Y directions about centroid:

X-X:	9205291 x10⁴ mm⁴
Y-Y:	3765639 x10⁴ mm⁴

Weight per meter(plus 20% to include connections): p1=1.2x78.5x0.145=6.8 kN/m

Steel S355

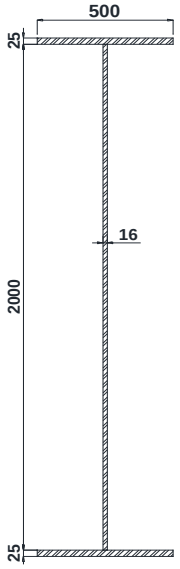

(mm)

Transversal beams

Area:	57000 mm²
Centroid:	X: 250 mm
	Y: 1025 mm
Radii of gyration:	X: 1298 mm
	Y: 265 mm

Principal moments and X-Y directions about centroid:

X-X:	3615886 x10⁴ mm⁴
Y-Y:	45133 x10⁴ mm⁴

Weight per meter: p3=78.5x0.057=4.5 kN/m

Steel S235

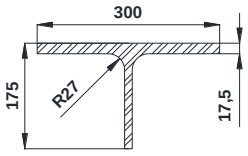

(mm)

1/2 HEA 360 braces

Weight per meter - p4=0.56 kN/m

Steel S235

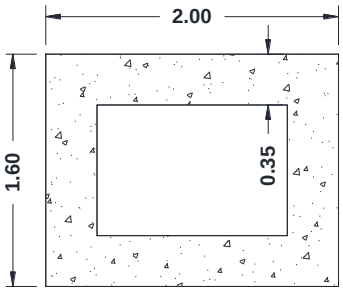

(m)

Concrete pylon leg cross section

Area:	4.37 m²
Centroid:	X: 1.00 m
	Y: 0.80 m
Radii of gyration:	X: 0.9024 m
	Y: 1.1322 m

Principal moments and X-Y directions about centroid:

X-X:	0.762 m4
Y-Y:	1.231 m4

Concrete C55/60

The next step, after modelling all these elements, is to set the connectivity properties between the elements. In the software it is possible to do it in two ways: connection by nodes or link elements. The first method is used when bars have a common point, then it is possible to introduce releases by changing the element properties. When elements have different position in the space, then the connectivity is made by links. A link (Figure 40) object connects two joints, i and j, separated by length L, such that specialized structural behaviour may be modelled. Linear, nonlinear, and frequency-dependent properties may be assigned to each of the six deformational degrees-of-freedom (DOF) which are internal to a link, including axial, shear, torsion, and pure bending.

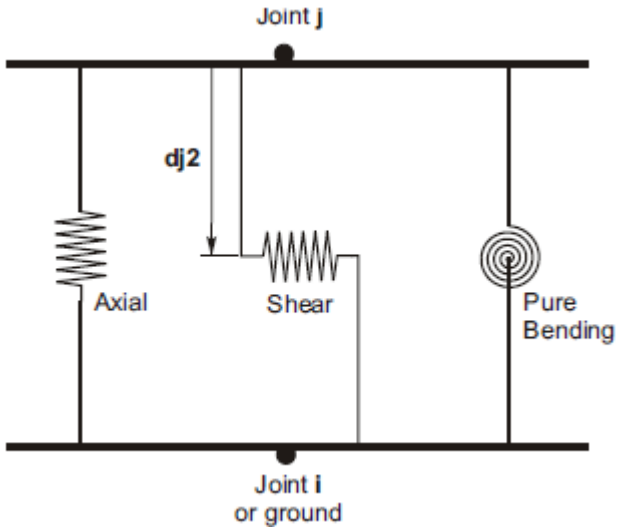

Figure 40 - Link element variations

In this project all the HEA600, transversal beams and braces were modelled in the same plane and then connected by a common node. This process requires offset application to correct the elements position. On this group of beams the connectivity properties were set so they work as pinned elements, so free rotation releases at the transversal XY axis were set.

In order to have the exact length of the cables, the double "I" beams were modelled exactly in their centroid position. Therefore, the transversal beams were connected to the double "I" beams by links with fixed displacement and free rotation. In the Figure 41, all the deck connections and links are exposed.

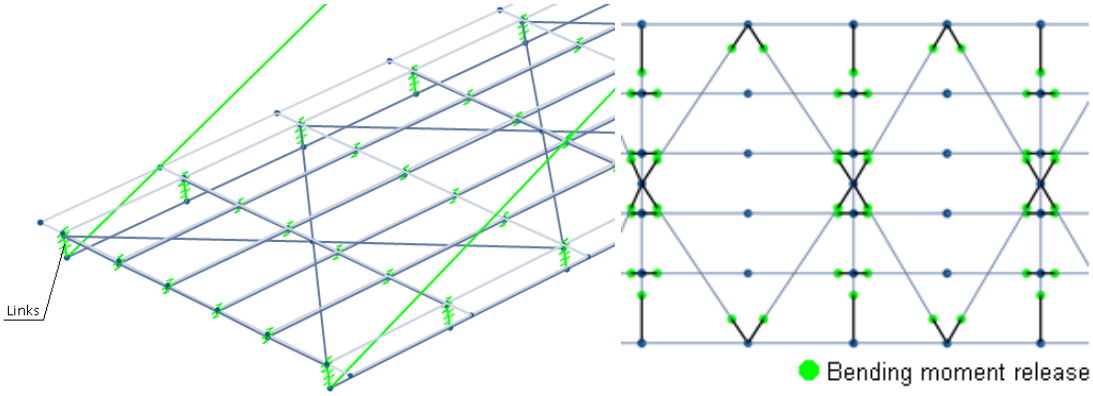

Figure 41 - Releases at the deck bar elements

The deck is also composed by a concrete slab with variable height between 0.13m and 0.20m. To model the slab shell objects were used, but to this type of elements the software only allows a constant height to be set, so an average height was input to this slab. Since connectors were not used to join the slab to

the steel deck, it was assumed that there is no relevant participation of the concrete slab in the bending resistance of the deck, so it is expected that the height simplification will not have a great influence in the final model. As a preliminary assumption, the connectivity between the shell and the steel frames was made with free longitudinal displacement links and free rotations about the longitudinal and transversal axes of the bridge(Figure 42).

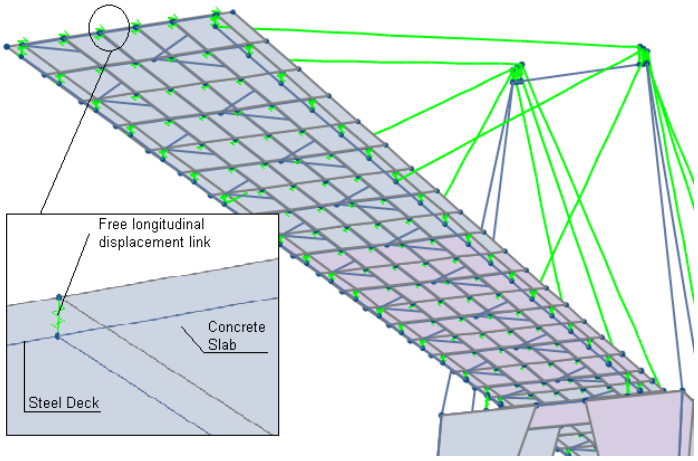

Figure 42 - Link between the steel deck and the concrete slab

The pylons are a less complex structure with no need for links or releases, they have four elements: columns, concrete laminate plate, top beam, and foundations. The four columns have the same section, that is described in the Table 1, and were assembled as bar elements. The concrete laminate plate has a thickness of 30 centimetres and was modelled as a shell element. The top beam has also been modelled as a bar element and the cross section is listed in the Table 1. Foundations were characterized by fixed supports that were applied on each pylon leg.

To support the deck 24 stays are anchored between the two “I” sections that compose the main longitudinal beam. In the real structure each two cables of the same plan are one single object that goes from deck anchorage in the central span to deck anchorage in the side span passing through a saddle on the top of the tower. However, in the 3D model cables are objects defined by a two-point line, so it is impossible to make a single object such as the real element. To simulate the correct cable behaviour a link element with free longitudinal displacement (Figure 43) was applied at the saddle position, in order to constrain vertical and transversal cable and tower movements, but allowing relative longitudinal displacements, to simulate the possible sliding and distribution of the force according to the applied loads.

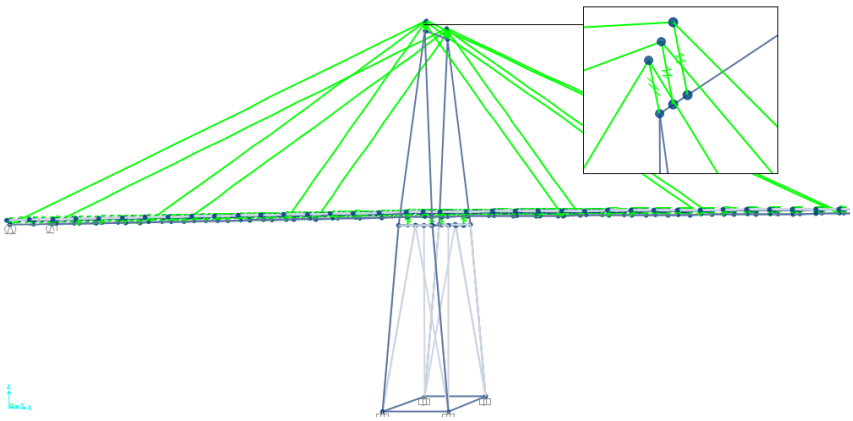

Figure 43 - Cable connection to the pylon to through link element.

In addition, 16 pinned bearings, eight on each tower, also support the deck of the bridge. The pin bearing allows rotation in one direction. In Figure 44, a copy from the original project shows a detail view from the element. To model this, support a link was used with free rotation along the longitudinal direction, but fixed about the transversal axis.

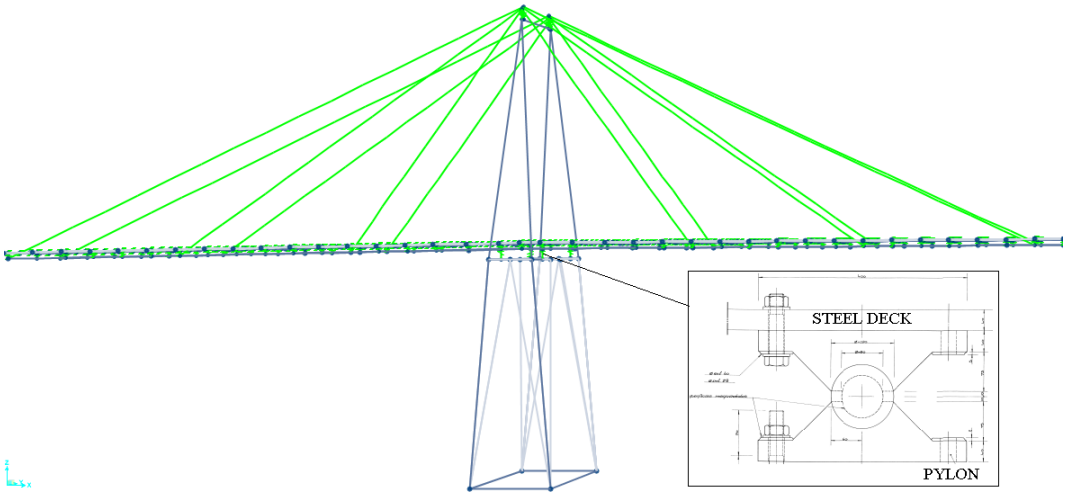

Figure 44 – Pin bearing in the pylon zone.

The simply supported deck segment in the central part of the bridge originates a non-symmetrical loading (with respect to the tower) of the deck which cannot be balanced, since the other two parts of the bridge are symmetrical. In order to transfer the added load to the supports, two vertical anchors to the transition columns have been placed on each side of the bridge (Figure 45). To simulate their effect, two supports with only vertical displacement restriction were set on both edges of the double "I" beams, as shown in the Figure 45.

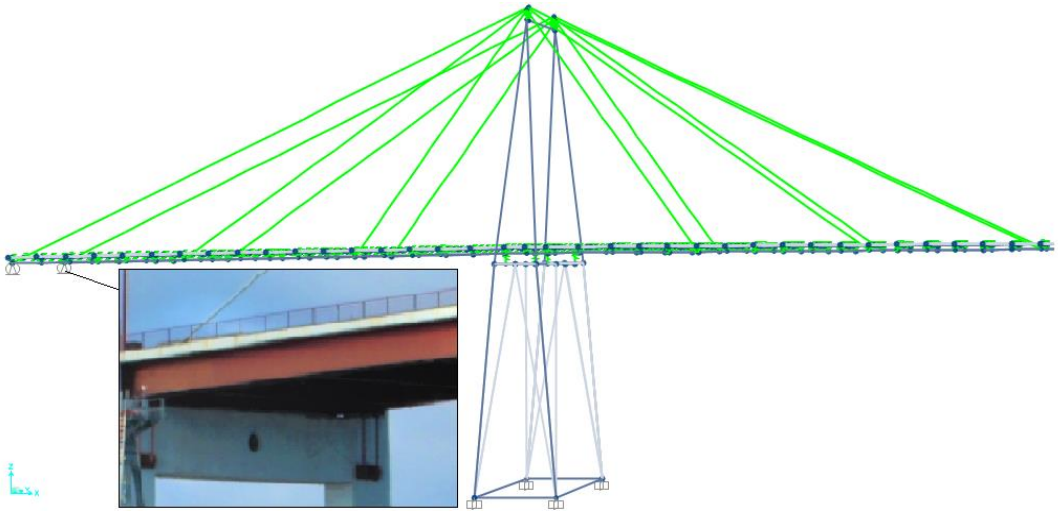

Figure 45 - Suspenders at the edge of the deck

4.2 LOAD CASES

The next step after modelling all the elements was to set the load cases. For this work, the load definition was based on the Eurocode 1 for wind [26] and traffic loads [27] and Eurocode 8 for seismic action and additional information available on the rehabilitation report [23].

4.2.1 DEAD LOAD

The Edgar Cardoso bridge has two main materials, concrete and steel. For the concrete members, a specific weight of 25 kN/m³ was considered that includes the reinforcement and 78,5 kN/m³ was used for the steel parts. The software automatically considers the self-weigh of the elements modelled, so it was not necessary to add a load for this case. In addition, the bridge is also composed by non-structural elements and their load must be assigned to the elements for latter analysis. The values adopted to calculate the extra permanent load are systematized in Table 2 and were extracted from the original project of this bridge and from the rehabilitation report [23]:

Table 2 - Other permanent loads

Description	Load (kN/m)
Parapets	6,0
Kerb	3,2
Footway floor	8,8
Central reservation floor	1,6
Pavement	18,8
Guard rails	5,0
Pipelines	5,0
Total	48,4

To reach these values a simple calculation was processed, multiplying the elements area by their self-weight. However, for this work the total load was equally distributed on the bridge deck. The results of this procedure are exposed bellow.

Linear load (L.L) – 48,4 kN/m ≈ 50 kN/m

Distributed load = L.L/Deck width = 50/20 = 2,50 kN/m²

However, after the validation that will be discussed latter on this chapter, was noticed that an increment on the self-weight was necessary to reach the axial forces measured on site on the cables. For this purpose, a permanent load of 3,5 kN/m² was applied to the deck on the FE model.

4.2.2 TRAFFIC LOAD

The Eurocode 1 part 2 (NP EN 1991-2) establishes the actual traffic load to be used for bridge design [27]. Following the European standard, there are four load models that can be applied to the structure. These are the following:

- Load Model 1 (LM1) - Concentrated and uniformly distributed loads, which cover most of the effects of the traffic of lorries and cars. This model is recommended to general and local verifications.
- Load Model 2 (LM2) - A single axle load applied on specific tire contact areas which covers the dynamic effects of the normal traffic on short structural members. Used mainly to local verifications.

- Load Model 3 (LM3) - A set of assemblies of axle loads representing special vehicles (e.g. for industrial transport) which can travel on routes permitted to abnormal loads. Applied for general and local verifications.
- Load Model 4 (LM4) - A crowd loading, intended only for general verifications.

For this work only the LM1 and the LM4 were used since only global verifications will be conducted.

These models are applied along the carriageway width that is defined by the standard. The Edgar Cardoso bridge has a permanent reservation area in the middle of the deck, so the carriageway is divided in two pieces as shown in the figure (Figure 46)

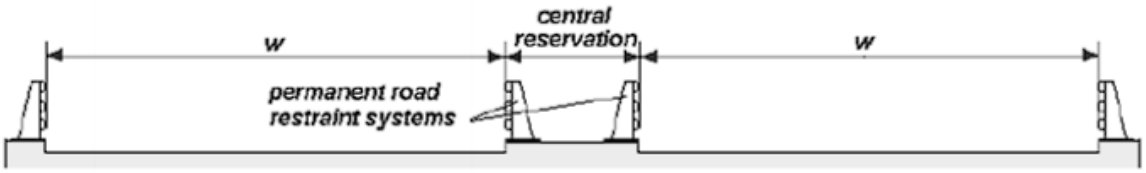

Figure 46 - Carriageway width

The carriageway is divided into lanes were the tandem systems are assigned. Figure 34 explains this distribution for the Load Model 1.

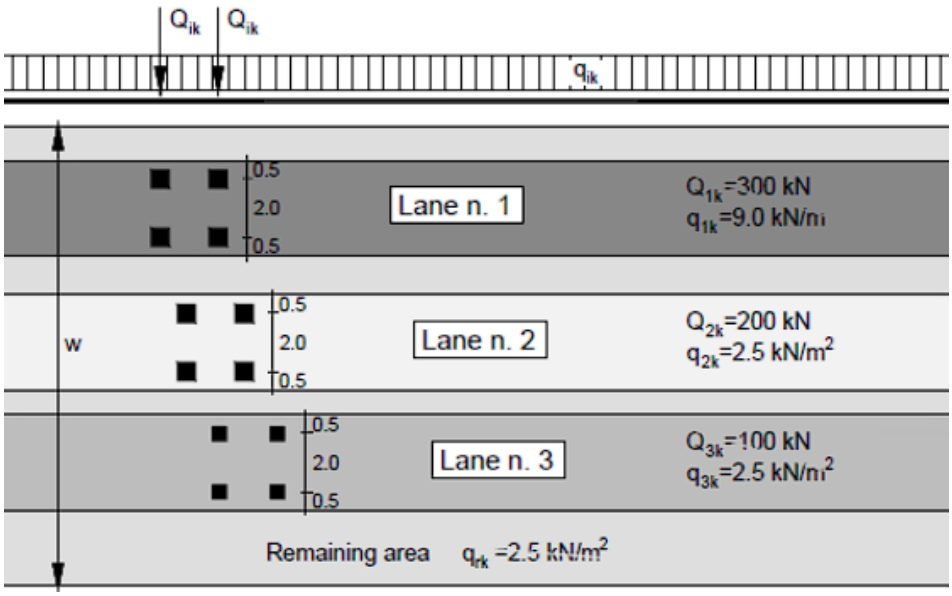

Figure 47 - Load Model 1 (LM1)

To apply the load on the structure deck, it is necessary first to calculate the transversal influence line so that the load is arranged to produce the maximum stresses required for a future analysis. To calculate the influence line of one of the main beams the Courbon method was adapted, which is based on the stiffness distribution of the girders. The equation 1 was used to construct this influence line.

$$R(j) = kj \cdot \left(\frac{1}{\sum ki} + \frac{xj}{\sum ki \cdot xi^2} \cdot x\right) \qquad (1)$$

The result of the influence line for the left double “I” beam is exposed in the Graphic 1.

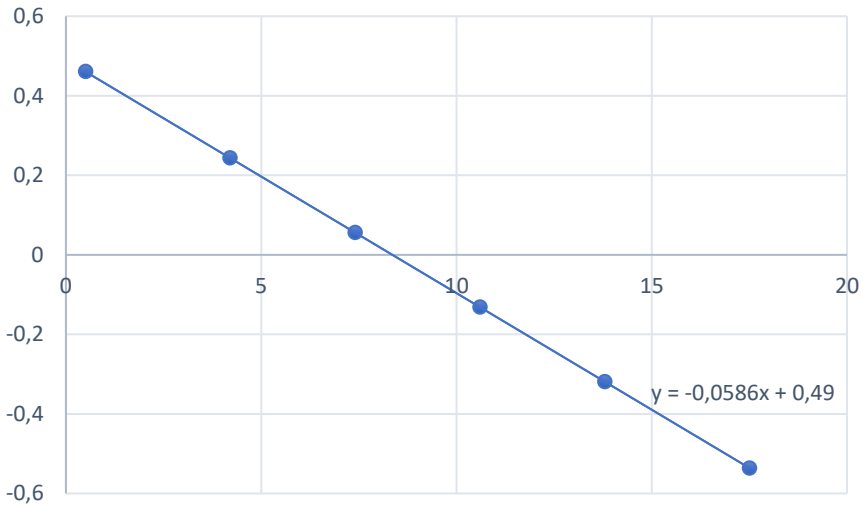

Graphic 1 - Transversal Influence Line

The null value was found at 8.37m from the extreme edge, as the bridge has a pedestrian passage of two meters only 6.37m remains for rolling track. It was possible to add 2 tracks, with the values described in Figure 34. Figure 48 shows the load distribution made for the LM1 respecting the influence line presented in the

Graphic 1 for future analysis.

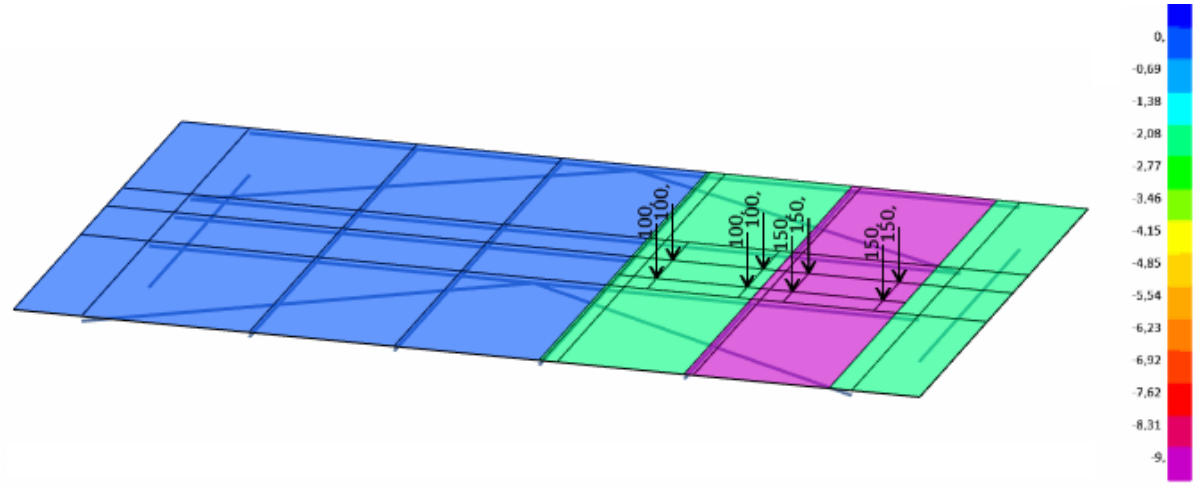

Figure 48 – Traffic load model 1 distribution

A similar process was done to set the longitudinal position of the load to maximize the forces on the cables and critical sections of the deck. However, by the complexity of the structure the formulation is too complex to be hand-calculated. Therefore, the longitudinal influence lines for the structure were calculated by the software SAP2000. Figure 49 shows the influence lines for the axial load in the central span cables.

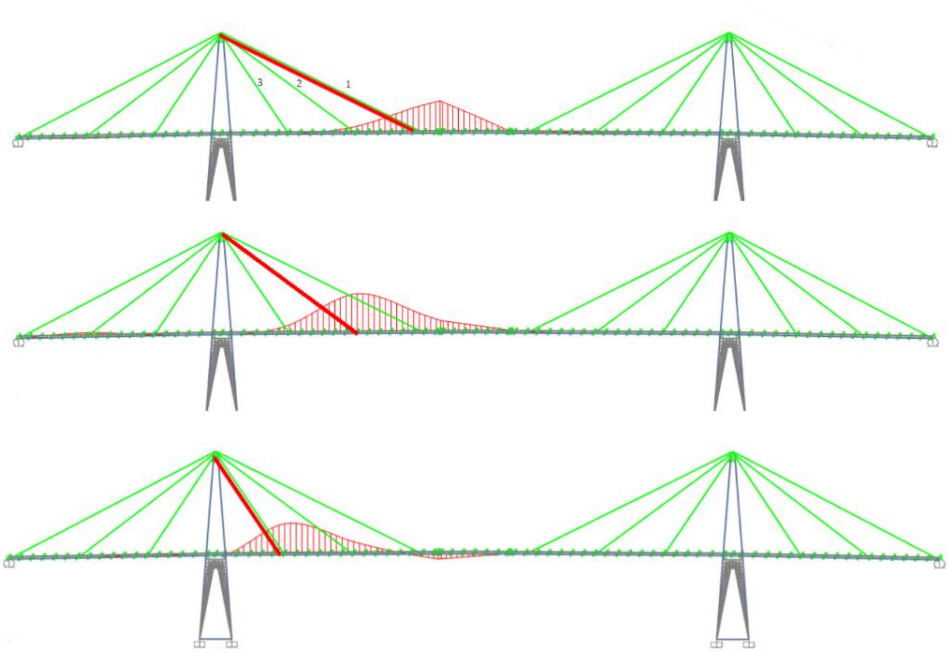

Figure 49 - Cable tension influence lines

Figure 50 illustrates the influence lines for the moments in the central span and for the anchorage section. It is now possible to place the load model so a maximum value is extracted for these internal forces.

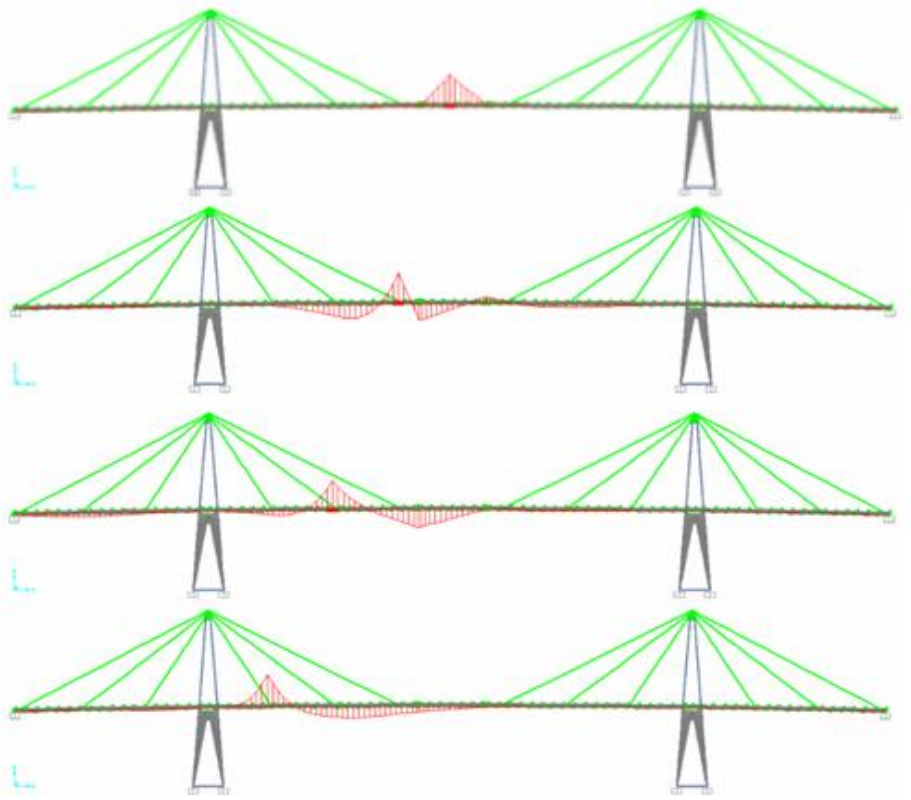

Figure 50 - Moment influence line

4.2.3 WIND ACTION

The wind forces are defined in the European standard NP EN1991-1-4 [26]. The following expression (2) defines the forces to be applied to the structure.

$$Fw = cscd \cdot cf \cdot qp(ze) \cdot Aref \quad (2)$$

Where,

Cscd – Structural coefficient

Cf – Force coefficient

qp(ze) – Peak velocity pressure

Aref – Element reference area

The calculation process starts by defining the peak velocity pressure, that is described in the Eurocode 1-4 by expression 3:

$$qp(z) = [1 + 7 \cdot Iv(z)] \cdot \frac{1}{2} \cdot \rho \cdot v_m^2(z) \quad (3)$$

Where,

ρ – Air density of 1,25 kg/m³

vm(z) – Mean wind velocity

Iv(z) – Turbulence intensity

For the mean wind velocity, the Portuguese annex of the Eurocode 1-4 for wind action describes the fundamental value of the wind speed for structures located in a range of 5 km from the coast as 30 m/s. Figure 51 shows that the bridge distance from the sea is about 2 km, what confirms that the base velocity is appropriated.

Figure 51 - Edgar Cardoso bridge location

The fundamental wind speed is one of the coefficients to calculate the mean wind velocity defined by the equation 4:

$$vm(z) = cr(z) \cdot ct(z) \cdot vb \quad (4)$$

The coefficients cr and c0 are, respectively, the rugosity and orography coefficients. As it is exposed in Figure 51 the land around the bridge is plan and is composed mostly by small constructions. This is important information to characterize the coefficients needed to calculate the mean wind velocity. The Portuguese National Annex of Eurocode 1-4 divides the terrain into four categories, as shown in Table 3.

Table 3 - Terrain category and terrain parameters

Terrain category		z0 m	zmin m
I	Sea or coastal area exposed to the open sea.	0,005	1
II	Area with low vegetation such as grass and isolated obstacles (tress, buildings) with separations of at least 20 obstacles heights.	0,05	3
III	Area with regular cover of vegetation or buildings or with isolated obstacles with separation of maximum 20 obstacles height (such as villages, suburban terrain, permanent forest).	0,3	8
IV	Area in which at least 15% of the surface is covered with buildings and their average height exceeds 15m.	1,0	15

In this work the terrain was considered as category one: sea or costal area exposed to the open sea. With the definition of the terrain category, it is possible to calculate the rugosity coefficient that is defined by the expressions below and is a function of the roughness length (z0) given in Table 3.

$$cr(z) = kr \cdot ln\left(\frac{z}{z0}\right), \text{ for } zmin \leq z \leq zmax \qquad (5)$$

$$cr(z) = cr(zmin), \text{ for } z \leq zmin \qquad (6)$$

Where,

z – structure height

z0 – is the roughness length (Table 3)

kr – terrain factor depending on the roughness length z0 given by the expression (7):

$$kr = 0{,}19 \cdot \left(\frac{z0}{z0,II}\right)^{0{,}07} \qquad (7)$$

Where,

z0,II = 0,05m (terrain category II)

zmin – minimum height defined by the Table 3

zmax – maximum height assumed as 200m.

The orography coefficient is meant to include acceleration effects due to the terrain slope around the structure, such as hills or cliffs. It was assumed a unitary orography coefficient since the ground around the bridge is flat. After the definition of these two coefficients it was possible to define the 10-minute mean wind velocity to be used in the calculation of the peak velocity pressure. The results obtained for that are exposed in Table 4.

Table 4 - Average wind velocities

Label	z	cr	Vm (m/s)
1	20,00	1,34	40,24
2	39,10	1,45	43,49
3	78,20	1,56	46,85

Before applying the loads into the model, a division in height was made in order not to insert on the towers extreme or low wind forces. For the deck, the second line of the Table 4 was used to characterize the peak velocity pressure.

Returning to the peak velocity pressure expression (3), the intensity of turbulence must be defined before finishing the calculation. This factor is a function of the orography coefficient already discussed in this section and the z0 value given by the Table 3 - Terrain category and terrain parameters, the expression for the turbulence factor is exposed below.

$$Iv(z) = \frac{1}{c0(z) \cdot ln(z/z0)}, \text{ for } zmin \leq z \leq zmax \qquad (8)$$

$$Iv(z)=Iv(zmin), \text{ for } z \leq zmin \qquad (9)$$

Where,

z – structure height

z0 – is the roughness length (Table 3)

After the definition of all the parameters needed to calculate the peak velocity pressure, it was possible to finally establish the values to be used. Table 5 includes a compilation of all the values used and the results obtained of the peak velocity pressure.

Table 5 - Peak velocity pressure

Results						Base values	
						Vb (m/s)	30
Label	**z (m)**	**cr**	**Vm (m/s)**	**Iv**	**qp (N/m²)**	**Cs,Co,Cd**	1
1	20,00	1,34	40,24	0,12	1866,03	**Z0 (m)**	0,005
2	39,10	1,45	43,49	0,11	2105,26	**Zmin (m)**	1
3	19,55	1,34	40,13	0,12	1858,14	**kt**	0,162

Now that the values for the peak velocity pressure are defined, it is possible to proceed to the determination of the force coefficient (cf) and the structural factor (cscd).

The force coefficient is a factor that adjusts the force applied into the structure based in their geometry. The most accurate process to determine these coefficients is to measure the pressure at several points of a scaled model of the structure submitted to wind loads inside a wind tunnel. To avoid the necessity of doing this test, Eurocode provides generic values of this coefficient that provide an approximation.

Whereas the definition and the methodology vary to the type of element, for this reason this section will be divided to discuss separated the results to each element.

4.2.3.1 Force coefficient - Bridge deck

The Graphic 2 below is available on the section 8.3.1 of the NP EN 1991-1-4 and is used to obtain the force coefficient along the cross-section direction based on the deck geometry. It is also shown in the graphic that the height to be considered (d,tot) is a sum of the deck depth with an extra length, defined by the standard as two meters, to consider the vehicles height.

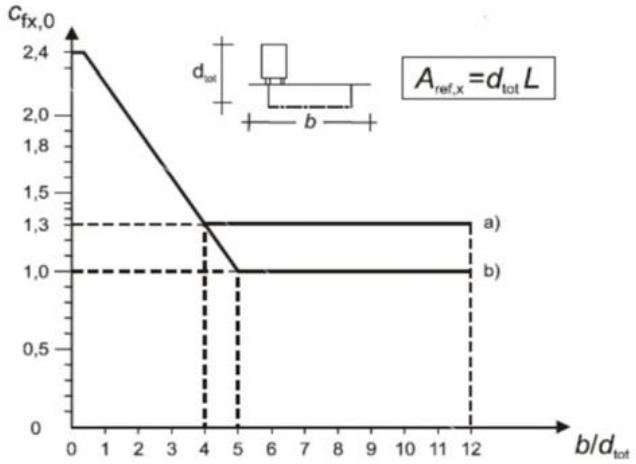

Graphic 2 - Force coefficient cfx,0 for bridge decks (NP EN 1991-1-4, 2019)

Furthermore, the national annex of the Eurocode 1-4 recommends a value of ±0,9 to be used as a force coefficient along the z direction, Figure 52. This force must be applied to the deck with an eccentricity of a quarter of the total width of the deck, what for the *Edgar Cardoso Bridge* represents 5 meters.

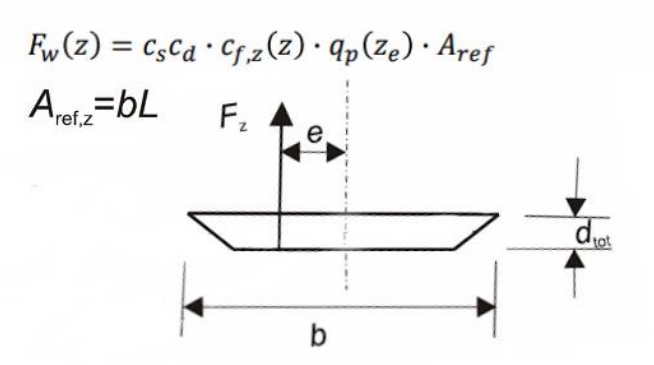

Figure 52 - Application of the wind force along the z direction, Fz(ze).

The Table 6 summarizes the values to the force coefficients used to the bridge deck.

Table 6 - Force coefficients applied to the bridge deck

Description	Values
cfx,0	1,05
cfz	0,90

4.2.3.2 Force coefficient – Tower

To calculate the tower force coefficient the section 7.6 of the Eurocode 1-4 was used. This section of the European standard describes how to obtain the force coefficient to rectangular sections. The expression 10 is given to obtain the force coefficient.

$$Cf = Cf,0 \cdot \psi r \cdot \psi\lambda \quad (10)$$

The variable cf,0 is the force coefficient to rectangular elements with sharp edges, what represents exactly the case of the structure of this study. Eurocode 1-4 presents the Graphic 3 in other to determinate the values for the cf,0 coefficient. The ψr variable is the Reynolds reduction value to sections with round corners, so it was assigned an unitary value because it does not apply to this structure.

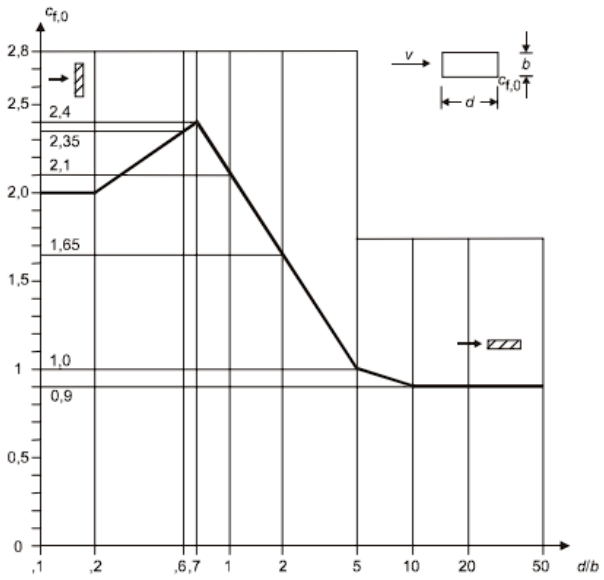

Graphic 3 - Force coefficient to rectangular sections with sharp edges

The ψλ variable is about boundary effects caused by the wind flow around the element. This coefficient depends on voids ratio and on the slenderness of the element. The Graphic 4 is available in the section 7.13 of the Eurocode 1-4 and was used to obtain this coefficient. In the Table 7 the values to obtain the coefficient forces to the tower are compiled.

Table 7 - Boundary effect determination values

B (m)	L (m)	A (m²)	Ac (m²)	λ	ϕ	ψλ	b/d	cf,0
14	78,2	22,4304	547,4	11,17	0,041	0,98	1	2,1

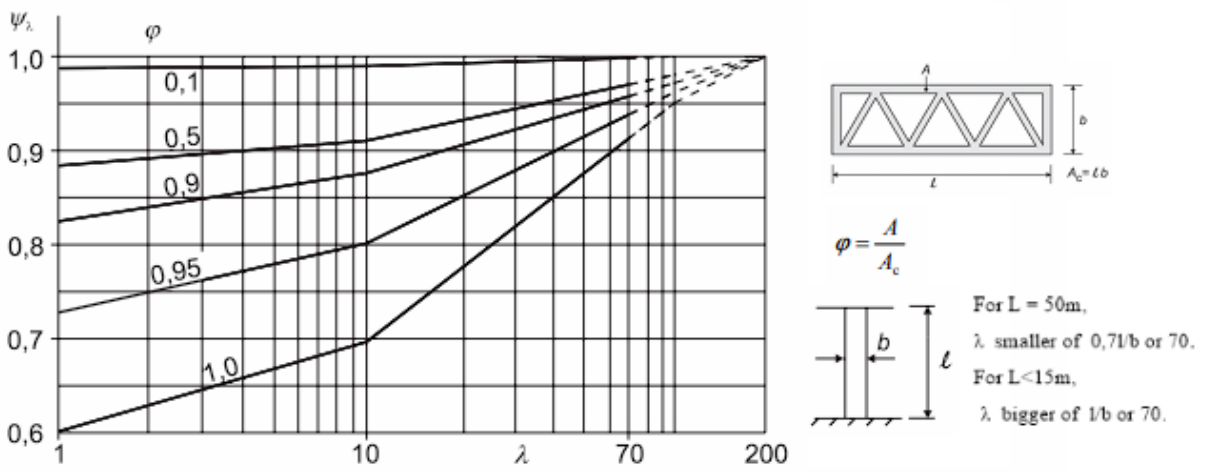

Graphic 4 - Boundary effect coefficient ψλ

4.2.3.3 Pressure coefficient – Cables

To define the pressure coefficient for the cables the section 7.9 of the Eurocode 1-4 to cylinders with circular section. The calculation of the coefficient of pressure for this type of elements depends on the Reynolds number that is defined by the given expression (11):

$$Re = \frac{b \cdot v(ze)}{v} \quad (11)$$

Where,

b – diameter

v – cinematic air viscosity (15 10^{-6} m²/s)

v(ze) – peak wind velocity

And the pressure coefficient is defined by:

$$cpe = cp,0 \cdot \psi\lambda\alpha \quad (12)$$

For this work the value of interest for ψλα is when this coefficient is equal to the ψλ, based on the Eurocode 1-4. Thus, the value can be obtained by the Graphic 4 where the values to the φ and λ, are respectively 1,0 and 70,0, concluding that the value to the ψλα is equal to 0,93. Table 8 shows the values obtained for the pressure coefficient of this cable.

Table 8 - Pressure coefficient for cylinders with circular cross-section

Description	**Values**		
ρ (kg/m³)	1,25	1,25	1,25
v(ze) (m/s)	60,05	60,05	60,05
Ø (cm)	15,00	11,62	9,88
L (m)	100,62	75,00	50,08
v (m²/s)	1,50E-05	1,50E-05	1,50E-05
Re	6,0E+05	4,7E+05	4,0E+05

L/b	670,62	645,33	507,04
ʎ	70	70	70
ϕ	1	1	1
ψʎ	1	1	1
cp,h	-0,4	-0,4	-0,4

The structural coefficient meant to correct the wind forces based on the structural behaviour, such as natural frequencies and geometry. A complete calculation was done based on the annex C of the Eurocode 1-4 to obtain the structural coefficient. The values found for this coefficient would reduce the forces, as shown in Table 9, so it was decided to use a unitary value for this coefficient in order to have the worst case scenario.

Table 9 - Structural coefficient (cscd) calculation

Variable	Value	Variable	Value	Variable	Value	Variable	Value
b (m)	200,00	**Iv**	0,11	**Vm (m/s)**	43,49	**Øy**	26,44
h (m)	2,20	**B²**	0,34	**fl(z,n)**	1,78	**Øz**	0,29
Z0 (m)	0,01	**R²**	0,02	**Sl(z,n)**	0,09	**Ks**	1,67
z (m)	39,10	**v**	0,12	**Gy**	0,41	**∂**	0,03
L(zs)	154,87	**kp**	3,14	**Gz**	0,50	**cscd**	**0,80**

With all the coefficients identified, it is possible to determinate the wind forces to be applied at the modelled elements. Table 10 and Table 11 show the values used to run the analysis in this work.

Table 10 - Wind force values and coefficients

Description	z	cr	Vm (m/s)	Iv	qp (N/m²)	cfx,0	cscd	Fw,x (kN/m)
Deck	39,10	1,45	43,49	0,11	2105,26	1,05	1	9,28
Long Cable	48,65	1,49	44,55	0,11	2186,11	0,372	1	0,12
Medium Cable	48,65	1,49	44,55	0,11	2186,11	0,372	1	0,09
Short Cable	48,65	1,49	44,55	0,11	2186,11	0,372	1	0,08
Tower - Base level	20,00	1,34	40,24	0,12	1866,03	2,1	1	7,84
Tower - Deck level	39,10	1,45	43,49	0,11	2105,26	2,1	1	8,84
Tower - Top Level	78,20	1,56	46,85	0,10	2366,52	2,1	1	9,94

Table 11 - Wind force value applied to the z direction on the deck

Description	Z (m)	cr	Vm (m/s)	Iv	qp (N/m²)	cfx0	cfz	cscd	Fw0 (kN/m)	Fw,z (kN/m)
Values	39,1	1,45	43,49	0,11	2105,26	1,05	0,90	1	9,28	37,89

To the deck and cable elements a distribution considering an average height was done, because the variation of pressures would not cause a big influence in the results. However, to the towers a trapezoidal

distributed load was assigned to the frame elements considering the values available on the Table 10 for the base, deck and top levels.

4.2.4 SEISMIC LOAD

For seismic analysis bridges must be classified by their importance depending on the consequences of failure for the human life, especially in the immediate post-earthquake period. Eurocode 8-3 [28] classifies bridges in three categories, based in their importance, general road and railway bridges belong to importance class II that is an average importance class.

The characterization by importance class is important to define what is the design seismic action, A_{ed}, to be used in the analyses. By definition, the reference seismic action, A_{ek}, is associated with the probability of exceedance in 50 years and the importance factor γ_I as exposed in the expression below. The importance factor differs with the bridge classification, for structures defined as importance class II the γ_I factor is equal to one.

$$A_{ED} = A_{Ek} \cdot \gamma_I \qquad (13)$$

To the ultimate limit state seismic action, the structure must be designed so after the occurrence its integrity and resistance remains adequate, even if some parts suffer some damage. Essentially, the bridge deck should be designed to avoid, other than locally to secondary components such as joints, continually slabs or parapets.

To characterize the seismic action countries, divide the territory in regions with the same average ground acceleration in case an earthquake occurs. For Portugal, the National Annex of the EN 1998-1 2010 divides the country in parts according to the action type 1 and 2. The division is shown in Figure 53.

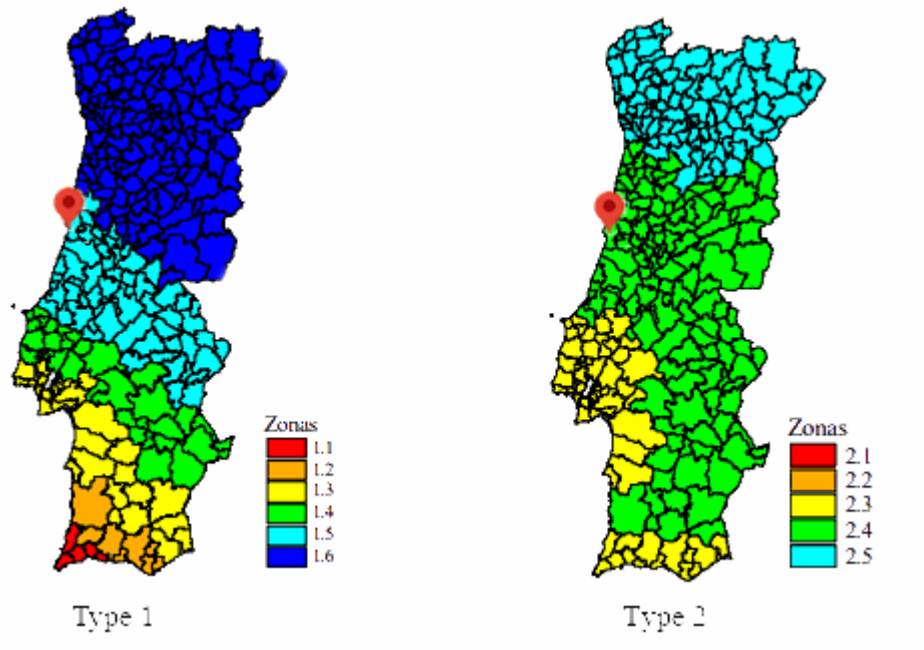

Figure 53 - Seismic zones for continental Portugal according to the action type.

The distinction between the seismic action is related to the fact that two seismic scenarios can affect Portugal. The first one is labelled as a “distant” situation, where the epicentre is in the Atlantic Ocean. The second type named as a “near” situation, where the epicentre is in the continental Portugal or in the Azores archipelago. For each one of the seismic actions’ types, there are different patterns for ground

acceleration and response spectrum. Table 12 describes the values of the ground acceleration related to each seismic zone.

Table 12 - Maximum base ground acceleration

Seismic acceleration type 1		**Seismic acceleration type 2**	
Seismic zone	**agr (m/s²)**	**Seismic zone**	**agr (m/s²)**
1.1	2,5	2.1	2,5
1.2	2	2.2	2
1.3	1,5	2.3	1,7
1.4	1	2.4	1,1
1.5	0,6	2.5	0,8
1.6	0,35	–	–

As it is exposed in Figure 53, the seismic zone for the city of *Figueira da Foz* where the Edgar Cardoso bridge is located is considered as 1.5 for the seismic action type 1, and for the type 2 is considered to be 2.4. With the definition of the seismic zone, it is possible determinate the ground acceleration to be used in the calculation of the seismic action. As it is described in the Table 12, the values for the ground acceleration are 0.6 and 1.1 m/s², respectively for the actions type 1 and 2.

The characterization of the actions in the seismic design is done through the response spectrum Graphic 5, defined in the Eurocode 8-1. The response spectrum shape is related with structural parameters (ductility and damping ratios) and with soil characterization by wave velocity, standard penetration test results and unconfined cohesive strength. For this work, a type of soil B was considered, what configures as a compact sand deposit. In Table 13 the parameters to define the response spectrum shape to each type of seismic action are defined.

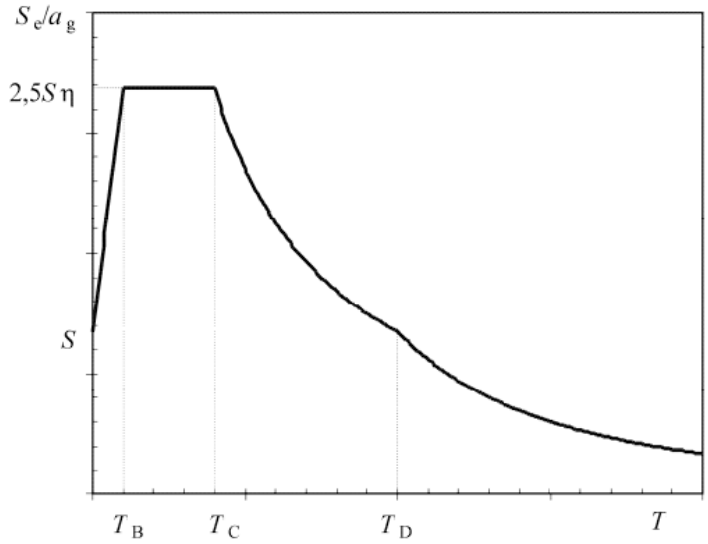

Graphic 5 - Response spectrum shape

Table 13 - Response spectrum parameters for soil type B

Tipo 1	**S**	1,35
	TB	0,1
	TC	0,6
	TD	2
Tipo 2	**S**	1,35
	TB	0,1
	TC	0,25
	TD	2

The variable η is a coefficient that adjusts the response spectrum based on the damping of the structure, it is defined by the following expression (14):

$$\eta = \sqrt{10/(5+\xi)} \geq 0{,}55 \qquad (14)$$

Where,

ξ - Viscous damping of the structure. Defined as 2% for this work structure.

Through the response spectrum the value for the spectral acceleration can be defined, so it is possible to calculate the shear force at the structure base. This value is given by the expression 15.

$$Fb = Sd(T1) \cdot m \cdot \lambda \qquad (15)$$

Where,

Sd(T1) – Spectral Acceleration of design

m – Total mass of the structure

λ – Correction factor, of 0,85 to T1≤2 Tc or 1 to the other cases

To obtain the design value for the spectral acceleration, Eurocode 8-1 defines equations to adjust the response spectra using a coefficient called behaviour factor, q. The behaviour factor adjusts the response of the structure based on its ductility capacity. The Graphic 6 below, from the Eurocode 8-3, explains the behaviour factor based on a force-displacement relationship. The base value to be used according to the type of structure are defined by the Eurocode 8-3, as disposed in the Table 14. However, for this work it was chosen to respect the option made by the rehabilitation report [23] to define the behaviour factor as 1,00.

Graphic 6 - Seismic behaviour factor

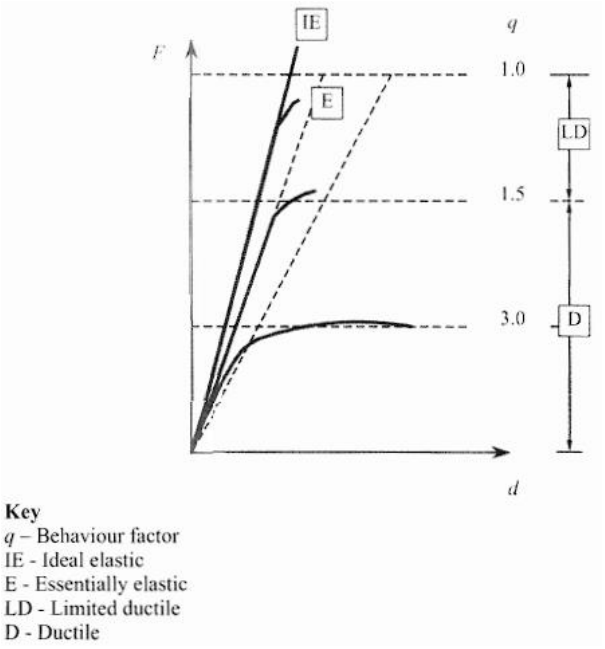

Table 14 - Maximum values of the behaviour factor q (EN 1998-2:2005+A2:2011)

Type of Ductile Members	Seismic Behaviour	
	Limited Ductile	Ductile
Reinforced concrete piers:		
Vertical piers in bending	1,5	3,5 $\lambda(\alpha_s)$
Inclined struts in bending	1,2	2,1 $\lambda(\alpha_s)$
Steel Piers:		
Vertical piers in bending	1,5	3,5
Inclined struts in bending	1,2	2,0
Piers with normal bracing	1,5	2,5
Piers with eccentric bracing	-	3,5
Abutments rigidly connected to the deck:		
In general	1,5	1,5
Locked-in structures (see. **4.1.6(9), (10)**)	1,0	1,0
Arches	1,2	2,0

*$\alpha_s = L_s/h$ is the shear span ratio of the pier, where L_s is the distance from the plastic hinge to the point of zero moment and h is the depth of the cross-section in the direction of flexure of the plastic hinge.

For $\alpha_s \geq 3$ $\quad \lambda(\alpha_s) = 1,0$

$3 > \alpha_s \geq 1,0$ $\quad \lambda(\alpha_s) = \sqrt{\frac{\alpha_s}{3}}$

The parameters for seismic action defined in this section were introduced in the FE Model, where the software allows to configure the response spectrum based on the standard load pattern. Figure 41 is a view of the SAP2000 screen where the response spectrum is defined. Adjustments must be done to respect the parameters defined by the National Annex of the NP EN 1998-1:2010.

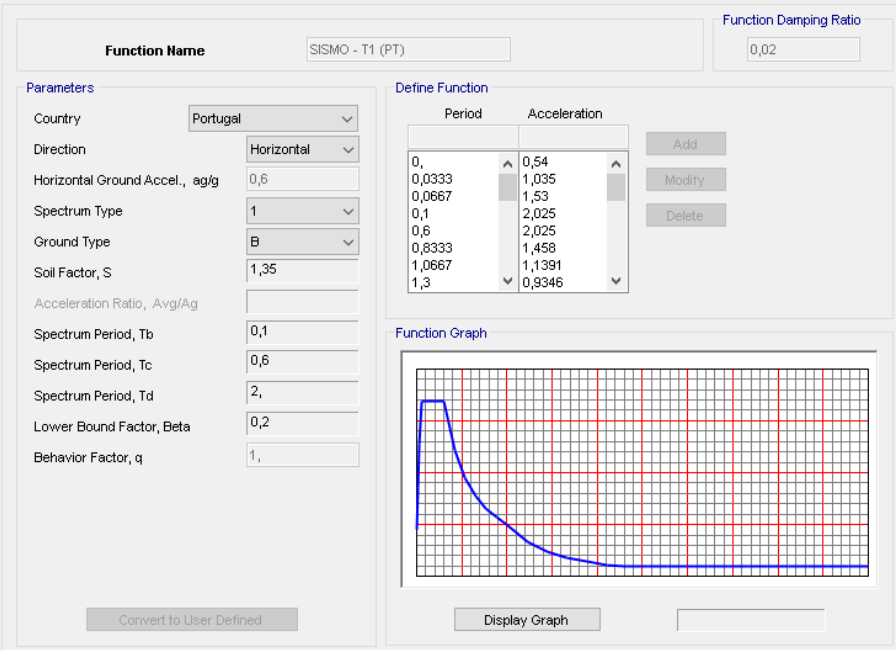

Figure 54- SAP2000 response spectrum by the Eurocode 8.

The final step is to set up the combination of the seismic effect in multiple directions. Since the maximum values for the modal response do not occur for the same time, they can be combined using statistical approaches. The following techniques are defined in the sections 4.3.3.5 of the EN 1998-1:2010 to combine multiple direction effects.

- Square Root of the Sum of the Squares (SRSS)

$$E_{i,max} = \sqrt{\sum_{j=1}^{N\ modes} E_{i,j,max}^2} \quad (16)$$

- Complete Quadratic Combination (CQC)

$$E_{i,max} = \sqrt{\sum_{j=1}^{N} \sum_{k=1}^{N} \rho \cdot E_{i,j,max} \cdot E_{i,k,max}} \quad (17)$$

As the modal periods differs more than 10% between each other, they are classified as independent by the Eurocode 8-1, so the recommended method to be used is the SRSS technique. The shear reactions for the seismic action after the combination are described.

Table 15 - Shear reactions for seismic action.

Descriptions	X	Y
S.A. Type 1 (kN)	12340,99	7724,83
S.A. Type 2 (kN)	9416,34	5894,63

4.2.5 LOAD COMBINATIONS

To combine the loads assigned to the structure, it was used the methodology presented by the standard EN 1990:2009 [24]. The basic principle of this process is to establish appropriated degrees of reliability

and in an economical way sustain the actions applied to the structure during the construction and work life, as indicated in the Table 16.

Table 16 - Indicative design working life

Design working life category	Indicative design working life (years)	Examples
1	10	Temporary structures
2	10 to 25	Replaceable structural parts, e.g. gantry girders, bearings
3	15 to 30	Agricultural and similar structures
4	50	Building structures and other common structures
5	100	Monumental buildings structures, bridges, and other civil engineering structures

To guarantee the safety and comfort to those how will use the structure, two scenarios must be evaluated when a structure is designed. The first one is the Serviceability Limit State (SLS), where the principal concern is the comfort of people, normal function of the structure and appearance of the construction work. Another situation to be evaluated is the Ultimate Limit State (ULS), which is focused on safety of people and structure.

The methodology to evaluate the risk of some damage or any other problem to affect the structure is based on probabilistic factors. The principle applied to this case is called “Reliability Theory”, where the probability of some effect (E) overcome the resistance (R) of the structure,

Graphic 7, must be acceptable to the society. In order to reduce susceptibility to the damage the European standard EN 1990:2009 defines coefficients to increase the design loads and decrease the design resistance that will be presented in this section

Graphic 7 - Probabilistic approach for load and resistance definition

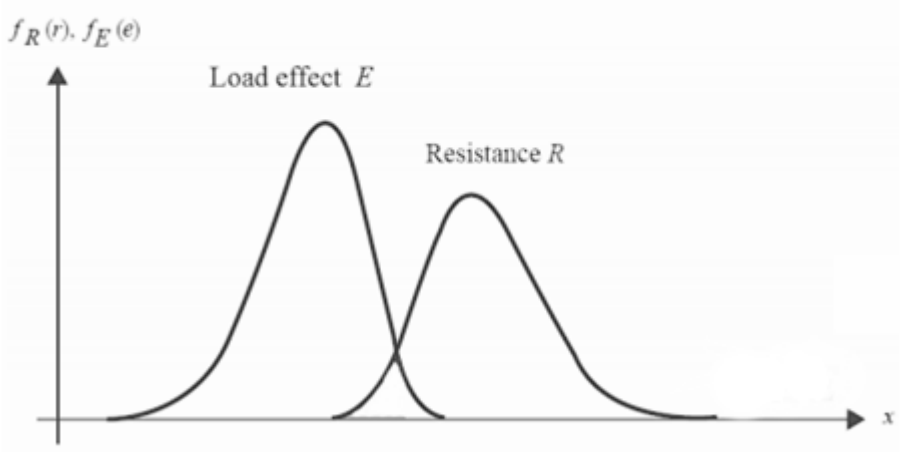

To evaluate the load probability of occurrence a classification by their variation in time is made according to the following:

- Permanent loads (G): Self-weight of structure, fixed equipment, and road surfacing.
- Variable actions (Q): Imposed loads on building floor, beam and roofs, wind action or snow loads;
- Accidental actions (A): Explosions, or impact from vehicles.

In addition, the actions shall also be classified by:

- their origin, as direct or indirect,
- their spatial variation, as fixed or free, or
- their nature and/or the structural response, as static or dynamic.

For this the loads described earlier in this chapter were classified and inputted in the FE model respecting the following criteria:

- Permanent loads (G):
  - Self-weight of the structural elements
  - Non-structural elements: Parapets, guardrails, kerbs, pipelines and other elements showed in the section 4.2.1.
- Variable actions (Q):
  - Traffic loads
  - Wind action
  - Seismic load

The combination of each load case shall occur with actions that are considered to act simultaneously. To each one of the combinations a leading variable action must be determined to be combined with the other load case that has a probability to occur at the same time.

4.2.5.1 Serviceability Limit State (SLS)

The EN 1990:2009 defines the following serviceability limit states:

- Characteristic combination, normally used for irreversible limit states:

$$E_d = \sum_{j\geq 1} G_{k,j} + P + Q_{k,1} + \sum_{i>1} \psi_{0,i} \cdot Q_{k,i} \qquad (18)$$

- Frequent combination, used for reversible limit states:

$$E_d = \sum_{j\geq 1} G_{k,j} + P + \psi_{1,1} \cdot Q_{k,1} + \sum_{i>1} \psi_{0,i} \cdot Q_{k,i} \qquad (19)$$

- Quasi-permanent combination, normally used for long-term effects and the appearance of the structure:

$$E_d = \sum_{j\geq 1} G_{k,j} + P + \sum_{i>1} \psi_{2,i} \cdot Q_{k,i} \qquad (20)$$

The values of the coefficient ψ are defined in the Table 17 below

Table 17 - Recommended values of ψ factor

Symbol			ψ0	ψ1	ψ2
Traffic loads (see EN 1991-2, table 4.4)	gr1a (LM1+pedestrian or cycle-track loads)	TS	0,75	0,75	0
		UDL	0,4	0,4	0
		Pedestrim+cycle-track loads	0,4	0,4	0

	gr1b (single axle)	0	0,75	0
	gr2 (horizontal force)	0	0	0
	gr3 (pedestrian loads)	0	0	0
	gr4 (LM4 - Crowd loading)	0	0,75	0
	gr5 (LM3 - Special vehicles)	0	0	0
Wind forces	Fwk			
	Persistent design situations	0,6	0,2	0
	Execution	0,8	-	0
	Fw	1	-	-
Thermal action	Tk	0,6	0,6	0,5
Snow loads	Qsn,k	0,8	-	-
Construction loads	Qc	1	-	1

All the load combination used to run the analysis of this work are compiled in the Annex A.

4.2.5.2 Ultimate Limit State (ULS)

For the Ultimate Limit State (ULS) the EN 1990:2009 defines the following expression 20:

$$E_d = \sum_{j\geq 1} \gamma_{G,j} \cdot G_{k,j} + \gamma_P \cdot P + \gamma_{Q,1} \cdot \psi_{0,1} \cdot Q_{k,1} + \sum_{i>1} \gamma_{Q,i} \cdot \psi_{0,i} \cdot Q_{k,i} \quad (20)$$

Besides that, the standard divides the application of this load combination for different types of analysis, all the categories are listed below.

- EQU: Loss of static equilibrium of the structure or any part of it considered as a rigid body;
- STR: Internal failure or excessive deformation of the structure or structural members, including footings, piles, basement walls, etc;
- GEO: Failure or excessive deformation of the ground where the strengths of soil or rock are significant in providing resistance;
- FAT: Fatigue failure of the structure or structural members.

For the model in discussion only the STR case will be applied, according to the objectives established for the work. According to the EN 1990:2009 the values given in Table 18 for the coefficients γ are defined.

Table 18 - Recommended values for γ factor

Situações de projecto persistentes e transitórias	Acções permanentes		Pré-esforço	Acção variável de base da combinação *)	Acções variáveis acompanhantes *)
	Desfavoráveis	Favoráveis			
(Expressão 6.10)	$\gamma_{Gj,sup} G_{kj,sup}$	$\gamma_{Gj,inf} G_{kj,inf}$	$\gamma_P P$	$\gamma_{Q,1} Q_{k,1}$	$\gamma_{Q,i} \psi_{0,i} Q_{k,i}$

*) *As acções variáveis são as consideradas no Quadro A1.1.*

NOTA 1: *As combinações de acções indicadas nas expressões (6.10a) e (6.10b) não devem ser utilizadas.*

NOTA 2: *Os valores de γ que devem ser adoptados são os seguintes:*
$\gamma_{Gj,sup} = 1,35$
$\gamma_{Gj,inf} = 1,00$
$\gamma_{Q,1} = 1,50$ *nos casos desfavoráveis (0 nos casos favoráveis)*
$\gamma_{Q,i} = 1,50$ *nos casos desfavoráveis (0 nos casos favoráveis)*
γ_P *- os valores deste coeficiente constam dos Eurocódigos aplicáveis.*
Para os valores de γa utilizar para as deformações impostas, ver os Eurocódigos aplicáveis.

NOTA 3: *Os valores característicos de todas as acções permanentes com a mesma origem são multiplicados por $\gamma_{Gj,sup}$, caso o efeito total das acções resultante seja desfavorável, e por $\gamma_{Gj,inf}$, caso o efeito total das acções resultante seja favorável. Por exemplo, todas as acções devidas ao peso próprio da estrutura podem ser consideradas como sendo da mesma origem; tal também se aplica se estiverem envolvidos diferentes materiais.*

NOTA 4: *Para determinadas verificações, os valores de γ_G e de γ_Q podem ser subdivididos em γ_g e γ_q e no coeficiente de incerteza do modelo γ_{Sd}. Na maioria dos casos correntes, pode utilizar-se um valor de γ_{Sd} variando entre 1,05 e 1,15.*

The combinations used in this work for the ULS are available at the Annex A.

4.3 VALIDATION OF THE FINITE ELEMENT MODEL

4.3.1 SELF-WEIGHT

After modelling all the elements and setting their properties, it is important to make some global verifications before further analysis. The first is to ensure that all the structure self-weight is well-applied, so the base reactions were compared with the values obtained in the rehabilitation report [23]. Results are shown in the Table 19.

Table 19 - Deck self-weight verification

Descriptions	Number	Weight p/ meter (kN/m)	Length p/ piece (m)	Totals (kN)
Main "I" section	4	6,8	405	11016
HEA600	4	1,8	405	2916
Transversal beams	47	4,5	15,5	3278,25
Braces	160	0,56	9,86	883,456
Slab	1	81,3	405	32926,5
Other permanent loads	1	70	405	28350
		Total estimated weight (kN)		79370,206
		Self-weight from the FE Model (kN)		79980
		Error		-0,8%

4.3.2 CABLE GEOMETRY

SAP2000 offers a variety of options to adjust the cable geometry. Since the values of the axial forces in the stays were available from measurements done in the bridge by Prof. Elsa Caetano [22], it was possible to correct the geometry of each stay to find the right load distribution between them. This process was done by changing the initial tension applied on each stay. In the Table 20 a comparison is made between the values extracted by the program and those measured on site.

Table 20 - Stay's axial forces

Stay	Size	Position	Ref.	Model	Variation
North - Middle Span	Large	West	8964	8828	-2%
North - Middle Span	Large	East	8789	8828	0%
North - Middle Span	Medium	West	5261	5040	-4%
North - Middle Span	Medium	East	5086	5040	-1%
North - Middle Span	Small	West	3184	3020	-5%
North - Middle Span	Small	East	3166	3020	-5%
South - Middle Span	Small	East	3357	3238	-4%
South - Middle Span	Small	West	3339	3238	-3%
South - Middle Span	Large	East	9218	8952	-3%
South - Middle Span	Large	West	9185	8952	-3%
South - Middle Span	Medium	East	4921	4769	-3%
South - Middle Span	Medium	West	4997	4769	-5%
North - Side Span	Large	West	8370	8390	0%
North - Side Span	Large	East	8106	8390	4%
North - Side Span	Medium	West	5390	5296	-2%
North - Side Span	Medium	East	5523	5296	-4%
North - Side Span	Small	West	3590	3470	-3%
North - Side Span	Small	East	3427	3470	1%
South - Side Span	Small	East	3510	3563	2%
South - Side Span	Small	West	3507	3563	2%
South - Side Span	Large	East	8320	8317	0%
South - Side Span	Large	West	8430	8317	-1%
South - Side Span	Medium	East	5449	5379	-1%
South - Side Span	Medium	West	5577	5379	-4%

4.3.3 MODE SHAPES AND NATURAL FREQUENCIES

Mode shapes and natural frequencies are very important aspects to verify the global functionality of the FE model. In Table 21 a comparison between the FE model natural frequencies extracted from the software and field measurements results was made to validate the modelling process. For this evaluation, two measurements taken on site were available, one from the rehabilitation report measured before the interventions and other made more recently by Prof.ª Elsa Caetano.

Table 21 - Comparison of the natural frequencies

Mode shape	FE Model (Hz)	Field measurements (Hz)			
		Rehabilitation Report	Variation	Prof.ª Elsa Caetano	Variation
Vertical flexure	0,5	0,51	2,0%	0,58	13,8%
Torsion	0,69	0,73	5,5%	0,72	4,2%
Transversal	0,84	0,87	3,4%	0,85	1,2%

In Figure 55 these three mode shapes are illustrated.

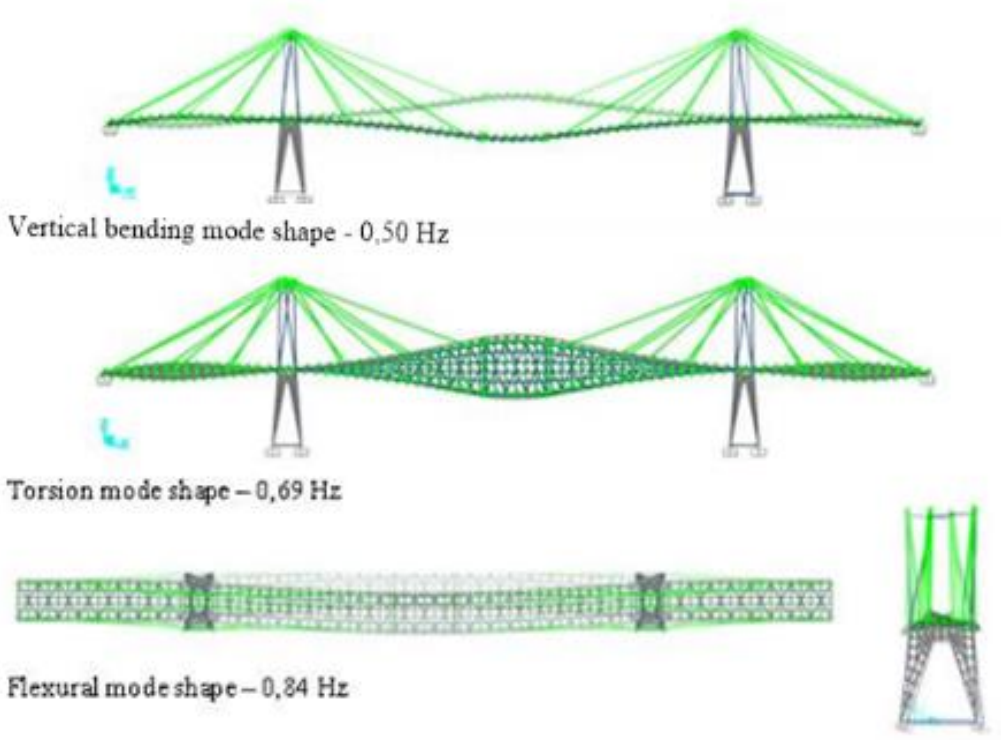

Figure 55 - Mode shapes for the Edgar Cardoso Bridge

4.4 SENSITIVITY ANALYSIS

In this section a discussion will be conducted about the results extracted of the model described in the last section. A detailed analysis was made to evaluate the bridge sections that are more susceptible to failure.

As the cables are the main object of study in this work, the results for them will be discussed first. For each cable of the main span the results were extracted for the maximum axial force, according to the influence line exposed earlier in this work. The values are exposed in the Table 22 below, divided by load case for the limit states according to the Eurocode 1.

Table 22 - Axial forces on the main span cables

	DEAD		SC		SLS		ULS	
Cables	Axial Load (MN)	Stress (MPa)	Axial Load (MN)	Stress (MPa)	Axial Load (MN)	Stress (MPa)	Axial Load (MN)	Stress (MPa)
VCTN_L_O	8,90	502,82	4,34	245,20	13,24	748,02	18,53	**1046,61**
VCTN_M_O	5,00	471,70	2,80	264,15	7,80	735,85	10,95	**1033,02**
VCTN_C_O	3,00	391,75	1,70	221,99	4,70	613,74	6,60	**861,84**

As the yielding strength of the cable steel is 1600 MPa, in the Ultimate Limit State the safety factor is, approximately, 60%, it means that they can support an increase of 40% of axial load. The cable stays are fundamental part of the structure, as they provide support to the bridge deck and act loading the main girders and the tower. It means that a rupture on a cable could lead to a progressive collapse scenario, as a result of load redistribution between the members of the structure. In Figure 56, the dead load diagram for axial load in the frame objects are displayed. This load pattern was chosen for a better analysis, as the load applied is uniform.

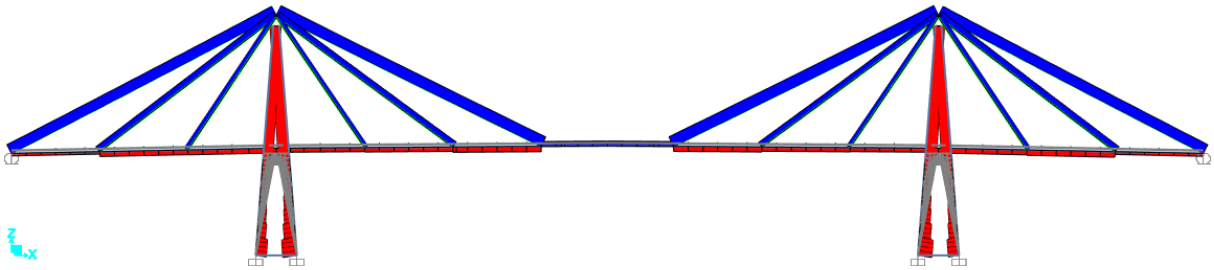

Figure 56 - Bridge axial load diagram

Regarding bending moments, as it was expected, the biggest value appears on the simply supported deck that is placed in the middle of the main span (Figure 57). For this section the worst situation is composed by a bending moment of 25,9 MN/m and a stress force of 17 MN, this composition results in a stress for the double "I" beam of 379 MPa, a value that represents 74% of the ultimate tensile strength and overcomes the yielding strength by 7%. As this is one of the members with higher levels of stress, it was chosen to monitor its reaction during the analysis run further on this work.

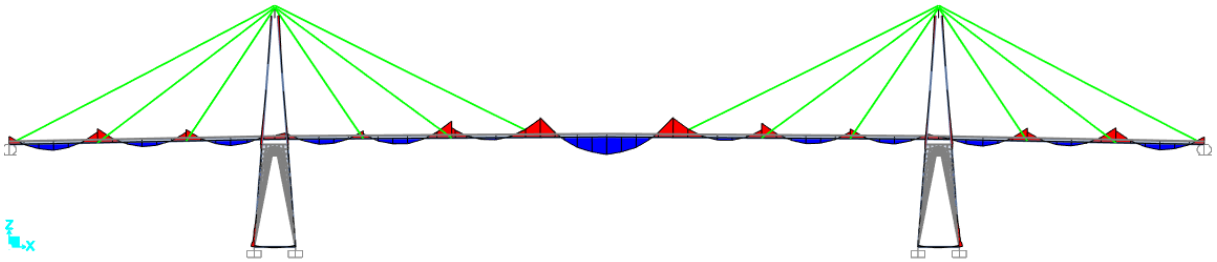

Figure 57 - YY bending moment diagram for the bridge deck (Dead load case).

The issue related to the tower is related with the displacement along the longitudinal direction, as it is represented in Figure 58 by a blue tone for the left tower and in red for the right (colour are different, because they move in opposite directions). This condition was not meant to happen, as the cables are one single object attached to the deck in both sides and the saddles would only receive axial force, but the friction between the elements results in forces that cause such displacement. The tower displacement will be a point of interest for the analysis run later in this work, because through this value it could be possible to see if some cable loss is evolving. In other hand the displacements are important because slight displacements could result in big bending moments in the pylon legs, and this effect can cause rupture of the element.

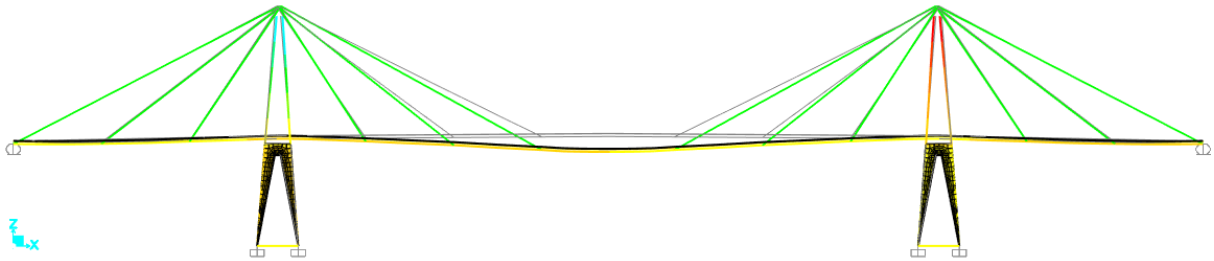

Figure 58 - Structure displacement (Dead load case).

In Table 23 the resultant forces and displacement for the most demanding combination are compiled.

Table 23 - Pylon section resistance analysis

Case for maximum stress	Δx (m)	Δy (m)	Axial Load (MN)	My (MN.m)	Mx (MN.m)	σ,max (Mpa)	σ,mr (Mpa)	Safety factor
1.35(DL)+1.5{T(L))+(0,6*W)}	0,17	0,06	-37,5	-6,76	9,78	39	55	40%

This section is very important to evaluate the safety of the structure in discussion and to set boundaries for the analysis that will be run in the next chapter. With the results obtained here it was possible to conclude that the deck girders are the elements with minimum safety factor, as for the Ultimate Limit Service characterized by the Eurocode 1, the tensile value already crosses the yielding limit. Besides, for the cables, the stress can rise 40% considering that these elements still have the full design section.

In this chapter a discussion about the main process for modelling the bridge structure using the SAP2000 software made, as well as a characterization of all the loads and an analysis of the results extracted from the software. Based on the model and in all the information obtained after this process, a study to characterize the cable damage that the structure support will be done in the following chapter.

In the Annex B the results for all the elements are listed in detail for all the load cases considered to calculate the values presented in this section.

5
SIMULATION OF DAMAGE SCENARIOS

The *Edgar Cardoso Bridge* is a cable-stayed bridge with its stays composed by parallel-wire cables, as it was exposed earlier in this work. Corrosion is one of the most problematic pathology that appears in this type of structure. With the corrosion the steel suffers loss of cross section and this problem is worst for small round section, that have most part of its body exposed to the air/corrosion. As the cables are formed by numerous wires (900,540,390) it is very difficult to inspect, and determinate the internal damage in the cable.

The main objective of this chapter is to develop scenarios of damage to describe further what is the implication of cable loss in terms of the structural behaviour of the bridge. Therefore, it was chosen to work basically in three hypotheses where a reduction of 10, 20 and 40% in the cable areas will be done and the results will be discussed after.

5.1 PARAMETERS FOR DAMAGE ANALYSIS

The procedure to determinate the damage scenario consists in reducing the cable properties in the FEM model. For this, a reduction of 10, 20 and 40% was set for this analysis. To define these values, a first try was made, were the reduction of ten percent was established. As the result did not cause a huge impact on the structural behaviour, it was decided to double the damage until the yielding tensile of 1600 MPa for the cables was reached.

In Table 22, a sample of these scenarios is exposed to show how the stress in the cable evolves along the reduction of the cross-section.

Table 24 - Axial forces on a medium cable of the main span after area reduction of the large cable.

	Normal case	-10%	-20%	-40%
Forces (kN)	10859,15	10871,44	11142,35	11556,35
Variation	-	0%	3%	6%

The purpose of this analysis is to define a pattern for the structure behaviour after the reduction of the section, so it is possible to determinate which parameter are important to analyse in case of a future structural health monitoring.

For the load distribution there was no reason to work based in cases that have complex assignments, such as the LM1 or wind actions, because they could make more difficult to identify the results of this process. Thus, it was decided to apply the load model 4, corresponding to a uniform load of 5kN/m² to

simulate effects of pedestrian action including dynamic effects, as it is shown in Figure 59. Besides, it is important to inform that the cross-section variation was done only by changing the area of the cable segment, so the weight remains the same for all the scenarios.

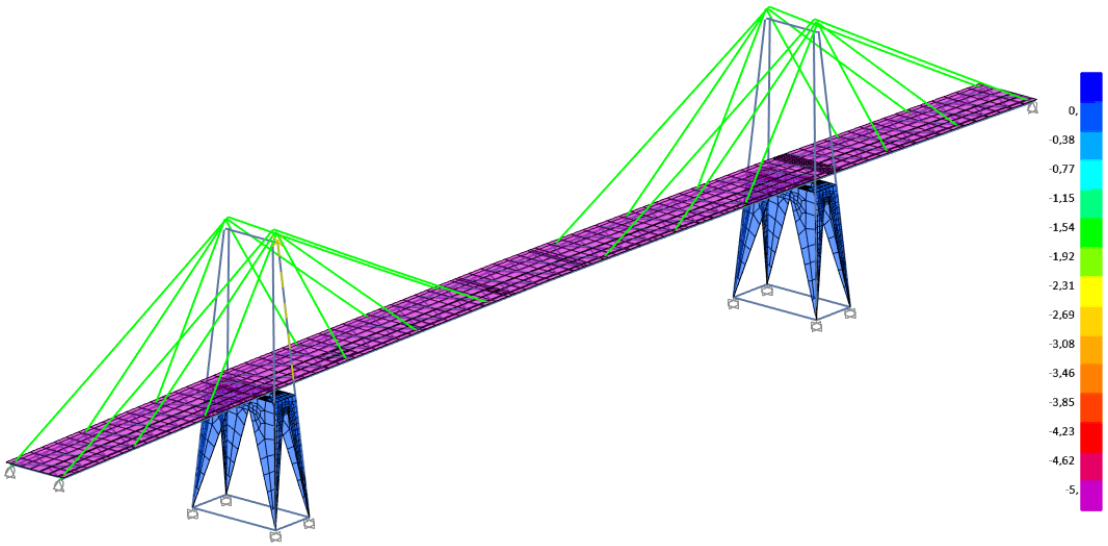

Figure 59 - LM4 distribution for the damage analysis

Thus, the LM4 was combined with the self-weight for ULS combination, so values that could lead to a failure situation could be presented. According to the formulation (21) presented in the section 0 the following configuration for this combination was applied to the structure in the model:

$$Fd = \gamma_g * G + \gamma_q * Q = 1{,}35 * G + 1{,}50 * Q \quad (21)$$

Based on the reasons presented in the end of the last chapter, the following parameters will be analysed to evaluate how the structure behaves after the occurrence of damage in the cables.

- All the 24 stays, to evaluate the variation of the axial load
- Top of the north to tower, for variation of displacement
- One of the four pylon legs of the north tower, for tensile check
- Abutment of the simply supported deck in the middle of the main span, for variation of displacement
- Main girder (Double "I" beam), for tensile check.
- Variations of natural frequencies

The members that will be analysed during the next sections are marked in Figure 60.

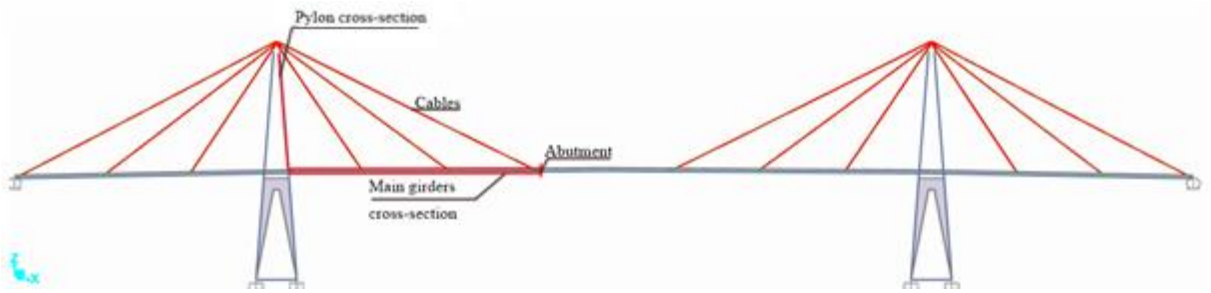

Figure 60 - Members analysed in the damage scenarios

5.2 DAMAGE SCENARIOS

The first damage scenario to be rehearsed was a damage occurring on the longest cable. This cable was chosen because it is the cable that carries the higher force and could cause more impact in the whole structure.

After the characterization of the first scenario, it was possible to evaluate the sequence of analyses. Besides, it was possible to conclude that each side of the deck is almost independent for this structure. This behaviour repeats for the other transversal and longitudinal bridge sides. Based in this behaviour, the damage characterization was focused only in one quarter of the structure, as the results would repeat for the other parts of the structure. Figure 61 represents the cables where the damage will be applied.

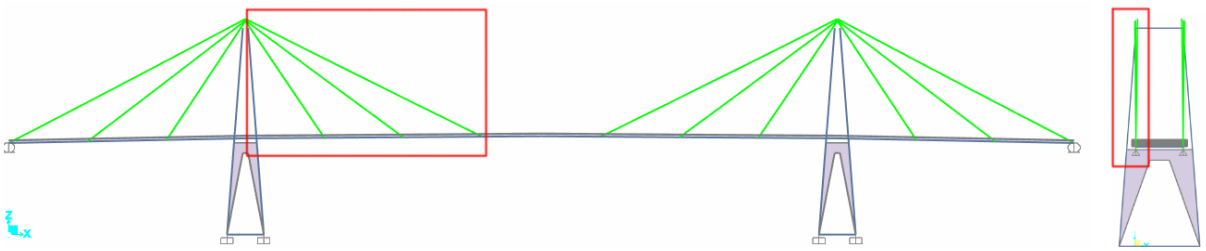

Figure 61 - Cables where the damage was applied

The following order was stablished for the damage scenarios:

- Damage in the long cable of the main span
- Damage in the medium cable of the main span
- Damage in the short cable of the main span
- Damage uniform to all the cables.

To each scenario of damage, the values for axial force in all the cables, displacements in de middle span and the efforts in the pylon and deck section were obtained. For a better understanding of the effects caused by the cross-section reduction for each scenario the values will be presented as ratios of a based value, the expression 22 was used.

$$\Delta E = (E_d - E_0)/(E_0) \qquad (22)$$

Where, E_0 is the base value and E_d is the effort for a damage scenario.

Presenting the values in the form of variation values is useful since it normalizes the resultant in ratios of a measurement. This is important, for example, to the axial loads in the cables where the values have a huge range of values. Graphic 8 is a representation of a graphic for a damage scenario run for a medium cable. It is possible to see in this example the most affected cables are the ones on the next side.

The results found after the analysis made in each one of the scenarios will be discussed in the next chapter, were a detailed analysis of the consequences of each scenario of damage and the limitation of the structure will be presented.

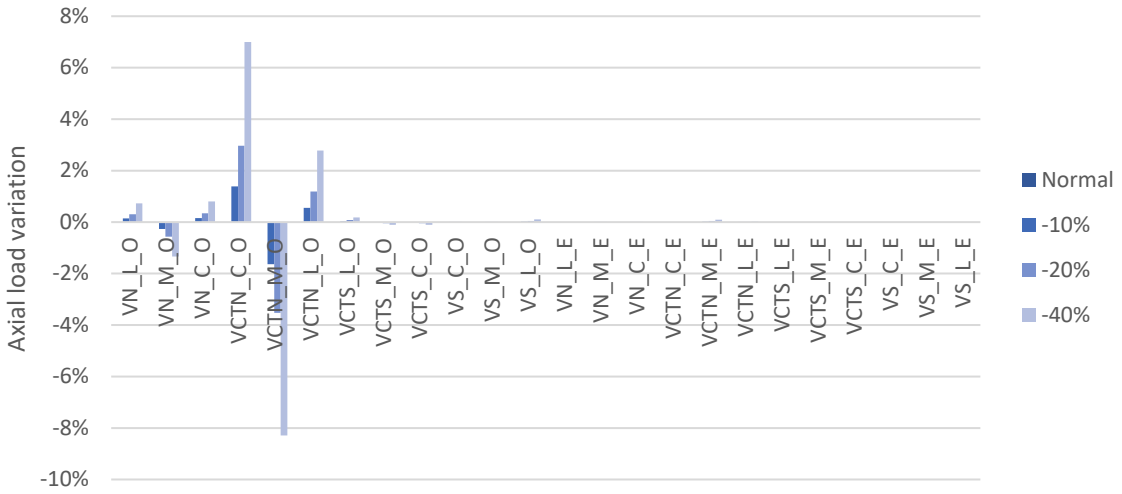

Graphic 8 - Example of a damage scenario done for a medium cable

6
RESULTS AND DISCUSSIONS

After several analysis of various scenarios of cable damage for the *Edgar Cardoso Bridge* it was possible to identify patterns for the structural response. The objective after this study is to have sufficient information to sustain a guideline to help on the measurement work in the structure.

This chapter contains a presentation of the findings for the analysis conducted in the structure under damage scenarios. During the research 4 scenarios of cable damage were considered, where the area of the cables was reduced by 10, 20 and 40% percent under the action of an uniform load, that represents a situation of pedestrian traffic covering the dynamic effects. For each damage case the results extracted from the FEM model are exposed below and discussed in section 6.5. It is also important to remember that the studies were done only for the north-west side of the bridge, as this structure is symmetrical, and the results would be the same for other sides.

6.1 DAMAGE SCENARIO 1 – LOSS ON THE LONG CABLE

This section will present the results for a simulation of damage in the longest cable of the *Edgar Cardoso Bridge*, indicated in the Figure 62.

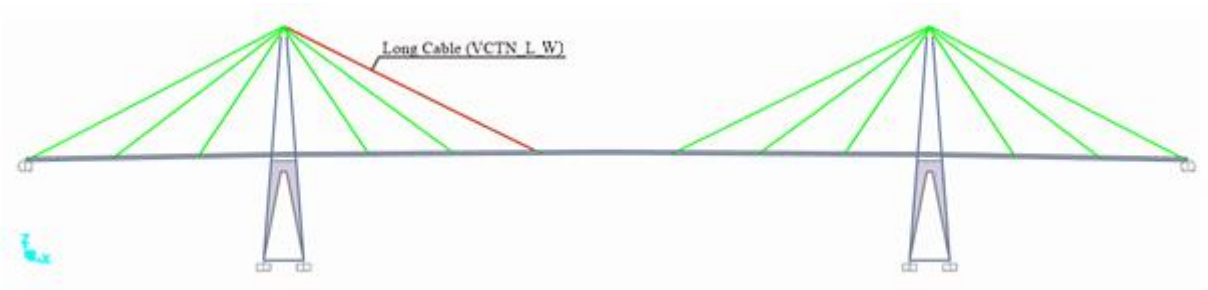

Figure 62 - Cable affected by the damage scenario 1 (loss on the long cable)

6.1.1 AXIAL LOAD

The section reduction on the cable results on a redistribution of the loads between other cables. In the Graphic 9 the variation of load for each scenario of damage are represented.

It is possible to see in the Graphic 9 that the distribution follows mainly for the medium cable (VCTN_M_W) with the damage progression. Another aspect to notice is that the redistribution does not cause huge impact on the east side of the bridge.

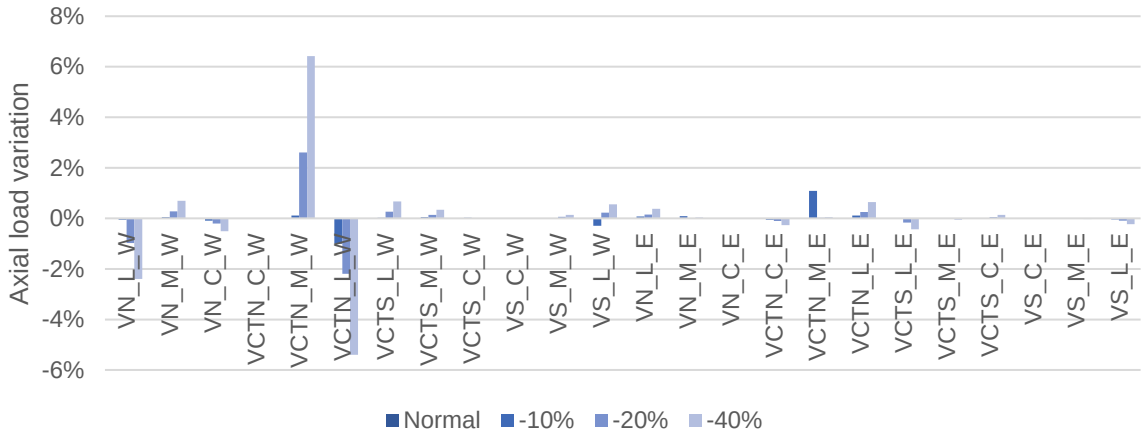

Graphic 9 - Axial load variation for damage scenarios 1 (loss of long cable on the West side)

The nomenclature used to identify the cables is explained in the Table 25

Table 25 – Cables identification

Longitudinal position	VN – North side span
	VS – South side span
	VCTN – North side of the central span
	VCTS – South side of the central span
Type of cable	L – Large
	M – Medium
	C – Short
Transversal position	W – West side
	E – East side

The stress increase during the damage evolution, as the variation of section is more pronounced than the load variation. Graphic 10 shows the variation of stress for the long and medium cables, that are the most affected in this scenario.

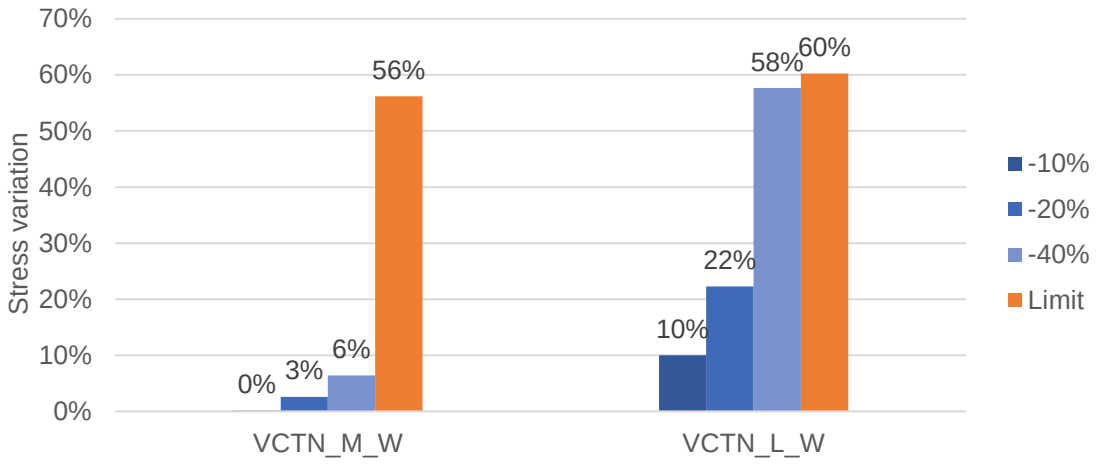

Graphic 10 - Variation of stress for the damage scenario 1 (loss of long cable)

6.1.2 DISPLACEMENT

Values for the displacement in the gravity direction were registered for the reductions on the long cable area, as shown in the Graphic 11.

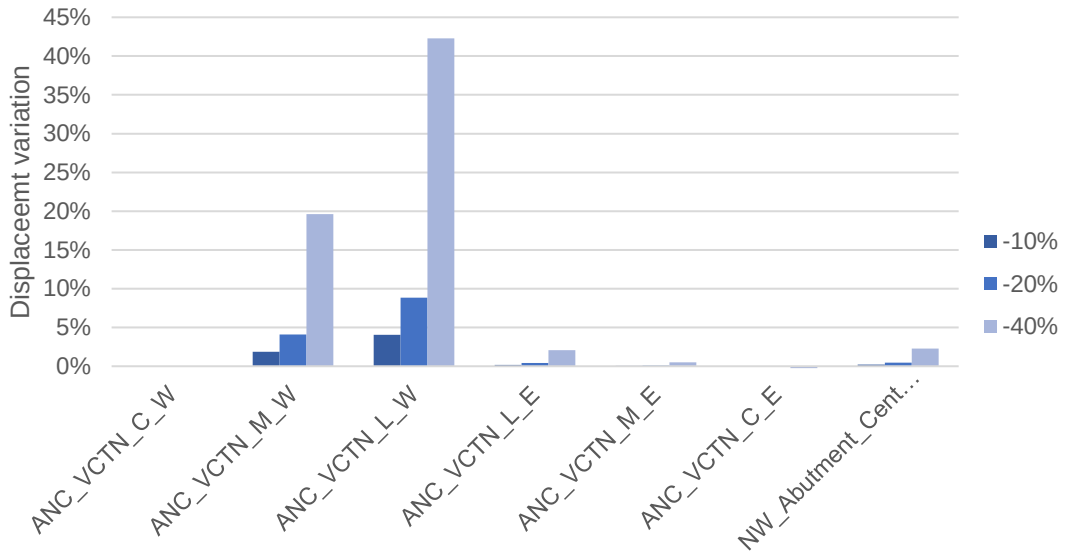

Graphic 11 - Variation of displacement for the damage scenario 1 (loss of long cable)

This result is very relevant for this work, as the variation of displacement is very large and develops essentially at the anchorage point of the cable affected. This result is meaningful also because it could be easily identified by measurement.

The nomenclature used to identify the points where the displacement was measured are explained in the Table 26.

Table 26 – Displacement points identification

Label	Description
ANC_VCTN_C_W	Anchorage of the short cable in the north-west side of the central span
ANC_VCTN_M_W	Anchorage of the medium cable in the north-west side of the central span
ANC_VCTN_L_W	Anchorage of the long cable in the north-west side of the central span
ANC_VCTN_C_E	Anchorage of the short cable in the north-east side of the central span
ANC_VCTN_M_E	Anchorage of the medium cable in the north-east side of the central span
ANC_VCTN_L_E	Anchorage of the long cable in the north-east side of the central span
NW_Abutment_CentralSpan	North-west abutment of the simply supported segment in the main span

The displacements on the top of the tower and their variation are shown in the Table 27.

Table 27 - Displacements on the tower top for the damage scenario 1 (loss of long cable).

Cable loss	XX	Δ_{xx}	YY	Δ_{yy}	ZZ	Δ_{zz}
0%	6,32	-	0	-	-0,337	-
-10%	6,31	-0,16%	0	0,00%	-0,336	-0,30%
-20%	6,29	-0,47%	0	0,00%	-0,335	-0,59%
-40%	6,25	-1,11%	0	0,00%	-0,333	-1,19%

6.1.3 MODAL RESPONSE

The impact of this damage scenario in the vibration modes is described in Table 28. As it was possible to detect, the reduction on the area of the longest cable affects mainly the primarily vibration modes (Annex C).

Table 28 - Modal variation for the damage scenario 1(loss of long cable)

Numb. modal case	-10%	-20	-40
1	0%	**-1%**	**-3%**
2	0%	**-1%**	**-2%**
3	0%	**-1%**	**-2%**
4	0%	0%	**-1%**
5	0%	0%	0%
6	0%	0%	0%
7	0%	0%	**-1%**
8	0%	0%	0%
9	0%	0%	0%
10	0%	0%	**-1%**
11	0%	0%	0%
12	0%	0%	0%
13	0%	0%	**-1%**
14	0%	0%	**-1%**
15	0%	0%	0%
16	0%	0%	0%
17	0%	0%	0%
18	0%	0%	0%
19	0%	0%	0%
20	0%	0%	0%

6.1.4 ADJACENT MEMBERS

The variation the of stress for the first damage scenario on the main beam of the deck, that is composed by a double “I” section described in 4, is displayed in the Table 29.

Table 29 - Variation of stress in the double "I" section for the damage scenario 1 (loss of long cable).

Area reduction	Axial Load (kN)	Bending moment (kN.m)	Stress (MPa)	Δ
0%	17048,47	25923,68	379,00	0,0%
10,0%	17358,98	25901,24	381,00	0,5%
20,0%	17728,44	25874,15	384,00	1,3%
40,0%	18701,61	25823,60	390,00	2,9%

Even with the stress values been in a high stage, the damage caused by the cable loss is not large enough to cause the beam failure. In addition, it is important to highlight that these stresses were obtained for an Ultimate Limit State, what does not mean that the bridge is unsafe for the current service condition.

The variation of stress in the pylon section was also obtained for each damage situation. The results are presented in Table 30.

Table 30 - Variation of stress in the pylon section for the damage scenario 1(loss of long cable).

Area reduction	Axial Load (kN)	Bending moment xx (kN.m)	Bending moment yy (kN.m)	Stress (MPa)	Δ
0	-35261,00	5404,00	9461,00	35,02	0,0%
10%	-35224,27	5409,93	-9462,59	35,01	0,0%
20%	-35180,79	5416,49	-9464,44	35	0,0%
40%	-35063,16	5433,48	-9470,02	34,97	0,0%

6.2 DAMAGE SCENARIO 2 – LOSS ON THE MEDIUM CABLE

In this scenario the medium cable will receive an area reduction. The element is indicated in Figure 63.

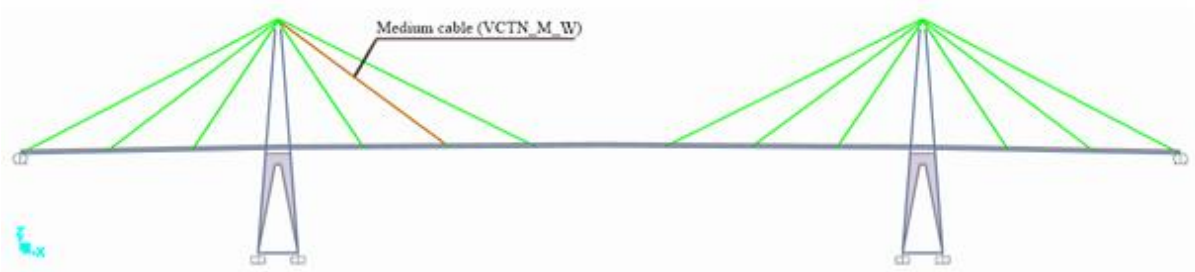

Figure 63 - Cable affected by the damage scenario 2 (loss on the medium cable)

6.2.1 AXIAL LOAD

The area reduction on the cable leads to a load redistribution. In Graphic 12 the load variation for each damage case are presented.

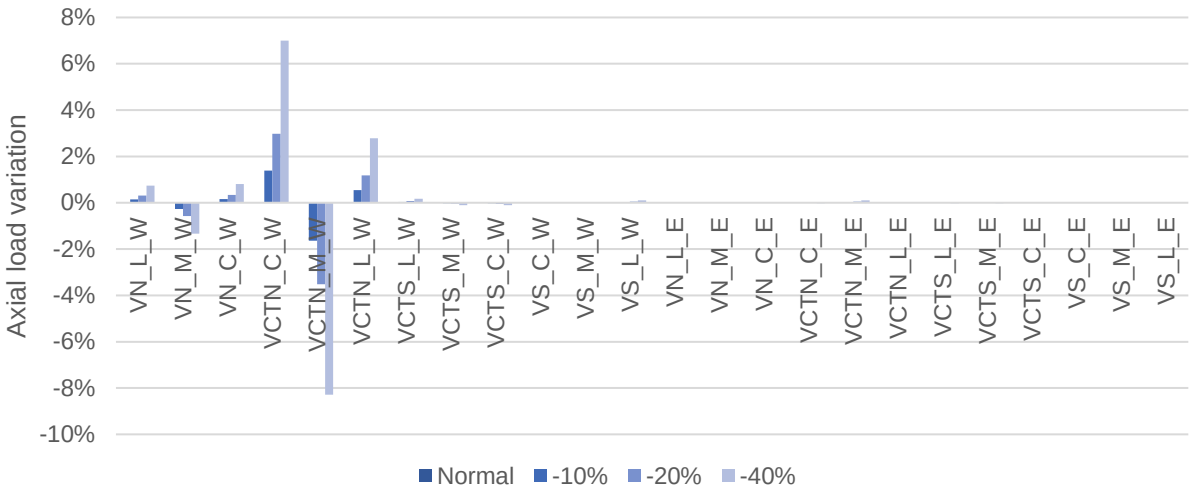

Graphic 12 - Axial load variation for damage scenario 2 (loss of medium cable)

As the variation of section is more pronounced than the load variation the stress increase during the damage evolution. The Graphic 13 below shows the variation of stress for the long and medium cables, that are the most affected by the reduction on the cross section of the cables in discussion.

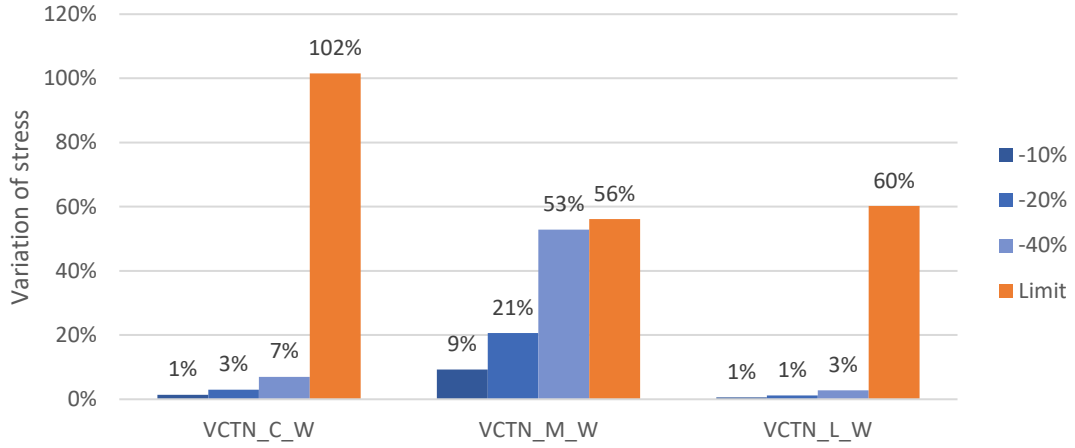

Graphic 13 - Variation of stress for the damage scenario 2(loss of medium cable)

6.2.2 DISPLACEMENT

Values for the displacement in the gravity direction were registered for each reduction on the medium cable section. As shown in the Graphic 14.

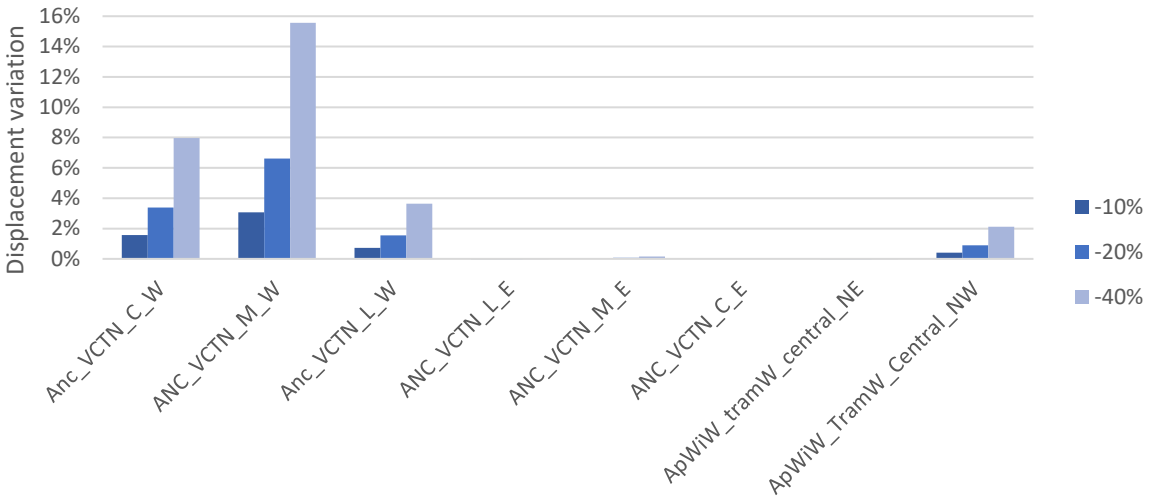

Graphic 14 - Variation of displacement for the damage scenario 2 (loss of medium cable).

The displacements on the top of the tower and their variation are shown in the Table 31.

Table 31 - Displacements at the tower top for the damage scenario 2 (loss of medium cable).

Cable loss	XX	Δ_{xx}	YY	Δ_{yy}	ZZ	Δ_{zz}
0%	6,32	-	0	-	0,337	-
-10%	6,29	-0,47%	0	0,00%	-0,337	0,00%
-20%	6,26	-0,95%	0	0,00%	-0,338	0,30%
-40%	6,18	-2,22%	0	0,00%	-0,34	0,89%

6.2.3 MODAL RESPONSE

As it is shown in the Table 32, the variation of section affects mainly the higher order vibration modes (Annex C).

Table 32 - Modal variation for the damage scenario 2 (loss of medium cable)

	-10%	-20%	-40%
1	0%	0%	0%
2	0%	0%	**-1%**
3	0%	0%	0%
4	0%	0%	**-1%**
5	0%	0%	0%
6	0%	0%	0%
7	0%	0%	0%
8	0%	0%	0%
9	0%	0%	0%

10	0%	0%	0%
11	0%	**-1%**	**-2%**
12	0%	0%	**-1%**
13	0%	0%	0%
14	0%	0%	0%
15	0%	0%	0%
16	0%	0%	0%
17	0%	**-1%**	**-2%**
18	0%	0%	0%
19	0%	0%	0%
20	0%	0%	0%

6.2.4 ADJACENT MEMBERS

The variation the of stress for the second damage scenario on the main beam of the deck is displayed in the Table 33.

Table 33 - Variation of stress in the double "I" section for the damage scenario 2 (loss of medium cable).

Area reduction	Axial Load (kN)	Myy (kN.m)	Stress (MPa)	Δ
0%	17048,47	25923,68	-379,80	0,0%
10,0%	17014,37	25926,99	-379,02	-0,2%
20,0%	16976,06	25927,08	-378,10	-0,4%
40,0%	16525,19	25891,60	-377,90	-0,5%

The variation of stress in the pylon section were also obtained for each one of these damage situations. The results are shown in the Table 34.

Table 34 - Variation of stress in the pylon section for the damage scenario 2(loss of medium cable).

Area reduction	Axial Load (kN)	Mxx (kN.m)	Myy (kN.m)	Stress (MPa)	Δ
0	-35261,00	5404,00	9461,00	35,02	
10%	-35218,28	5374,91	-9422,63	34,92	-0,29%
20%	-35169,04	5340,90	-9378,38	34,8	-0,34%
40%	-35045,44	5255,28	-9266,82	34,5	-0,86%

6.3 DAMAGE SCENARIO 3 – LOSS ON THE SHORT CABLE

In this scenario the shorter cable will receive an area reduction, the element is indicated in the Figure 64.

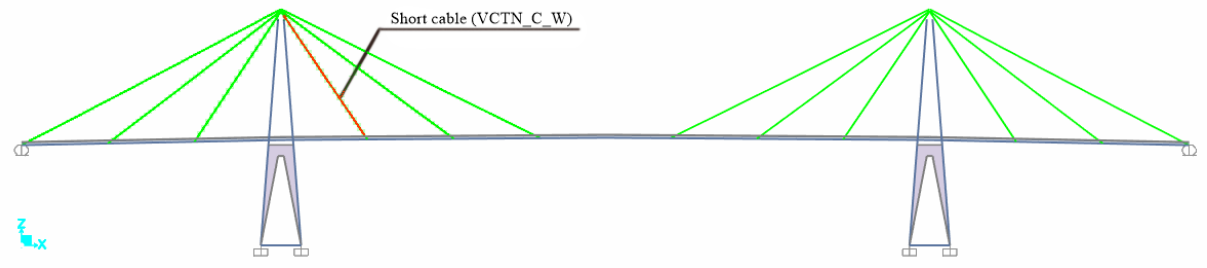

Figure 64 - Cable affected by the damage scenario 3 (loss of short cable).

6.3.1 AXIAL LOAD

The area reduction on the cable lead to a redistribution of the loads. In the Graphic 15 the load variation for each damage case are presented.

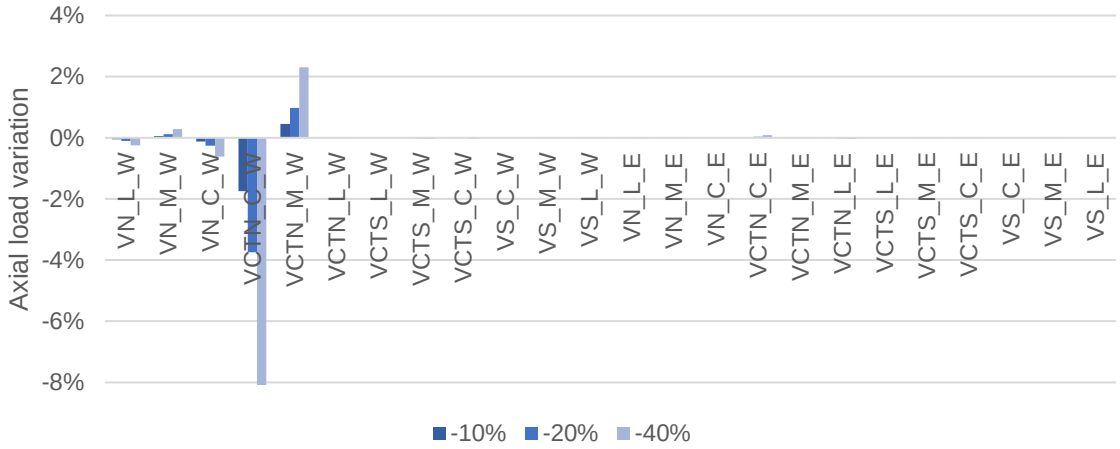

Graphic 15 - Axial load variation for damage scenarios 3 (loss of short cable).

As the variation of section is more pronounced than the load variation the stress increase during the damage evolution. The Graphic 16 below shows the variation of stress for the long and medium cables, that are the most affected by the reduction on the cross section of the cables in discussion.

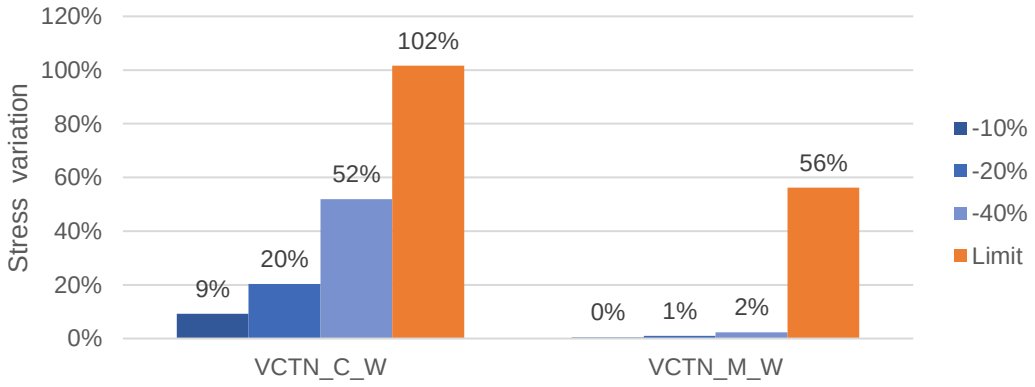

Graphic 16 - Variation of stress for the damage scenario 3 (loss of short cable)

6.3.2 DISPLACEMENT

Values for the displacement in the gravity direction were registered for each reduction on the medium cable section. As shown in the Graphic 17.

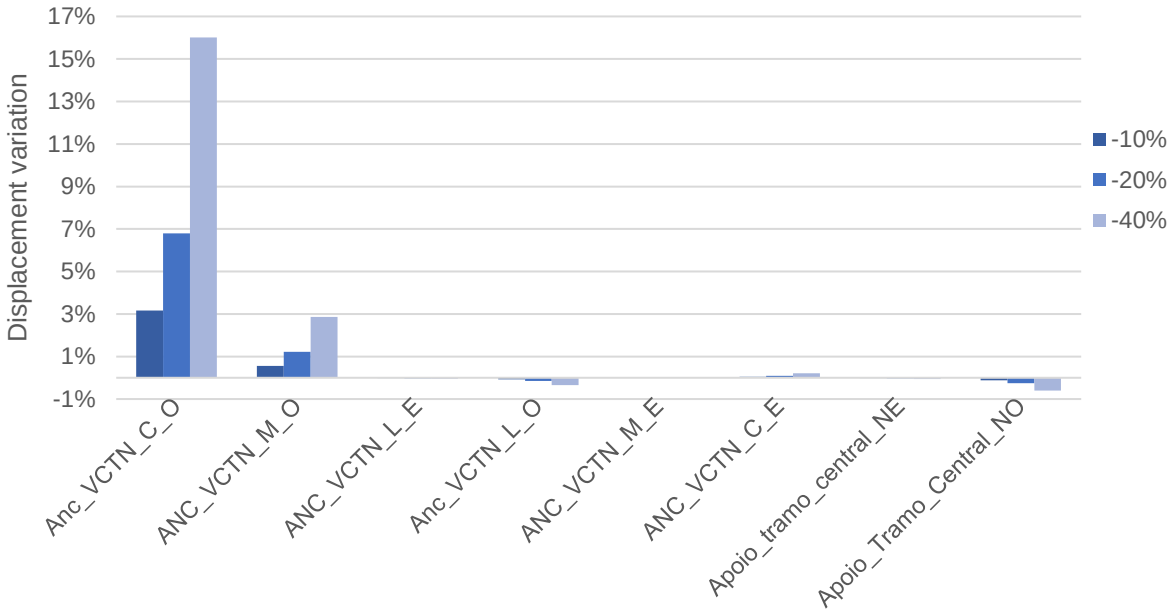

Graphic 17 - Variation of displacement for the damage scenario 3 (loss of short cable)

The displacements on the top of the tower and their variation are shown in the Table 35.

Table 35 - Displacements on the tower top for the damage scenario 3 (loss of short cable).

Cable loss	XX	Δ_{xx}	YY	Δ_{yy}	ZZ	Δ_{zz}
0%	6,32	-	0	-	0,337	-
-10%	6,3	-0,32%	0	0,00%	-0,335	-0,59%
-20%	6,23	-1,42%	0	0,00%	-0,333	-1,19%
-40%	6,22	-1,58%	0	0,00%	-0,327	-2,97%

6.3.3 MODAL RESPONSE

As it is shown in the Graphic 17 the variation of the section for the shorter cable does not have a big influence in the results of the modal shape (Annex C).

Table 36 - Modal variation for the damage scenario 3 (loss of short cable)

	-10%	-20%	-40%
1	0%	0%	0%
2	0%	0%	0%
3	0%	0%	0%
4	0%	0%	0%

5	0%	0%	0%
6	0%	0%	0%
7	0%	0%	0%
8	0%	0%	0%
9	0%	0%	0%
10	0%	0%	0%
11	0%	0%	**-1%**
12	0%	0%	0%
13	0%	0%	0%
14	0%	0%	0%
15	0%	0%	0%
16	0%	0%	0%
17	0%	0%	**-1%**
18	0%	0%	0%
19	0%	0%	0%
20	0%	0%	**-1%**

6.3.4 ADJACENT MEMBERS

The variation the of stress for the third damage scenario on the main beam of the deck, that is composed by a double “I” section described in the section 4, is displayed in the Table 37.

Table 37 - Variation of stress in the double "I" section for the damage scenario 3 (loss of short cable)

Area reduction	Axial Load (kN)	Myy (kN.m)	Stress (MPa)	Δ
0%	17048,47	25923,68	379,80	0,0%
10,0%	16944,54	25919,94	379,02	-0,2%
20,0%	16824,99	25912,63	378,10	-0,4%
40,0%	16525,19	25891,60	377,90	-0,5%

Besides the variation the stress in the beam section is a high stage its variation is not larger enough to reach the rupture value of 510 MPa. In addition, it is important to highlight that these stresses were obtained for an ultimate limit state, what does not mean that the bridge is unsafe for the current service condition.

The variation of stress in the pylon section were also obtained for each damage situations. The results are shown in the Table 38.

Table 38 - Variation of stress in the pylon section for the damage scenario 3 (loss of short cable)

Area reduction	Axial Load (kN)	Mxx (kN.m)	Myy (kN.m)	Stress (MPa)	Δ
0	-35261,00	5404,00	9461,00	35,02	
10%	-35169,98	5349,21	-9459,37	34,9	-0,34%
20%	-35065,24	5285,70	-9457,32	34,8	-0,63%
40%	-35045,44	5255,28	-9266,82	34,5	-1,48%

6.4 DAMAGE SCENARIO 4 – UNIFORM LOSS ON ALL THE CABLES

The objective of this last scenario is to analyse the structure behaviour under the condition of a uniform evolution of damage on a Serviceability Limit State (SLS). The damage simulation will be in the same ratio that was used in the last sections, with an area reduction of 10%, 20%, 40% and an additional case of 60%.

6.4.1 AXIAL LOAD

Graphic 18 shows the variation of axial force on the cables after the uniform area reduction.

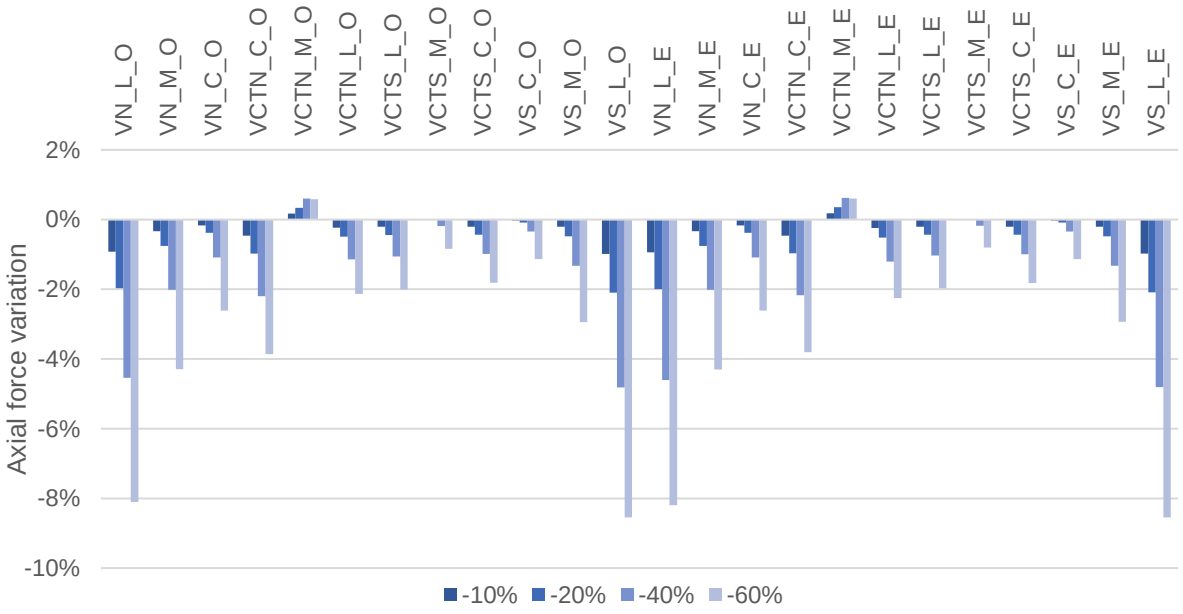

Graphic 18 - Axial Force variation for the damage scenario 4 (uniform loss)

As the variation of the loads are lower than the reduction on the cables area, it does not have an expressive participation on the stress variation. In the Graphic 19 it is notable that the variation in stress is manly caused by the section reduction, as they have almost the same variation value.

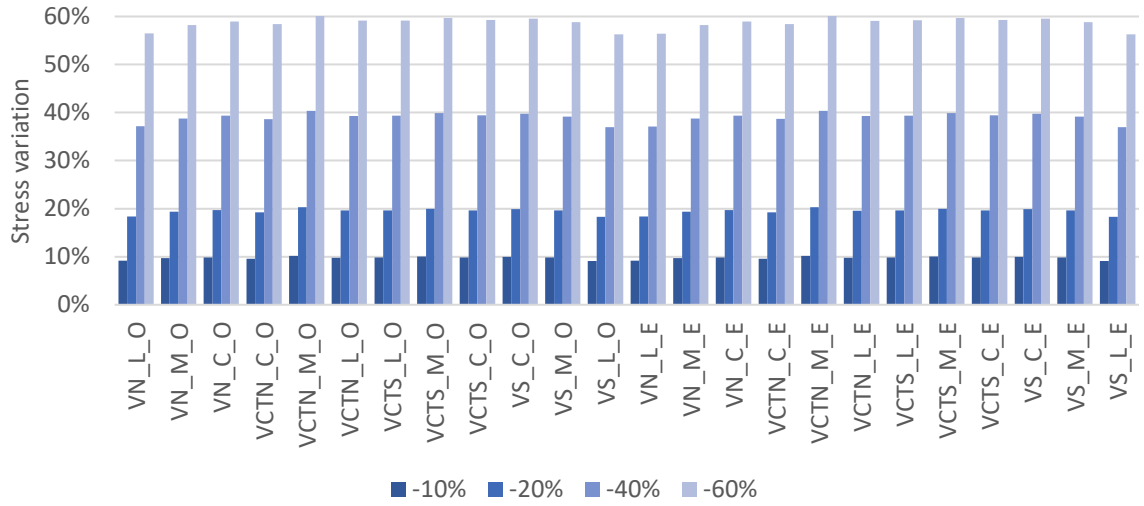

Graphic 19 - Stress variation in the cables for the damage scenario 4

6.4.2 DISPLACEMENT

Values for the displacement in the gravity direction were registered for each damage. The variation values found after the reduction on the cable cross section are displayed in the Graphic 20.

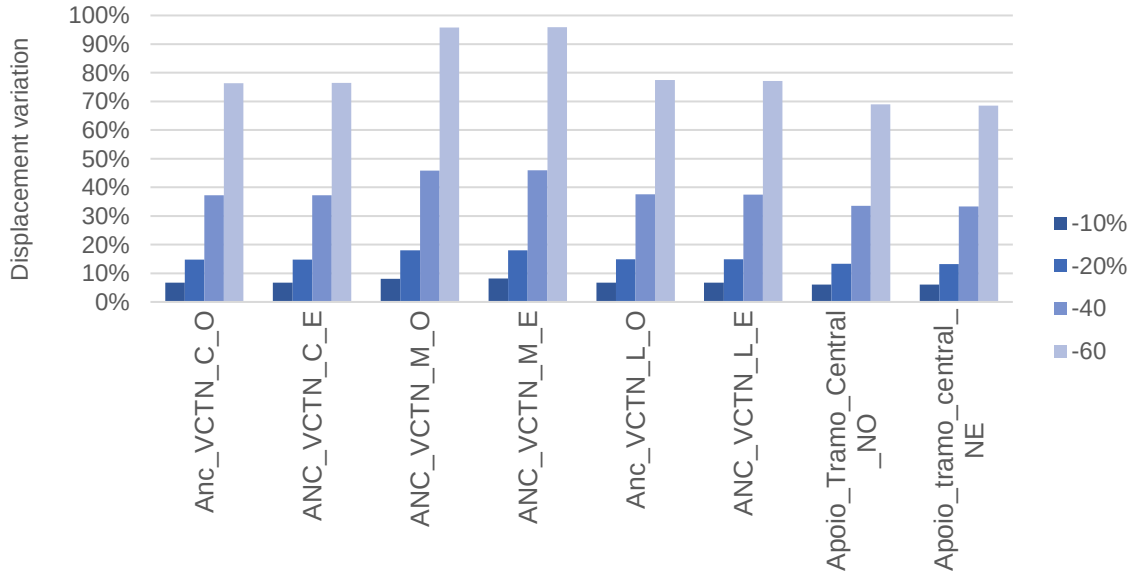

Graphic 20 - Displacement variation for the damage scenario 4 (uniform loss).

The displacements on the top of the tower and their variation are shown in the Table 35.

Table 39 - Displacements at the tower top for the damage scenario 4 (uniform loss).

Cable loss	XX	Δ_{xx}	YY	Δ_{yy}	ZZ	Δ_{zz}
0%	6,32	-	0	-	-0,337	-
-10%	6,71	6,17%	0	0,00%	-0,334	-0,89%
-20%	7,16	13,29%	0	0,00%	-0,33	-2,08%
-40%	8,3	31,33%	0	0,00%	-0,319	-5,34%

6.4.3 MODAL RESPONSE

Table 40 exposes the variation on the vibration modes and it is possible to identify that this scenario leads to a large distortion in this parameter.

Table 40 - Modal response variation for the damage scenario 4 (uniform loss).

	-10%	**-20%**	**-40**	**-60**
1	-3%	-7%	-14%	-24%
2	-3%	-6%	-12%	-21%
3	-3%	-6%	-13%	-23%
4	-2%	-4%	-9%	-16%
5	0%	0%	-4%	-10%
6	0%	0%	-2%	-9%
7	-2%	-3%	-4%	-4%
8	0%	-1%	-5%	-6%
9	-1%	-3%	-4%	-5%
10	-1%	-1%	-1%	-5%
11	-3%	-7%	-14%	-20%
12	-3%	-6%	-14%	-20%
13	-1%	-3%	-7%	-12%
14	-2%	-5%	-10%	-18%
15	0%	0%	-7%	-16%
16	0%	-1%	-5%	-13%
17	-3%	-6%	-8%	-8%
18	-3%	-6%	-8%	-8%
19	0%	0%	0%	-2%
20	-1%	-2%	-5%	-6%

6.4.4 ADJACENT MEMBERS

The variation of stress for the fourth damage scenario on the main beam of the deck is displayed in the Table 37.

Table 41 - Variation of stress in the double "I" section for the damage scenario 4 (uniform loss).

Area reduction	**Axial load (kN)**	**Myy (kN.m)**	**Stress (MPa)**	**Δ**
0%	-10079,89	18318,26	254,79	
10%	-10351,10	18345,64	256,94	0,8%

20%	-10672,29	18377,89	260,23	2,1%
40%	-11544,03	18464,46	267,1	4,8%
60%	-13017,39	18607,76	278,68	9,4%

As exposed in Table 41 for a serviceably condition this section can support a stress increase of 27% before the failure of the first cable.

For this scenario, the variation of stress in the pylon section are shown in the Table 42.

Table 42 - Variation of stress in the pylon section for the damage scenario 4 (uniform loss).

Area reduction	Axial load (kN)	Mxx (kN.m)	Myy (kN.m)	Stress (MPa)	Δ
0%	-22133,3	2504,752	-5017,24	-19,8	
10%	-22498,2	2663,798	-5229,76	-20,97	5,9%
20%	-22916,2	2846,839	-5474,63	-21,13	6,7%
40%	-23967,0	3311,288	-6097,65	-22,96	16,0%
60%	-25445,5	3978,553	-6998,57	-25,57	29,1%

6.5 DISCUSSION

With the results presented in the last sections of this chapter it was possible to extract some conclusions about the bridge structural behaviour under the four damage scenarios. Based on that, this section will discuss and review the obtained results.

First, the higher variation of stress is presented in Table 43 for each of the damage scenarios studied in this work.

Table 43 - Variation of stress in the cables most affected in each damage scenario.

Scenario	Cable with higher variation	-10%	-20%	-40%
1	VCTN_L_W	+10%	+22%	+58%
2	VCTN_M_W	+9%	+21%	+53%
3	VCTN_C_W	+9%	+20%	+52%
4	VS_L_O	+10%	+20%	+40%

Section 4.4 shows that the safety factor for the cables is 40%. As shown above, area reductions between 20% and 40% can lead to a state of risk to the structure. However, this value is not simple to determine, because the identification of cable loss is something complex to be done.

As shown in the Table 44, the variation of the cable stress is very low, even for the most affected cable in each case. Besides, this monitoring process could be inaccurate, as its value can suffer variation under

different weather condition. However, with a fixed monitoring system, that measures the weather parameters and cable forces, very accurate results could be obtained.

Table 44 - Variation of the axial force for each damage scenario.

Scenario	Cable with higher variation	-10%	-20%	-40%
1	VCTN_L_W	-1%	-2%	-5%
2	VCTN_M_W	-2%	-4%	-8%
3	VCTN_C_W	-2%	-4%	-9%
4	VS_L_O	0%	1%	1%

The displacements in each damage case is one of the most important values of this work. As it is shown in the Table 45, for early stages the variation of position is large and could be easily identified with a measurement work.

Table 45 - Displacement variation for each damage scenario.

Scenario	Cable with higher variation	-10%	-20%	-40%
1	ANC_VCTN_L_W	4%	9%	42%
2	ANC_VCTN_M_W	3%	7%	16%
3	ANC_VCTN_L_W	3%	7%	16%
4	ANC_VCTN_M_E	8%	18%	46%

The displacement in the top of the tower also could be measured, in order to monitor the damage progression in the stays. The results obtained for the displacements in the tower top are presented in the Table 46. However, these values are less expressive then those found for the deck.

Table 46 - Displacements on the tower top for the all the damage scenarios.

Scenario	Cable loss	XX	Δ_{xx}	YY	Δ_{yy}	ZZ	Δ_{zz}
1	-40%	6,25	-1,11%	0	0,00%	-0,333	-1,19%
2	-40%	6,18	-2,22%	0	0,00%	-0,34	0,89%
3	-40%	6,22	-1,58%	0	0,00%	-0,327	-2,97%
4	-40%	8,3	31,33%	0	0,00%	-0,319	-5,34%

The structure presents large variation in the vibration modes for a uniform damage scenario. This response is manly caused because the cable loss decreases the structural stiffness. However, in scenarios where only one cable is damaged the variation of the global stiffness is smaller and the vibration modes variation is less expressive.

Table 47 - Variation in the vibration modes for different damage scenarios

	Scenario 1	Scenario 2	Scenario 3	Scenario 4
% Area reduction	**40%**	**40%**	**40%**	**40%**
1	-3%	0%	0%	-14%
2	-2%	-1%	0%	-12%
3	-2%	0%	0%	-13%
4	-1%	-1%	0%	-9%
5	0%	0%	0%	-4%
6	0%	0%	0%	-2%
7	-1%	0%	0%	-4%
8	0%	0%	0%	-5%
9	0%	0%	0%	-4%
10	-1%	0%	0%	-1%
11	0%	-2%	1%	-14%
12	0%	-1%	0%	-14%
13	-1%	0%	0%	-7%
14	-1%	0%	0%	-10%
15	0%	0%	0%	-7%
16	0%	0%	0%	-5%
17	0%	-2%	1%	-8%
18	0%	0%	0%	-8%
19	0%	0%	0%	-0%
20	0%	0%	1%	-5%

For the deck and pylon section the stress variation is very low for most cases the damage reduces slightly the stress on these members.

Table 48 and Table 49 shoes the variation in the stress for the all the damage scenarios studied. For the main beam, the stress variation for all the scenarios considered is less than 5%. For the pylon, in the scenario where an uniform damage was applied to the cables a higher variation of 16% was noticed. Furthermore, in ULS the 40% variation would cause a cable rupture and for any of the cases presented below neither the beam nor the pylon would be close to failure.

Table 48 – Stress variation for the double "I" beam

Scenario	Area reduction	Axial load (kN)	Myy (kN.m)	Stress (MPa)	Δ
1	40%	16525,19	25891,6	377,9	-0,50%
2	40%	16525,19	25891,6	377,9	-0,50%
3	40%	18701,61	25823,6	-390	2,90%

4	40%	-11544	18464,46	267,1	4,80%

Table 49 - Stress variation for the pylon section

Scenario	Area reduction	Axial load (kN)	Mxx (kN.m)	Myy (kN.m)	Stress (MPa)	Δ
1	40%	-35063,2	5433,48	-9470,02	34,97	0,00%
2	40%	-35045,4	5255,279	-9266,82	34,5	-0,86%
3	40%	-35045	5255,28	-9266,8	34,5	-1,48%
4	40%	-23967	3311,288	-6097,65	-22,96	16,00%

7
CONCLUSIONS

The major objective of this work was to identify the structural behaviour of the *Edgar Cardoso Bridge* under various scenarios of damage. The structural analysis was done through a finite element model of the structure validated with previous data from a rehabilitation report and from measurement works done in the bridge.

The first conclusion of this work is that measurement is a very helpful tool to create a reliable finite element model. As it was exposed in this work, a 95% correspondence was obtained when comparing the data collected in the real structure with the values obtained by the FEM software.

After running all the FE analysis, a safety evaluation of the most susceptible sections of the structure was done. Through this process, it was possible to verify the structural safety of the bridge elements and evaluate the structural condition. The conclusion taken from this analysis was that for the pylon and for the cables the safety factor is at least 40%. For the double "I" beam, it was found that this element has already reached the yielding stage but it is far from the rupture strength (values presented for an ultimate limit stage). Resuming, it was found that cables could lose less than 40% of their section before failure, without considering the fatigue effects .

In chapters 5 and 6 an evaluation and discussion of four scenarios of cable loss was done. After that it was possible to conclude that a force redistribution occurs as the cables lose section, but this effect is less conditioning, because the reduction in the axial load of the cable affected by the damage is smaller than the area reduction and leads to a stress rise. In addition, it was possible to conclude that the pylon and the main beam of the deck are in a safe condition and the failure would occur first in the cables. The dynamic behaviour of the bridge was also analysed for every scenario. It was observed that only in a uniform damage distribution scenario more pronounced frequency variations occurred. The most evident effect during the damage evolution was found in the deck displacements, where large values were noticed even for scenarios with less damage.

Concluding, it is possible to state that all the objectives set for this dissertation were reached. A reliable model of the bridge was achieved through its validation with parameters measured in the real structure. The FEM analysis allowed to verify the structural behaviour for each degradation scenario. Furthermore, this work can be used as a guideline for further monitoring process, as it was possible to identify which effects are more pronounced during a failure process.

REFERENCES

[1] Gimsing, N., Georgakis, C. *Cable Supported Bridges.* John Wiley & Sons, Chichester, 2012.

[2] Chaussin, R., et al. *Cable Stays*. Service d'Etudes Techniques des Routes et Autoroutes (SETRA), Paris, 2002.

[3] Manterola, J. *Puentes: apuntes para su diseño, cálculo y construcción.* Colegio de Ingenieros de Caminos Canales y Puertos, Madrid, 2006.

[4] Caetano, E. S. *Cable vibrations in cable-stayed bridges*. IABSE, Zürich, 2007.

[5] Caetano, E. S. *Dynamics of Cable-stayed Bridges: Experimental Assessment of Cable-Structure Interaction.* Doctorate Dissertation, Faculty of Engineering of University of Porto, 2001.

[6] Podolny, W. & Scalzi, J. *Construction and Design of Cable-Stayed Bridges*. John Wiley &

Sons, Michigan, 1976.

[7] Yang, Y., Wang, X., Wub, Z. *Long-span cable-stayed bridge with hybrid arrangement of FRP cables.* Elsevier, 17/01/2020, 0263-8223, Elsevier.

[8] Caetano, E. S. Cables. In *Innovative Bridge Design Handbook: Construction, Rehabilitation and Maintenance*, 555-593, Elsevier, Waltham, 2015.

[9] Zoli, T., Steinhouse, J. *Some considerations in the design of long span bridges against progressive collapse*, 2007.

[10] Starossek, U. *Progressive Collapse of Bridges-Aspects of Analysis and Design*. International Symposium on Sea-Crossing Long-Span Bridges, Mokpo, Korea, Feb. 15-17, 2006.

[11] Wolff, M and Starossek, U, *Cable-loss analyses and collapse behavior of cable-stayed bridges.* The Fifth International Conference on Bridge Maintenance, Safety and Management, July 11-15, 2020, Philadelphia, USA.

[12] Ruiz-Teran, A, Aparicio, A. *Response of under-deck cable-stayed bridges to the accidental breakage of stay cables*. Engineering Structures, July 2009, pp. 1425-1434, Elsevier.

[13] Jungwirth, D., et al. *Acceptance of stay cable systems using prestressing steels*. FIB Bulleting No. 30, 2005, FIB..

[14] Starossek, U. *Progressive Collapse of Bridges — Aspects of Analysis and Design Previous Research*. Symposium A Quarterly Journal In Modern Foreign Literatures, pp. 1–22. 2006.

[15] Starossek, U. *Typology of progressive collapse*. Engineering Structures, September 2007, pp. 2302–2307. Elsevier.

[16] Olamigoke, O. *Structural Response Of Cable-Stayed Bridges To Cable Loss*. Doctorate Dissertation. Faculty of Engineering and Physical Sciences of University of Surrey Guildford. 2017.

University of Surrey. Guildford, Surrey. March 2017

[17] Khan, S. Z. (2010). *Design audit of the Phu My cable-stayed bridge, Vietnam.* Proceedings of the ICE - Bridge Engineering, 01/12/2020, pp. 203–211, Ice Publishing.

[18] Ngeljaratan, L., Moustafa, M. *Structural health monitoring and seismic response assessment of bridgestructures using target-tracking digital image correlation.* Engineering Structures, 15 June 2020 Elsevier, Reno.

[19] Caetano, E. S. *Experimental Identification of Dynamic Parameters in Structural Systems.* Maters Dissertation, Faculty of Engineering of University of Porto, 1992.

[20] Cunha, A., Caetano, E. S. *Experimental Modal Analysis of Civil Engineering Structures.* Sound and Vibration, Vol. 6, No. 40, 2006, pp. 12-20, Faculty of Engineering of University of Porto, Porto.

[21] Azevedo, A. *Método dos elementos finitos*. Faculty of Engineering of University of Porto, Porto, 2003.

[22] Caetano, E. S. *Determinação das forças instaladas nos tirantes da Ponte Edgar Cardoso na Figueira da Foz*. Technical Report. Faculty of Engineering of University of Porto. 2018

[23] Rito, A., Appleton, J., et al. *Ponte da Figueira da Foz e sues acessos: Inspecção e Elaboração de Estudo de Reabilitação de Obra de Arte.* Rehabilitation report. A2P. 1998.

[24] Eurocode 0: Basis of structural design (EN 1990). European Committee for Standardization (CEN), 2000.

[25] Eurocode 1: Actions on structures – Part 1-1: General actions – Densities, self-weight, imposed loads for buildings (EN 1991-1-1). European Committee for Standardization (CEN), 2009.

[26] Eurocode 1: Actions on structures – Part 1-4: General actions – Wind actions (EN 1991-1-4). European Committee for Standardization (CEN), 2010.

[27] Eurocode 1: Actions on structures – Part 2: Traffic loads on bridges (EN 1991-2). European Committee for Standardization (CEN), 2017.

[28] Eurocode 8: Design of structures for earthquake resistance - Part 1: General rules, seismic actions and rules for buildings (EN 1998-1). European Committee for Standardization (CEN), 2004.

ANNEX

Annex A – Load combination.

Annex B - Results extracted from the FEM model.

Annex C – Vibration modes.

ANNEX A: Load combinations.

Coefficients used to the Ultimate Limit State (ULS)

	Permanent	Base Action	Other Actions	
	γg	γq	γg + ψ	
1	**1,35** Dead	**1,5** Traf.	1,5	0,7
2	**1,35** Dead	**1,5** Traf.	1,5	0,7 Vento
3	**1,35** Dead	**1,5** Traf.	1,5	0,7 Sismo
4	**1,35** Dead	**1,5** Vento	1,5	0,7
5	**1,35** Dead	**1,5**	1,5	0,7 Traf.
6	**1,35** Dead	**1,5**	1,5	0,7 Sismo
7	**1,35** Dead	**1,5** Sismo	1,5	0,7
8	**1,35** Dead	**1,5** Sismo	1,5	0,7 Traf.
9	**1,35** Dead	**1,5** Sismo	1,5	0,7 Vento

Serviceability Limit State (SLS)

Characteristic combination

	Permanent	Base Action	Other Actions
	γg	ψ	ψ
1	**1** Dead	**1** Traf.	0,7
2	**1** Dead	**1** Traf.	0,7 Vento
3	**1** Dead	**1** Traf.	0,7 Sismo
4	**1** Dead	**1** Vento	0,7
5	**1** Dead	**1**	0,7 Traf.
6	**1** Dead	**1**	0,7 Sismo
7	**1** Dead	**1** Sismo	0,7
8	**1** Dead	**1** Sismo	0,7 Traf.
9	**1** Dead	**1** Sismo	0,7 Vento

Frequent combination

	Permanent		Base Action		Other Actions	
	γg		ψ		ψ	
1	**1**	Dead	0,7	Traf.	0,5	
2	**1**	Dead	**0,7**	Traf.	**0,5**	Vento
3	**1**	Dead	**0,7**	Traf.	**0,5**	Sismo
4	**1**	Dead	**0,7**	Vento	**0,5**	
5	**1**	Dead	**0,7**		**0,5**	Traf.
6	**1**	Dead	**0,7**		**0,5**	Sismo
7	**1**	Dead	**0,7**	Sismo	**0,5**	
8	**1**	Dead	**0,7**	Sismo	**0,5**	Traf.
9	**1**	Dead	**0,7**	Sismo	**0,5**	Vento

Quasi-Permanent Load combination

	Permanent		Base Action		Other Actions	
	γg		ψ		ψ	
1	**1**	Dead	**0,5**	Traf.	**0,5**	
2	**1**	Dead	**0,5**	Traf.	**0,5**	Vento
3	**1**	Dead	**0,5**	Traf.	**0,5**	Sismo
4	**1**	Dead	**0,5**	Vento	**0,5**	
5	**1**	Dead	**0,5**		**0,5**	Traf.
6	**1**	Dead	**0,5**		**0,5**	Sismo
7	**1**	Dead	**0,5**	Sismo	**0,5**	
8	**1**	Dead	**0,5**	Sismo	**0,5**	Traf.
9	**1**	Dead	**0,5**	Sismo	**0,5**	Vento

ANNEX B: Results extracted from the FEM model.

Axial load variation for damage scenario 1

	Normal	-10%	-20%	-40%
VN_L_W	13987,29	13980,402	13850,929	13651,636
VN_M_W	10413,613	10418,302	10442,929	10485,775
VN_C_W	7073,618	7066,945	7059,018	7037,667
VCTN_C_W	6078,277	6078,421	6078,583	6079,171
VCTN_M_W	10859,151	10871,445	11142,346	11556,348
VCTN_L_W	17674,231	17496,973	17286,631	16719,452
VCTS_L_W	17825,674	17830,852	17873,179	17945,034
VCTS_M_W	10604,441	10609,05	10619,093	10640,31
VCTS_C_W	6299,539	6300,701	6299,483	6299,088
VS_C_W	7166,872	7166,727	7166,556	7166,118
VS_M_W	10505,017	10506,71	10510,943	10519,682
VS_L_W	13966,131	13924,904	13997,421	14044,276
VN_L_E	14007,99	14017,666	14029,198	14061,173
VN_M_E	10417,602	10427,003	10419,138	10421,463
VN_C_E	7078,928	7078,715	7078,466	7077,831
VCTN_C_E	6077,301	6074,305	6070,742	6060,972
VCTN_M_E	10870,299	10988,619	10872,804	10876,217
VCTN_L_E	17699,835	17720,549	17745,218	17813,578
VCTS_L_E	17844,526	17847,319	17814,497	17768,225
VCTS_M_E	10610,029	10611,146	10607,906	10605,11
VCTS_C_E	6299,187	6299,524	6302,519	6307,734
VS_C_E	7170,791	7170,63	7170,439	7169,9
VS_M_E	10507,282	10507,724	10506,029	10504,139
VS_L_E	13982,617	13976,758	13969,748	13949,864

Axial load variation for damage scenario 2

	Normal	**-10%**	**-20%**	**-40%**
VN_L_W	13987,29	14007,551	14030,817	14090,004
VN_M_W	10413,613	10386,059	10354,374	10274,242
VN_C_W	7073,618	7084,84	7097,746	7130,399
VCTN_C_W	6078,277	6162,291	6258,982	6503,674
VCTN_M_W	10859,151	10681,32	10476,781	9959,126
VCTN_L_W	17674,231	17771,501	17883,266	18166,639
VCTS_L_W	17825,674	17831,949	17839,28	17857,545
VCTS_M_W	10604,441	10602,374	10599,988	10593,975
VCTS_C_W	6299,539	6298,228	6296,708	6292,891
VS_C_W	7166,872	7166,886	7166,904	7166,945
VS_M_W	10505,017	10505,028	10505,043	10505,074
VS_L_W	13966,131	13968,907	13972,153	13980,231
VN_L_E	14007,99	14007,907	14007,87	14007,621
VN_M_E	10417,602	10417,777	10417,98	10418,498
VN_C_E	7078,928	7078,981	7079,045	7079,216
VCTN_C_E	6077,301	6076,977	6076,597	6075,845
VCTN_M_E	10870,299	10872,387	10874,765	10880,744
VCTN_L_E	17699,835	17700,577	17701,557	17703,662
VCTS_L_E	17844,526	17843,789	17842,835	17840,643
VCTS_M_E	10610,029	10609,597	10609,109	10607,864
VCTS_C_E	6299,187	6299,119	6299,054	6298,866
VS_C_E	7170,791	7170,736	7170,671	7170,51
VS_M_E	10507,282	10507,269	10507,251	10507,214
VS_L_E	13982,617	13982,478	13982,268	13981,84

Axial load variation for damage scenario 3

	Normal	**-10%**	**-20%**	**-40%**
VN_L_O	13987,29	13980,438	13972,557	13952,55
VN_M_O	10413,613	10419,405	10426,073	10442,95
VN_C_O	7073,618	7064,964	7055,024	7029,886
VCTN_C_O	6078,277	5972,349	5850,557	5542,421
VCTN_M_O	10859,151	10908,614	10965,492	11109,441
VCTN_L_O	17674,231	17674,23	17674,215	17673,985
VCTS_L_O	17825,674	17825,926	17826,193	17827,004
VCTS_M_O	10604,441	10603,743	10602,945	10600,92
VCTS_C_O	6299,539	6299,248	6298,918	6298,065
VS_C_O	7166,872	7166,927	7166,99	7167,153
VS_M_O	10505,017	10504,827	10504,607	10504,057
VS_L_O	13966,131	13965,801	13965,413	13964,49
VN_L_E	14007,99	14007,395	14006,711	14005,049
VN_M_E	10417,602	10417,556	10417,497	10417,349
VN_C_E	7078,928	7078,985	7079,039	7079,167
VCTN_C_E	6077,301	6078,448	6079,723	6082,883
VCTN_M_E	10870,299	10870,116	10869,921	10869,44
VCTN_L_E	17699,835	17698,525	17697,02	17693,361
VCTS_L_E	17844,526	17845,135	17845,852	17847,519
VCTS_M_E	10610,029	10610,001	10609,967	10609,9
VCTS_C_E	6299,187	6299,048	6298,885	6298,493
VS_C_E	7170,791	7170,821	7170,856	7170,943
VS_M_E	10507,282	10507,247	10507,208	10507,104
VS_L_E	13982,617	13982,709	13982,822	13983,041

Axial load variation for damage scenario 4

	Normal	**-10%**	**-20%**	**-40%**	**-60%**
VN_L_O	11004,7	10903,05	10788,07	10504,79	10113,27
VN_M_O	7670,665	7645,098	7612,678	7516,332	7341,556
VN_C_O	5131,766	5123,294	5112,161	5075,884	4997,835
VCTN_C_O	4436,472	4415,92	4393,214	4339,036	4265,32
VCTN_M_O	7753,316	7766,912	7779,782	7799,874	7798,449
VCTN_L_O	12937,68	12908,2	12874,66	12789,91	12661,44
VCTS_L_O	13108,62	13081,31	13050,07	12970,14	12845,63
VCTS_M_O	7498,047	7499,122	7497,932	7483,789	7435,508
VCTS_C_O	4654,941	4645,408	4634,87	4609,162	4570,578
VS_C_O	5225,009	5223,519	5220,681	5206,921	5166,034
VS_M_O	7762,291	7746,152	7724,979	7659,147	7533,92
VS_L_O	10995,47	10887,36	10765,27	10465,68	10055,48
VN_L_E	11025,94	10922,62	10805,86	10518,67	10122,71
VN_M_E	7674,697	7649,117	7616,644	7520,01	7344,565
VN_C_E	5135,184	5126,725	5115,597	5079,271	5000,962
VCTN_C_E	4434,724	4414,394	4391,957	4338,494	4265,77
VCTN_M_E	7760,133	7774,175	7787,466	7808,231	7806,932
VCTN_L_E	12971,55	12940,12	12904,44	12814,63	12679,58
VCTS_L_E	13113,52	13086,89	13056,37	12978,04	12855,33
VCTS_M_E	7501,044	7502,353	7501,432	7487,977	7440,668
VCTS_C_E	4656,336	4646,7	4636,063	4610,204	4571,652
VS_C_E	5227,13	5225,642	5222,806	5209,042	5168,086
VS_M_E	7763,779	7747,718	7726,627	7660,96	7535,841
VS_L_E	11001,75	10893,84	10771,91	10472,45	10061,89

Displacement for the damage scenario 1

	Normal	**-10%**	**-20%**	**-40%**
ANC_VCTN_C_O	-0,236773	-0,236754	-0,236732	-0,236605
ANC_VCTN_M_O	-0,530332	-0,540238	-0,551999	-0,634272
ANC_VCTN_L_O	-0,959514	-0,998261	-1,044258	-1,365339
ANC_VCTN_L_E	-0,961874	-0,963707	-0,965891	-0,981909
ANC_VCTN_M_E	-0,531568	-0,531824	-0,53213	-0,534312
ANC_VCTN_C_E	-0,237044	-0,236988	-0,23692	-0,23647
Apoio_tramo_central_NE	-1,104578	-1,106874	-1,10961	-1,129817
Apoio_Tramo_Central_NO	-1,103804	-1,147986	-1,20043	-1,566219

Displacement for the damage scenario 2

	Normal	**-10%**	**-20%**	**-40%**
Anc_VCTN_C_W	-0,236773	-0,240498	-0,244784	-0,255636
ANC_VCTN_M_W	-0,530332	-0,546621	-0,565365	-0,612857
Anc_VCTN_L_W	-0,959514	-0,966423	-0,974356	-0,994483
ANC_VCTN_L_E	-0,961874	-0,961858	-0,961854	-0,961804
ANC_VCTN_M_E	-0,531568	-0,531725	-0,531905	-0,532355
ANC_VCTN_C_E	-0,237044	-0,237054	-0,237065	-0,237102
Apoio_tramo_central_NE	-1,104578	-1,104565	-1,104569	-1,104524
Apoio_tramo_Central_NW	-1,103804	-1,108413	-1,11369	-1,127112

Displacement for the damage scenario 3

	Normal	**-10%**	**-20%**	**-40%**
Anc_VCTN_C_O	-0,236773	-0,24426	-0,252875	-0,274678
ANC_VCTN_M_O	-0,530332	-0,533328	-0,536772	-0,545486
Anc_VCTN_L_O	-0,959514	-0,958875	-0,95814	-0,956259
ANC_VCTN_L_E	-0,961874	-0,961778	-0,961668	-0,961405
ANC_VCTN_M_E	-0,531568	-0,531579	-0,531594	-0,531634
ANC_VCTN_C_E	-0,237044	-0,237143	-0,237255	-0,237536
Apoio_tramo_central_NE	-1,104578	-1,104449	-1,1043	-1,103944
Apoio_tramo_Central_NO	-1,103804	-1,102512	-1,101023	-1,097231

Displacement for the damage scenario 4

	0	**-10%**	**-20%**	**-40**	**-60**
Anc_VCTN_C_O	-0,11214	-0,11966	-0,1287	-0,15385	-0,19781
ANC_VCTN_C_E	-0,11235	-0,11989	-0,12896	-0,15417	-0,19827
ANC_VCTN_M_O	-0,2292	-0,24784	-0,27045	-0,33439	-0,44874
ANC_VCTN_M_E	-0,23016	-0,2489	-0,27164	-0,33591	-0,45076
Anc_VCTN_L_O	-0,44687	-0,4771	-0,51347	-0,61494	-0,79327
ANC_VCTN_L_E	-0,45022	-0,48057	-0,51707	-0,61881	-0,79737
Apoio_Tramo_Central_NO	-0,53438	-0,56668	-0,60551	-0,71364	-0,90323
Apoio_tramo_central_NE	-0,53778	-0,57012	-0,60897	-0,71706	-0,90638

Variation on the vibration modes for damage scenario 1

	Normal	**-10%**	**-20**	**-40**
1	0,493331763	0,491063043	0,488209605	0,479718111
2	0,575567438	0,573792458	0,571722485	0,566475944
3	0,68831529	0,685369166	0,682041841	0,674006396
4	0,830813081	0,829136648	0,827113975	0,821801589
5	0,843837994	0,843678675	0,843577866	0,843256177
6	0,844540034	0,844473464	0,844440965	0,844411286
7	0,873280569	0,872072293	0,870794051	0,868101576
8	0,908142274	0,90769711	0,90720966	0,906104677
9	0,931500408	0,931479931	0,931497313	0,931021715
10	0,939669165	0,937671643	0,935731729	0,932500045
11	1,13942723	1,139408461	1,13938581	1,139317223
12	1,156704542	1,1563059	1,155828582	1,154537985
13	1,188115172	1,186520469	1,184816202	1,181124623
14	1,310759097	1,30775051	1,304642987	1,298264683
15	1,442076871	1,442130319	1,442186741	1,44218426
16	1,468019771	1,468031996	1,468040374	1,468037334
17	1,562283154	1,562284121	1,562281348	1,56224013
18	1,587574925	1,587149759	1,586609172	1,58545132
19	1,679854171	1,679853502	1,679853892	1,679851821
20	1,790666979	1,790392038	1,790101318	1,789463537

Variation on the vibration modes for damage scenario 2

	Normal	**-10%**	**-20**	**-40**
1	0,493331763	0,492938798	0,492474607	0,49123996
2	0,575567438	0,5749756	0,574287031	0,572510997
3	0,68831529	0,687746836	0,687069213	0,685349278
4	0,830813081	0,830014428	0,829072801	0,826598924
5	0,843837994	0,843851045	0,843847347	0,843865057
6	0,844540034	0,844541087	0,844539645	0,844541802
7	0,873280569	0,873164998	0,873031002	0,872697391
8	0,908142274	0,908031489	0,90790126	0,907570393
9	0,931500408	0,931513486	0,931511348	0,931531242
10	0,939669165	0,939666429	0,939661896	0,939650431
11	1,13942723	1,135120704	1,129021143	1,111661679
12	1,156704542	1,154159906	1,152456612	1,150668939
13	1,188115172	1,188086744	1,188036761	1,187991788
14	1,310759097	1,310628478	1,310441141	1,310064993
15	1,442076871	1,442153447	1,442153203	1,442266885
16	1,468019771	1,468033135	1,468030725	1,468043338
17	1,562283154	1,556874281	1,550101431	1,533328325
18	1,587574925	1,585115988	1,583322408	1,581259082
19	1,679854171	1,679853752	1,679853182	1,679852327
20	1,790666979	1,790113981	1,789531772	1,788287076

Variation on the vibration modes for damage scenario 3

	Normal	**-10%**	**-20%**	**-40**
1	0,493331763	0,493324057	0,493315096	0,493292115
2	0,68831529	0,688303513	0,688301488	0,688290348
3	0,575567438	0,575513581	0,575450795	0,575286973
4	0,830813081	0,830756412	0,83068679	0,83050176
5	0,843837994	0,843835941	0,843833099	0,843952639
6	0,844540034	0,844505336	0,844465071	0,844354547
7	0,873280569	0,872836127	0,872302423	0,870836803
8	0,908142274	0,908118397	0,908090512	0,908016689
9	0,931500408	0,931499314	0,931499006	0,931597719
10	0,939669165	0,939342311	0,938954091	0,93790919
11	1,13942723	1,137364002	1,13434211	1,124250904
12	1,156704542	1,154768175	1,153024137	1,150477057
13	1,188115172	1,187706929	1,187348593	1,186649426
14	1,310759097	1,310614748	1,310494604	1,310101138
15	1,442076871	1,442075737	1,442130267	1,4421983
16	1,468019771	1,468017935	1,46802789	1,468030919
17	1,562283154	1,559580259	1,555882837	1,544280268
18	1,587574925	1,585565682	1,583795292	1,580736156
19	1,679854171	1,679853903	1,679853599	1,679854148
20	1,790666979	1,787346161	1,783225997	1,772251613

Variation on the vibration modes for damage scenario 4

	Normal	**-10%**	**-20%**	**-40**	**-60**
1	0,493332	0,477686	0,460827	0,422312	0,373825
2	0,575567	0,560082	0,543276	0,504503	0,455142
3	0,688315	0,668226	0,646325	0,595527	0,530361
4	0,830813	0,815871	0,798306	0,754593	0,695136
5	0,843838	0,843075	0,840845	0,806818	0,755335
6	0,84454	0,843175	0,842492	0,824773	0,76921
7	0,873281	0,859646	0,844327	0,841474	0,840618
8	0,908142	0,904531	0,899966	0,863967	0,850128
9	0,9315	0,920784	0,902595	0,898182	0,883726
10	0,939669	0,931079	0,930651	0,929685	0,895536
11	1,139427	1,102841	1,064166	0,9796	0,908181
12	1,156705	1,120504	1,08244	1,000022	0,927906
13	1,188115	1,170864	1,151541	1,104547	1,040661
14	1,310759	1,281995	1,250365	1,175758	1,079692
15	1,442077	1,442024	1,441954	1,344867	1,214884
16	1,46802	1,467982	1,459848	1,395802	1,282219
17	1,562283	1,512497	1,467869	1,441814	1,434431
18	1,587575	1,544063	1,497703	1,468093	1,467118
19	1,679854	1,679843	1,679832	1,679793	1,643401
20	1,790667	1,771058	1,749791	1,701439	1,679605

ANNEX C – Vibration modes.

Vibration modes

1 – 0,50 Hz

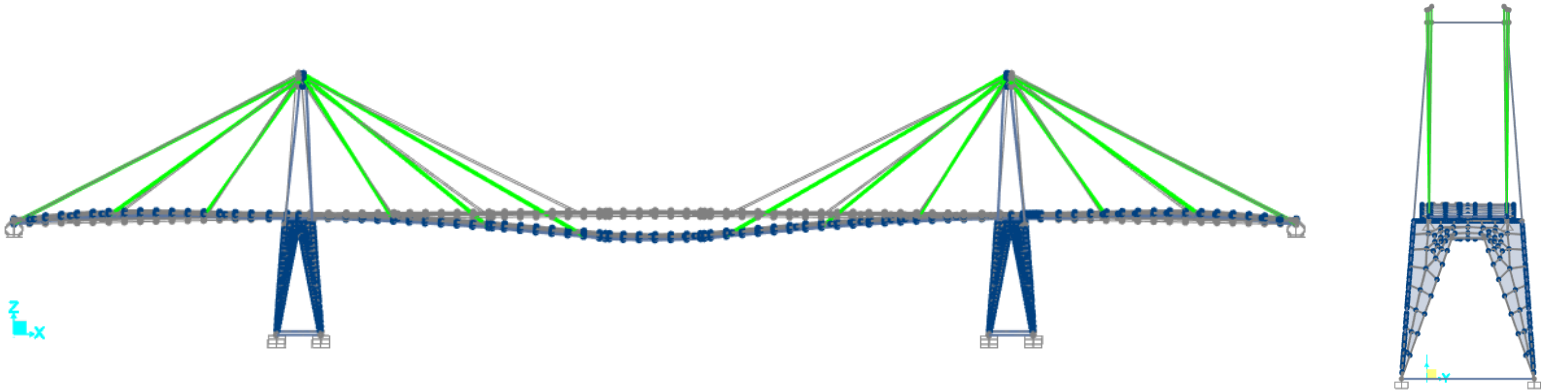

2 – 0,58 Hz

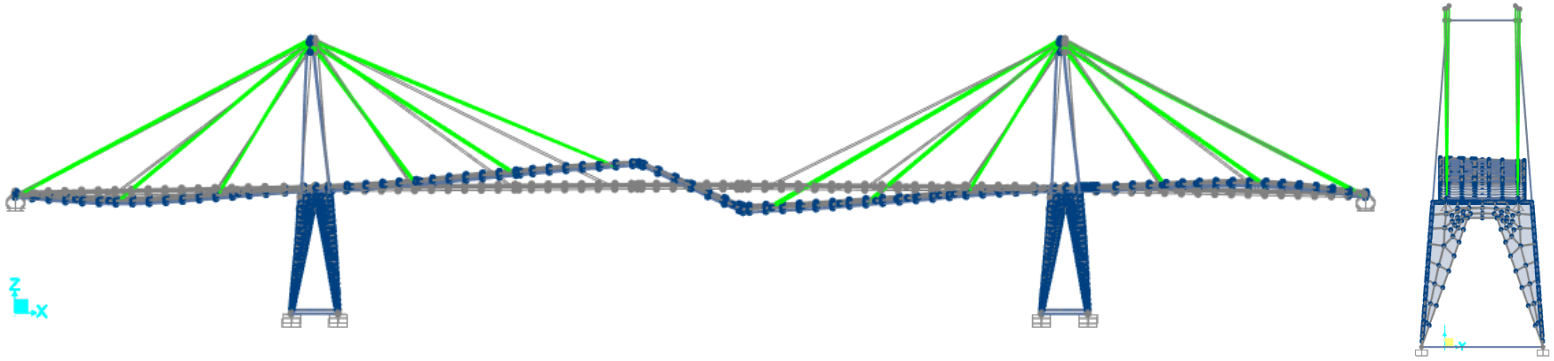

3 – 0,69 Hz

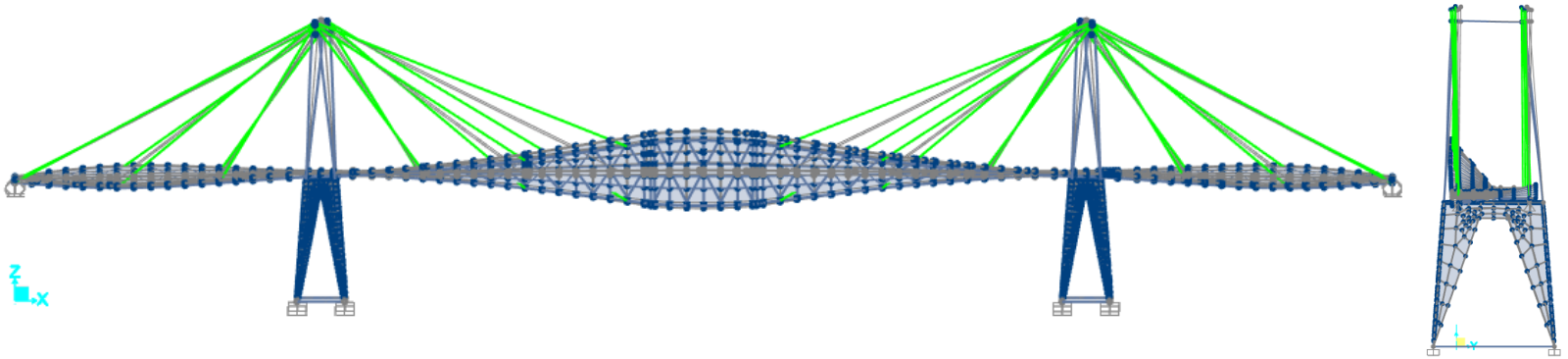

4 - 0,83 Hz

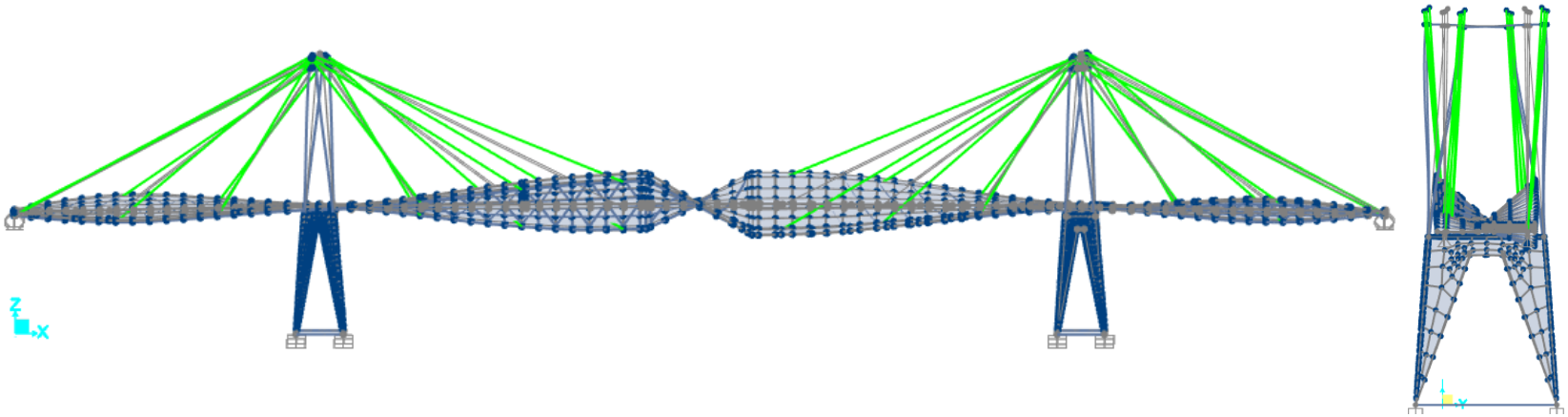

5 – 0,843 Hz

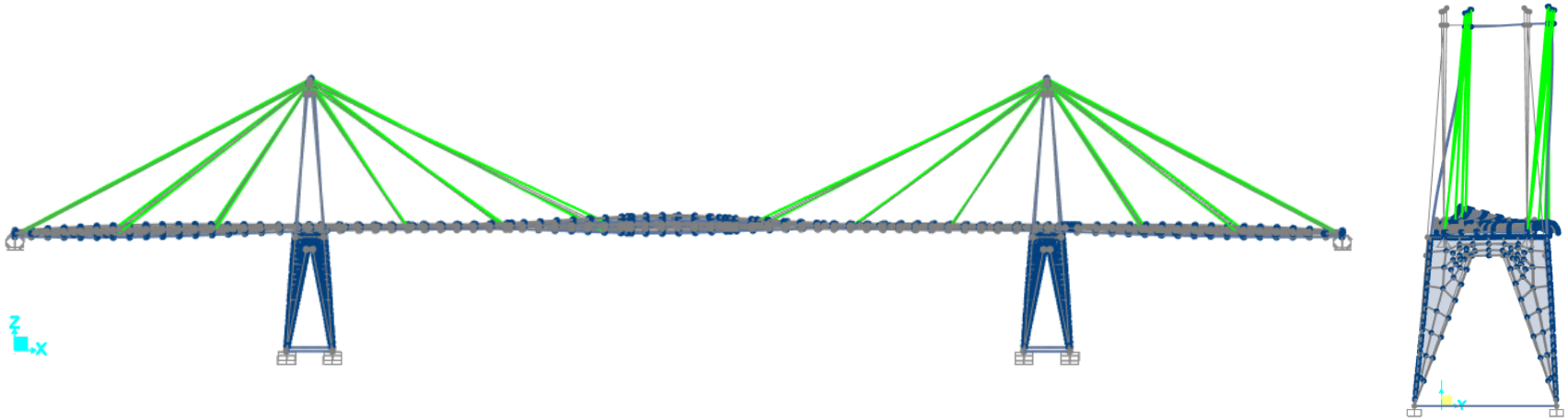

7 – 0,844

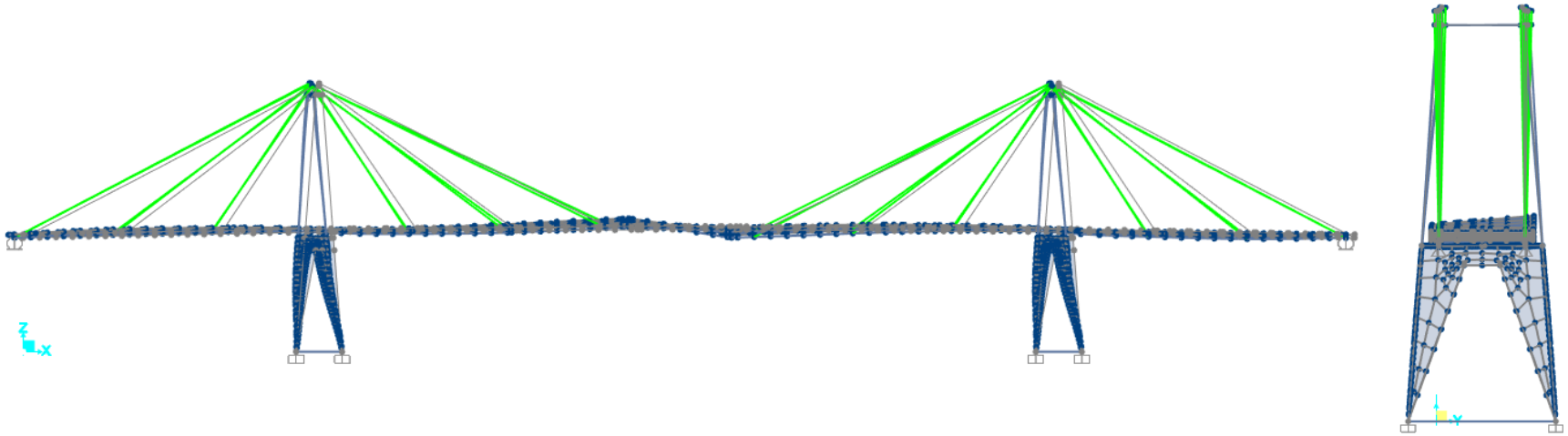

8 – 0,873 Hz

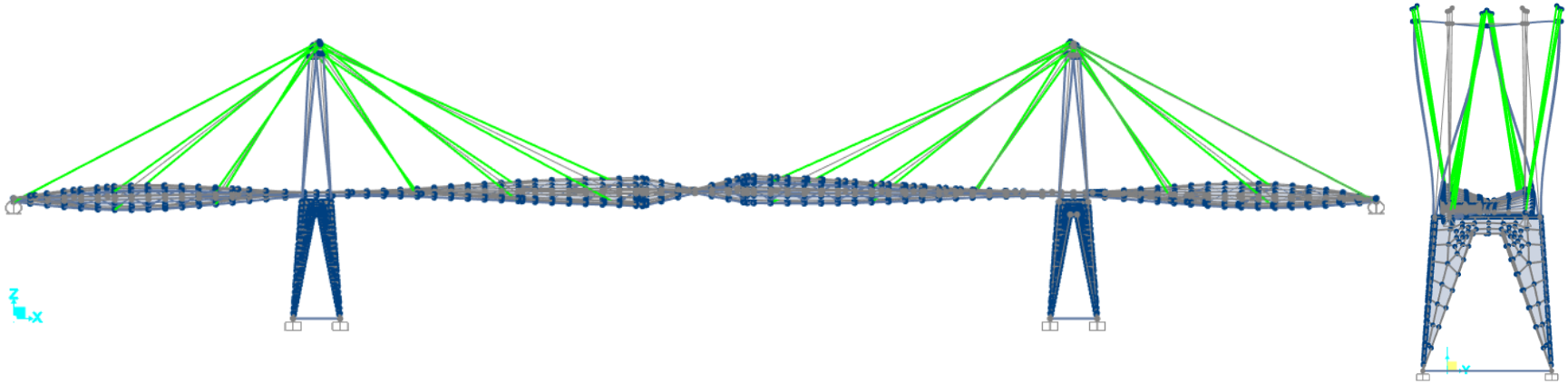

9 – 0,908 Hz

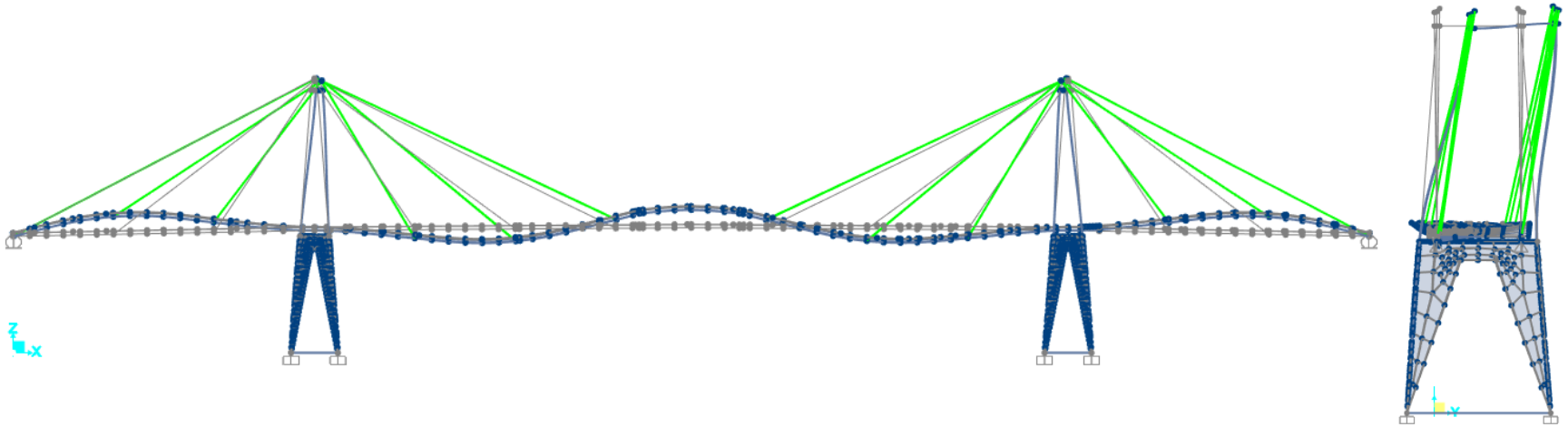

10- 0,94 Hz

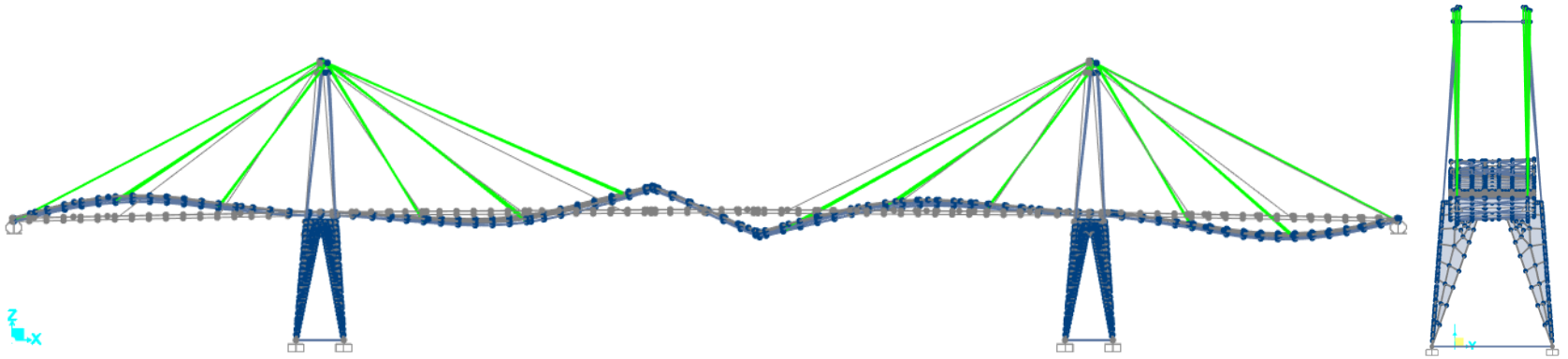

11 – 1,13 Hz

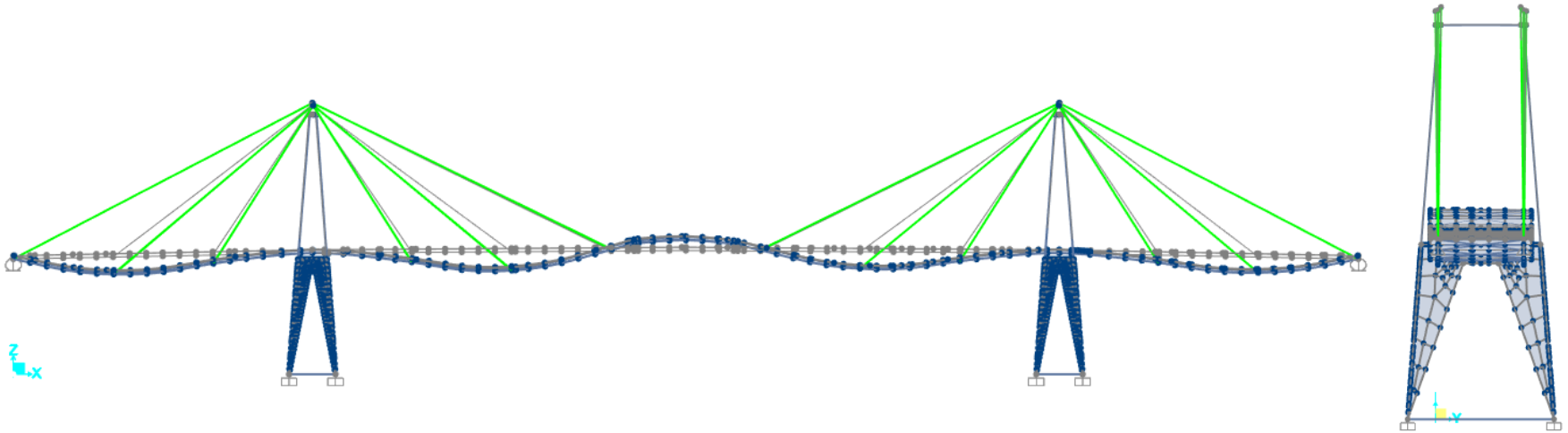

12 – 1,157 Hz

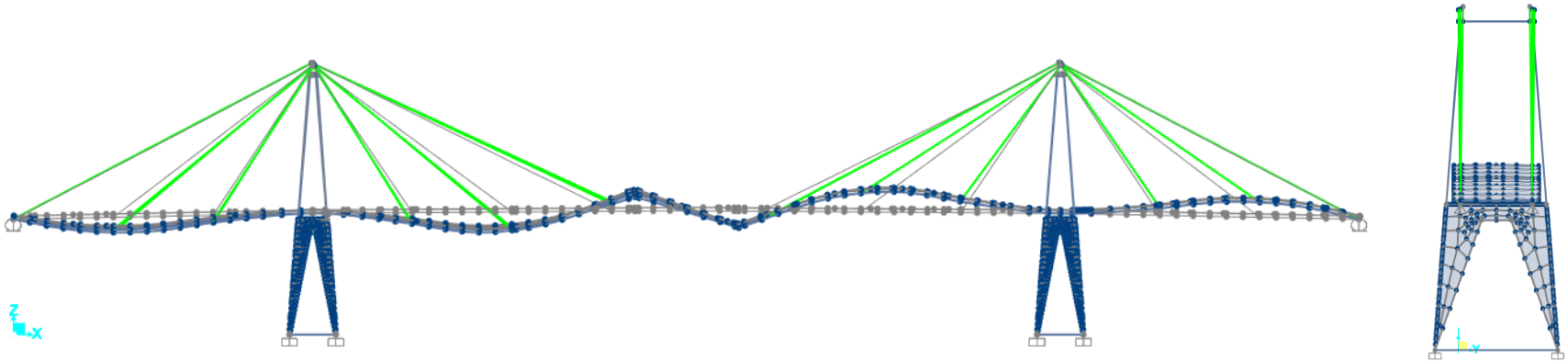

13 – 1,188 Hz

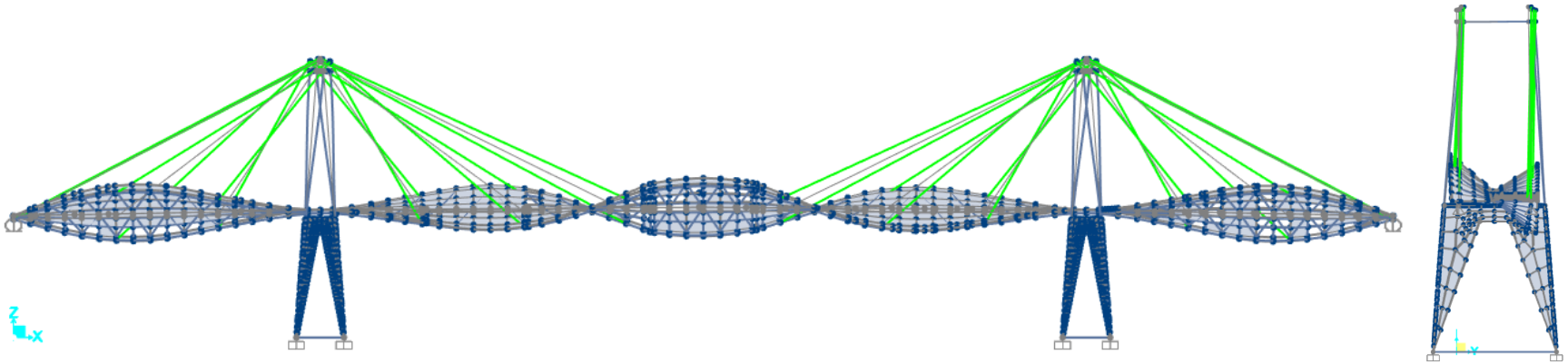

14 – 1,31 Hz

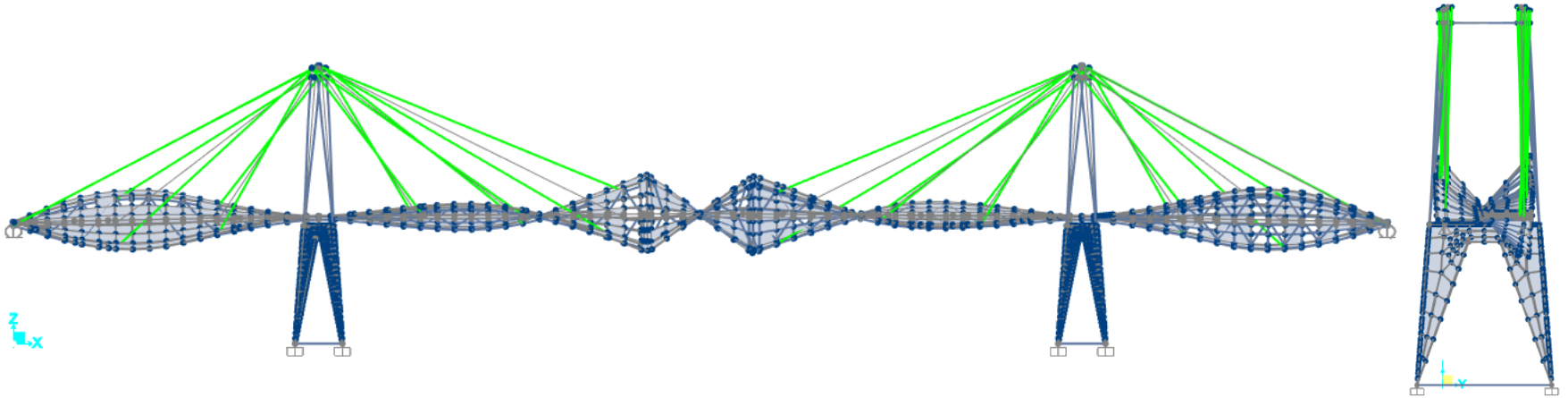

15 – 1,44 Hz

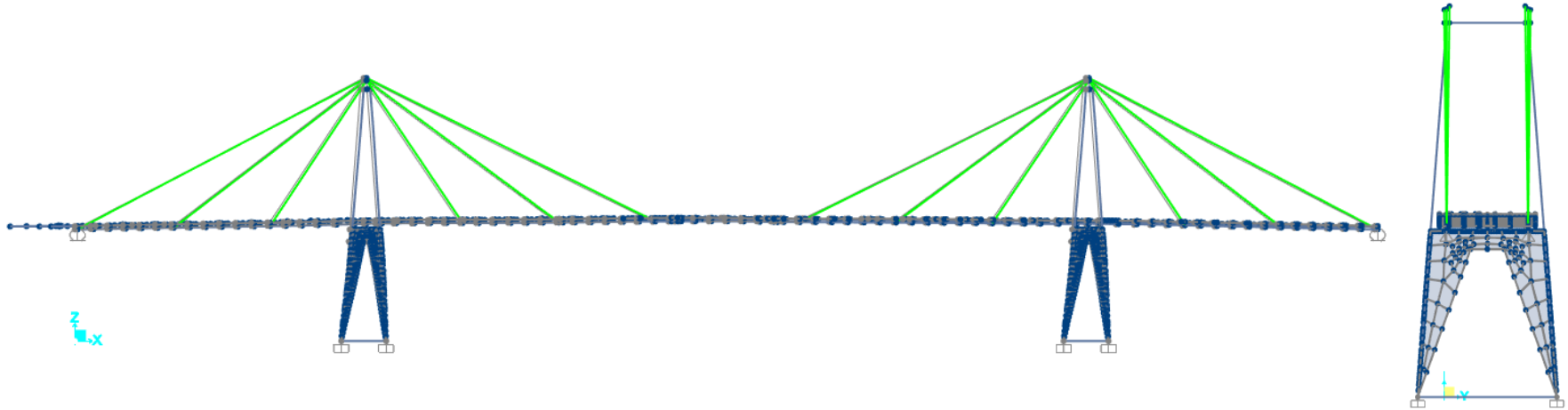

16 -1,47 Hz

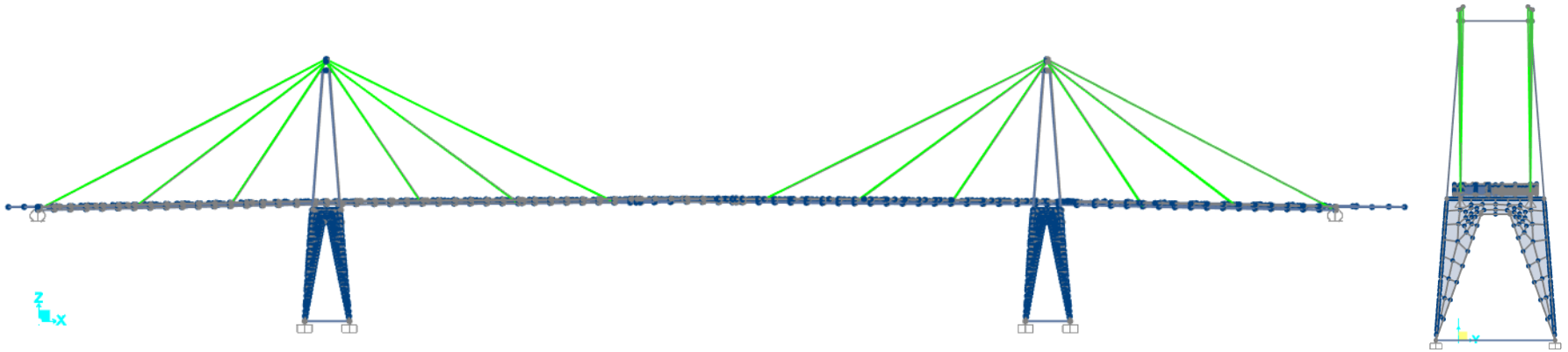

17 – 1,56 Hz

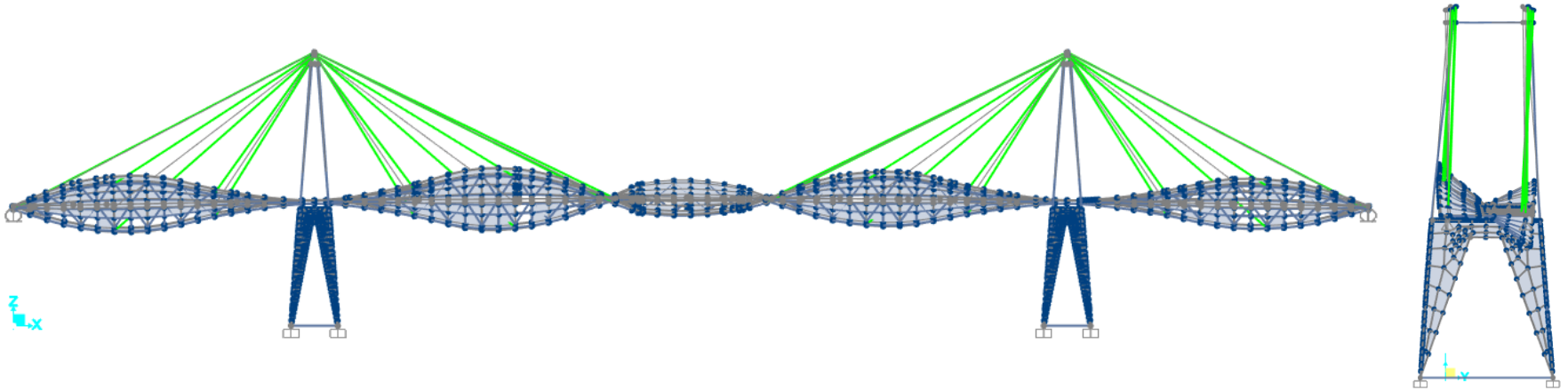

18 – 1,587 Hz

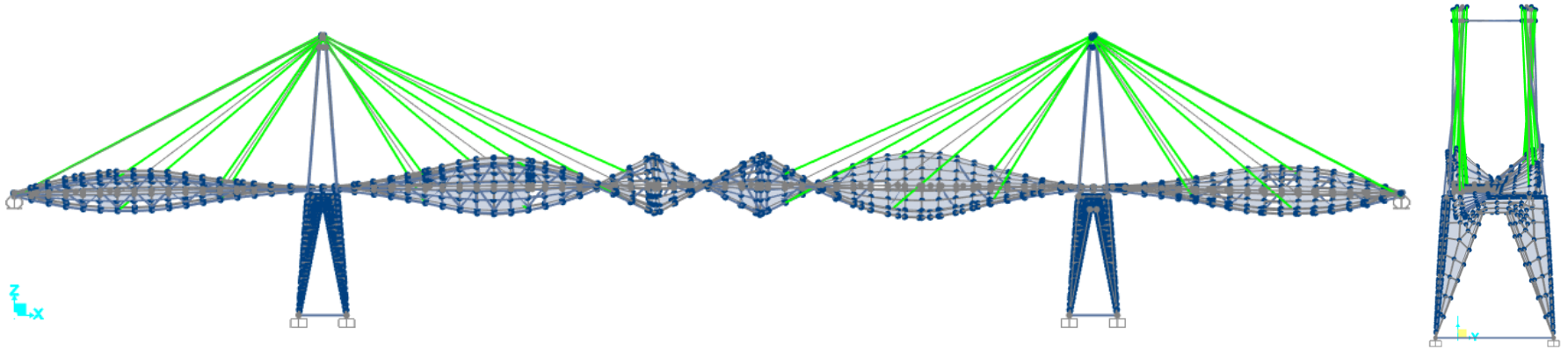

19 – 1,68 Hz

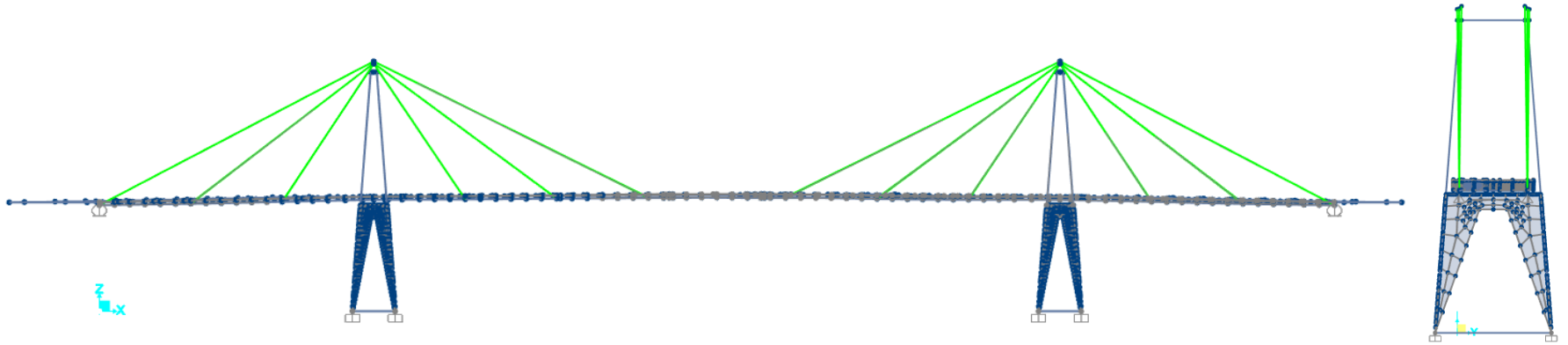

20 – 1,79 Hz